PHOSPHOPEPTIDE ADSORPTION ON ZIRCONIUM PHOSPHATE AND ZIRCONIUM PHOSPHONATE SOLIDS

By

EMILY J. POLLARD

A DISSERTATION PRESENTED TO THE GRADUATE SCHOOL
OF THE UNIVERSITY OF FLORIDA IN PARTIAL FULFILLMENT
OF THE REQUIREMENTS FOR THE DEGREE OF
DOCTOR OF PHILOSOPHY

UNIVERSITY OF FLORIDA

2013

To my family, especially my husband, who made this possible, and all for the glory of God

ACKNOWLEDGMENTS

I would like to express my gratitude to my family for all of their support throughout my graduate studies. Of special note is my husband whose day in and day out efforts made my degree progression possible. My parents were exceptionally helpful during the busiest times of my graduate career traveling long distances to lend a hand. My children, who bring so much joy to my life, always turned my bad days into good days with their bright smiles, contagious giggles, and amusing antics. Many thanks go out to my advisor and my research group for their instruction and aide in my research; I could not have come this far without them. I would also like to thank the Air Force Institute of Technology and the National Science Foundation (NSF) who funded my graduate work and the NSF award 10400016, which provided our department with the MALDI TOF-TOF referred to in this work. Last, but not least, I would like to say thank you to all of my friends and extended family members both near and far who gave me moral and spiritual support thought my time in graduate school.

DISCLAIMER: The views expressed in this document are those of the author and do not reflect the official policy or position of the United States Air Force, Department of Defense, or the U.S. Government.

TABLE OF CONTENTS

page

LIST OF TABLES

LIST OF FIGURES

Abstract of Dissertation Presented to the Graduate School
of the University of Florida in Partial Fulfillment of the
Requirements for the Degree of Doctor of Philosophy

PHOSPHOPEPTIDE ADSORPTION ON ZIRCONIUM PHOSPHATE AND ZIRCONIUM PHOSPHONATE SOLIDS

By

Emily J. Pollard

December 2013

Chair: Daniel R. Talham
Major: Chemistry

Phosphorylation is one of the most common post-translational modification of proteins, and it serves a regulatory or signaling function in numerous biological processes such as metabolism, gene expression, and differentiation. Studying the tryptic digests of proteins is an important aspect of understanding these processes. Mass spectrometry is the tool of choice for the study of phosphopeptides, but the substoichiometric amounts of phosphopeptides, the poor ionization of them in typical processes, and signal suppression from non-phosphopeptides necessitates an enrichment step before mass spectrometry analysis.

Typical phosphopeptide enrichment uses immobilized metal affinity chromatography (IMAC) or metal oxide affinity chromatography (MOAC) to separate phosphopeptides for focused study. To successfully employ these systems, it is often necessary to pre-treat protein digests or work near pH 3 in efforts to minimize competitive, acidic non-phosphopeptide binding. Even still, enrichment is often incomplete either losing some phosphopeptides or retaining some non-phosphopeptides. Increasing and applying an understanding of the enrichment

mechanism on IMAC or MOAC or developing a new material with improved properties could improve enrichment efforts.

Titania, a MOAC material, is perhaps the most common phosphopeptide enrichment material in use today, but its enrichment mechanism is not well understood. Zirconium phosphate has been reported once as a viable enrichment material, but little is known about its enrichment mechanism. Zirconium phosphonate particles have not been previously reported for this purpose. This work discusses research efforts to probe the enrichment mechanism on titania and to develop and explore new enrichment materials derived from zirconium phosphate and zirconium phosphonate. It will include quantitative and semi-quantitative comparisons of the binding of model peptides to titania, zirconium phosphate, and zirconium phosphonate.

CHAPTER 1
INTRODUCTION

Phosphopeptide Significance and the Need for Enrichment

Phosphorylation is a common post-translational modification of proteins. It plays a key regulatory roll in biology as it may control important cellular activities such as cell division, growth, differentiation, metabolism, and apoptosis.[1-5] Kinases and phosphatases, which respectively phosphorylate and de-phosphorylate proteins, signal changes for these cellular activities and, when malfunctioning, may have a role in the development of some cancers.[1, 5] Studying the phosphorylation characteristics of proteins will provide insight into these important biological mechanisms. This transient modification is observed primarily on amino acids serine (S), threonine (T), or tyrosine (Y) at approximately the ratio of 90:10:0.05, respectively.[1] However, estimates on the extent of protein phosphorylation are varied. The high end speculates that almost all eukaryotic proteins are phosphorylated at some point,[1] and about 30% of proteins might be phosphorylated at a given time.[4] Phosphorylated forms of proteins are present at substoichiometric concentrations.[5] The low ratio of the phosphorylated to the non-phosphorylated forms of a given protein and the transient nature of the modification make it difficult to study the phosphoproteome and drives the need for enrichment.

Common Enrichment Materials

Mass spectrometry (MS) is the method of choice for studying the phosphoproteome. It is sensitive enough to detect fmol levels of protein under the appropriate conditions, and it can identify unknown materials using tandem technologies.[2] Typically, proteins are enzymatically digested to yield peptides for MS

analysis. The substiochiometric phosphorylated peptides' signals are suppressed by the abundant non-phosphorylated peptides making phosphopeptides difficult to detect.

Enrichment techniques are used to separate phosphorylated and non-phosphorylated peptides before MS analysis to improve detection. Several enrichment techniques exist; immobilized metal affinity chromatography (IMAC) and metal oxide affinity chromatography (MOAC) are the most common.[1-5]

IMAC systems complex phosphate via immobilized metals such as Fe^{3+} and Ga^{3+} held to a support by chelating ligands such as iminodiacetic or nitrilotriacetic acid (Figure 1-1A).[1-5] When a mixture of peptides are exposed to the IMAC material, both the phosphate on a phosphopeptide and the carboxylate on acidic amino acid side chains are able to displace the ligands surrounding the metal center and can coordinate to the metal center (Figure1-1D). In order to improve the enrichment of phosphopeptides, researchers using IMAC will frequently invoke a methyl esterification reaction for the peptide mixture prior to IMAC. In methyl esterification, the carboxylic acids are converted to methyl esters by the addition of methanolic HCl to a solution of digested peptides.[6] While this step reduces non-specific binding of acidic non-phosphopeptides, methyl esterification does not prevent non-specific binding, and it introduces an additional handling step that can result in the loss of material. Additionally, IMAC suffers from metal leaching which can also contribute to the loss of phosphopeptides or the contamination of sample with metal ions.[2]

MOAC materials such as TiO_2 have a positively charged surface under acidic conditions (Figure 1-1B). Under the same conditions, phosphopeptides and acidic peptides can have a negative charge. Thus an electrostatic mechanism controls MOAC

enrichment (Figure 1-1E).[5] If the pH is sufficiently low, around pH 3, carboxylates will protonate and become neutral thereby reducing non-specific binding to some extent. However, some non-specific binding still occurs.[1, 2, 4, 5] Additionally, since the metals in MOAC are covalently bound to in the metal oxide structure, the materials are much less prone to leaching.[2, 5]

Zirconium based forms exist for both IMAC and MOAC materials. ZrO_2 is an alternative MOAC material to TiO_2, and Zr^{4+} can be chelated by a phosphonate to make a Zr^{4+}-IMAC material.[2, 7-9] These materials demonstrate different, and in some cases perhaps improved, enrichment capabilities compared to their more traditional counterparts. An explanation for this observation has not been provided, but instead it raises some interesting questions about the role the metal might play in the enrichment mechanism. The role of zirconium in phosphopeptide enrichment must be explored further.

α-Zirconium Phosphate and Zirconium Phosphonates

Crystalline α-ZrP (α-ZrP) was first synthesized by Clearfield and Stynes in 1964.[10] It is a layered material with the formula $Zr(HPO_4)_2 \bullet H_2O$. Each layer consists of a plane of zirconium atoms, each bridged by six phosphate groups with three from above and three from below (Figure 1-2). Three oxygen atoms from each phosphate group bind to three different zirconium atoms, and the fourth oxygen exists as a hydroxyl group that extends into the interlayer space. Thus an octahedral zirconium sheet is formed at the center of the layer with tetrahedral phosphate sheets on either side. The layers of α-ZrP are held together by van der Waals forces. The interlayer space houses one water molecule per unit cell. About two decades after the preparation of crystalline α-ZrP, Dines *et al.* demonstrated pillared zirconium

phosphonates made from α,ω-bisphosphonic acids.[11-13] These materials have a similar structure to α-ZrP except that an aryl group or alkyl chain takes the place of two hydroxyl groups on two phosphates and connects the layers of the material; an example is shown in Figure 1-3.[14] Clearfield provides a compendium of metal phosphonate chemistry including α-ZrP and a large number of zirconium phosphonates.[15]

The Zou group has demonstrated α-ZrP as a phosphopeptide enrichment material.[16] In their work they compared α-ZrP to TiO_2 and Fe^{3+}-IMAC using MALDI-TOF MS to analyze their enrichments. They used tryptic digests of purified phosphoproteins α-casein and β-casein, dilutions of the same with tryptic digest of bovine serum albumin (a non-phosphoprotein), mouse liver cell protein extracts and leukemia cell protein extracts. The authors noted several interesting observations. First, the post-synthetic treatment of α-ZrP with additional zirconyl chloride increased the affinity of the material for phosphopeptides (Figure 1-4). In Figure 1-4C, we see every expected phosphopeptide from the tryptic digest of α-casein and good exclusion of non-phosphopeptides from the spectra. Second, the inclusion of free zirconyl chloride in the system prevented the binding of phosphopeptides to α-ZrP while the inclusion of $FeCl_3$ largely did not (Figure 1-5). We think that the free Zr^{4+} present in the experimental conditions for Figure 1-5B, bound to the phosphates of the phosphopeptides and thus prevented the phosphopeptides from binding to the α-ZrP nanoplatelets. Third, α-ZrP had no bias for different amino acid sites of phosphorylation. Fourth, more phosphopeptides were identified with α-ZrP than with TiO_2 or Fe^{3+}-IMAC, however some phosphopeptides were uniquely enriched by each material (Figure 1-6). For this experiment, proteins were extracted from mouse liver lysate and were digested with

trypsin according to a previously published protocol.[17] Similar results were observed for the REH human leukemia cell line (data not shown here). Fifth, non-phosphopeptides were largely excluded from binding to the α-ZrP surface. In spite of these important observations, the authors do not offer a possible mechanism that could explain their observations other than the suggestion that Zr may be the cause.

Zou's group has also published additional work along similar lines using zirconium and a phosphonate in several materials for the enrichment of phosphopeptides. These materials coordinate zirconium using a phosphonate intrinsically available or chemically added onto the surface of each of the following materials: a surface modified porous silicon wafer, surface modified polymeric beads, monolithic particles, surface modified magnetic Fe_3O_4/SiO_2 core/shell nanoparticles, and bifunctionalized periodic mesoporous organosilicas.[18-22] The group's work consistently shows good qualitative selectivity for phosphopeptides over non-phosphopeptides and sensitivity down to the fmol level in some cases.

This work will build upon the work of Zou's group. We will further explore α-ZrP as a phosphopeptide enrichment material with an exploration of the zeta potential of the particle in suspension and a specific emphasis on the adsorption step in the overall enrichment process. Our work will define the isoelectric point of α-ZrP and detail quantitative adsorption capacity and selectivity through the study of two model peptides' interaction with α-ZrP. We propose a coordinate covalent binding mechanism on α-ZrP(Figure 1-1C,F) similar to the mechanism of traditional IMAC and highlighting the role of zirconium in allowing phosphopeptide adsorption and preventing non-phosphopeptide adsorption. In cases where zirconium is not fully coordinated within the

material, only the phosphate on a phosphopeptide is strong enough to displace the ligands surrounding the zirconium center. Competing carboxylates on non-phosphopeptides are not strong enough to displace the ligands around. This should reduce non-specific binding, which is a common problem in IMAC. Our proposed mechanism explains the good selectivity reported previously.[16] We present data in support of our proposed mechanism.

Additionally, we introduce a known zirconium phosphonate particle synthesized using an α,ω-bisphosphonic acid as a novel phosphopeptide enrichment material.[23] This material was chosen to increase the availability of zirconium on the surface of the particle, a point that will be discussed in Chapter 2. Our zirconium phosphonate material should have similar enrichment capability to the various zirconium anchored by a phosphonate materials described by Zou's group.[18-22] Additionally, it should have a binding mechanism comparable to our proposed mechanism for α-ZrP. We explore the binding capacity and selectivity of this material in comparison to α-ZrP and compare both of our synthesized materials to commercially available TiO_2. Since the enrichment mechanism with TiO_2 is electrostatic, and we suspect a coordinate covalent mechanism on our zirconium phosphate/phosphonate materials, we expect, and in fact observe, differences in the pH dependent binding of these materials. In order to understand the effect of pH on the particles, we begin our study with the exploration of isoelectric points for the materials of interest in this work.

Isoelectric Points

The first aspect of this study will consist of the characterization of the materials including the intrinsic electrokinetic properties of the particles in suspension. Suppose a particle exists in aqueous suspension with some innate charge on the surface. Counter

ions and water molecules will align at the surface forming a tight layer, the Stern layer, which ends at the inner Helmholtz plane (Figure 1-7). A second layer forms, the diffuse layer, with less tightly bound counter ions and water molecules. The potential within this layer gradually decreases as you move away from the particle surface until it reaches zero. These two layers together are considered the electrical double layer. If a particle in suspension is put in motion, all the molecules within the Stern layer and those some distance from the surface in the diffuse layer will move with the particle. The boundary between molecules that move with the particle and those that do not has several names: the outer Helmholtz plane, the slipping plane, or the shear plane. The zeta potential (ζ) for a material is the electrokinetic potential at the slipping plane of a particle in suspension.[24-26] The ζ of a material in suspension provides information about the stability of the suspension. If the ζ has a magnitude larger than ± 30 mV, the suspension is likely to be stable.[25]

The pH and ionic strength of a suspension can affect the ζ of a material. Increasing the ionic strength will dampen the ζ without affecting the sign of the potential. In some cases, such as adjusting the stability of a suspension, it can be useful to titrate the ζ as a function of ionic strength. Conversely, a change in pH can change the sign of the ζ. As such, it is often useful to titrate the ζ as a function of pH. The titration results will reveal the isoelectric point (IEP) of the material, the point at which the ζ is 0 mV. At pH values below the IEP, the ζ will be positive, and at pH values above the IEP, the ζ will be negative. The titration of ζ as a function of pH can also show pH regions where the suspension is expected to be stable.

The ζ is usually a dampened value with the same sign as the surface potential (Figure 1-3), and thus it is reasonable to approximate the surface potential from ζ data. There are some cases, however where this assumption might not be accurate. One such case exists when the surface is electrokinetically anisotropic.[26] Since the ζ is some distance from the surface of the particle, in principle it represents a weighted average of the surface potentials of various sites present on the particle. Nonetheless, the ζ still accurately portrays what a molecule "sees" as it approaches a charged particle in suspension.

In this work we will consider the ζ as a function of pH and the corresponding IEP as a means for estimating the surface potential of a material in suspension at different pH values. As we study the adsorption of peptides onto the various materials across a range of pH values, we will be able to comment on the binding mechanism from a standpoint of whether or not electrostatic attraction is contributing.

Adsorption Isotherms

Enrichment can be considered a multi-step process that includes adsorption, washing, desorption, and regeneration.[27] Characteristics of a successful enrichment system include adsorption of the desired analyte, reasonable separation of the desired analyte from competing components of the mixture, and good recovery of the desired analyte for further work. Additionally, it is beneficial if the system can be regenerated and used more than once. The first step of enrichment and the first characteristic of successful enrichment centers around adsorption. Chronologically, adsorption occurs first, and without successful adsorption of the desired analyte enrichment cannot occur. Adsorption of competing components can also occur; if it occurs, the second characteristic, separation, can be brought about by the washing step where non-

specifically adsorbed components are removed and the desired analyte remains adsorbed. Alternatively, if non-specific binding can be avoided during the adsorption step, two characteristics of successful enrichment, analyte adsorption and separation from competition, can be achieved in a single step. The final characteristic of successful enrichment, good recovery of the desired analyte, occurs during the desorption step. This step can also be called the elution step.

The second aspect of this study will consist of the focused study on the adsorption step of model peptides onto novel and known phosphopeptide enrichment materials. The adsorption step was chosen because it occurs first and because it can provide two characteristic features of successful enrichment, adsorption and separation. We will conduct batch adsorption studies and model binding with adsorption isotherms, which have been widely used to study adsorbents and adsorbates.[28-34] Using adsorption isotherms, we can quantitatively compare adsorption using the metrics binding capacity, efficiency, and favorability, and we can also quantitatively compare separation during the adsorption step as the metric selectivity.

Adsorption isotherms provide for a focused and quantitative study of the adsorption step of the larger chromatographic process, but alone they are not capable of predicting a full chromatographic system.[27] Additionally, our adsorption isotherms reflect the adsorption of a peptide from a single-component buffered solution whereas chromatographic enrichment processes handle complex mixtures of peptides. However, even under these conditions, adsorption isotherms still provide useful information for material/method development of more complete systems.[35-38] We will

use adsorption isotherms as a means to study the first step of enrichment on phosphopeptide enrichment materials.

This Work

In this work we combine our knowledge of the IEP and ζ for phosphopeptide enrichment materials with adsorption isotherm data across a range of pHs to understand the conditions that favor enrichment and probe the binding mechanism that controls the enrichment process. We test a relatively recently demonstrated enrichment material α-ZrP and a novel enrichment material Zr-OBP, and we compare them to a well-established enrichment material TiO_2. The materials are tested against a model phosphopeptide and a non-phosphorylated analogue of the same sequence under strongly ionic conditions, and the results are modeled with adsorption isotherms revealing quantitative binding parameters. These parameters are then compared to describe the differences and similarities between the materials.

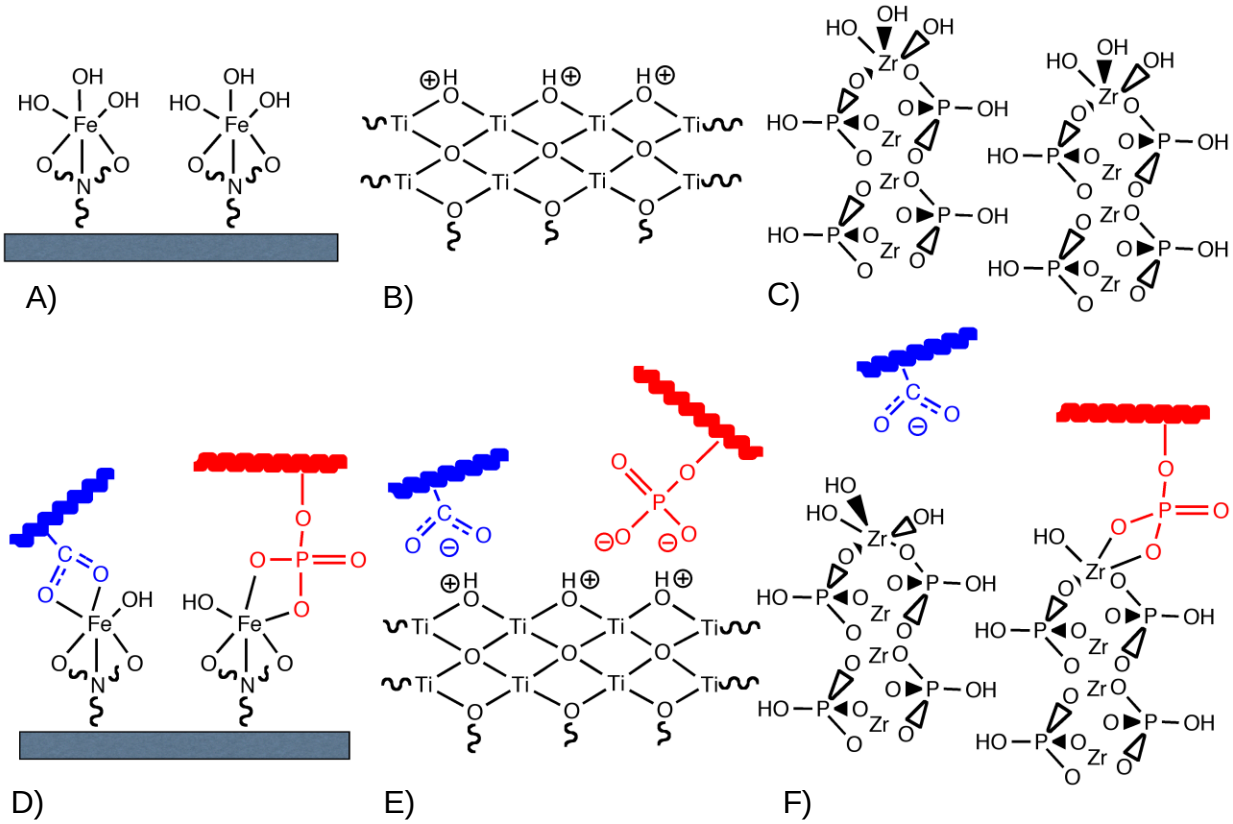

Figure 1-1. Schematics showing the surfaces of phosphopeptide enrichment materials (A-C) and the possible mechanism by which enrichment occurs (D-F) for IMAC, MOAC, and α-ZrP (left to right).

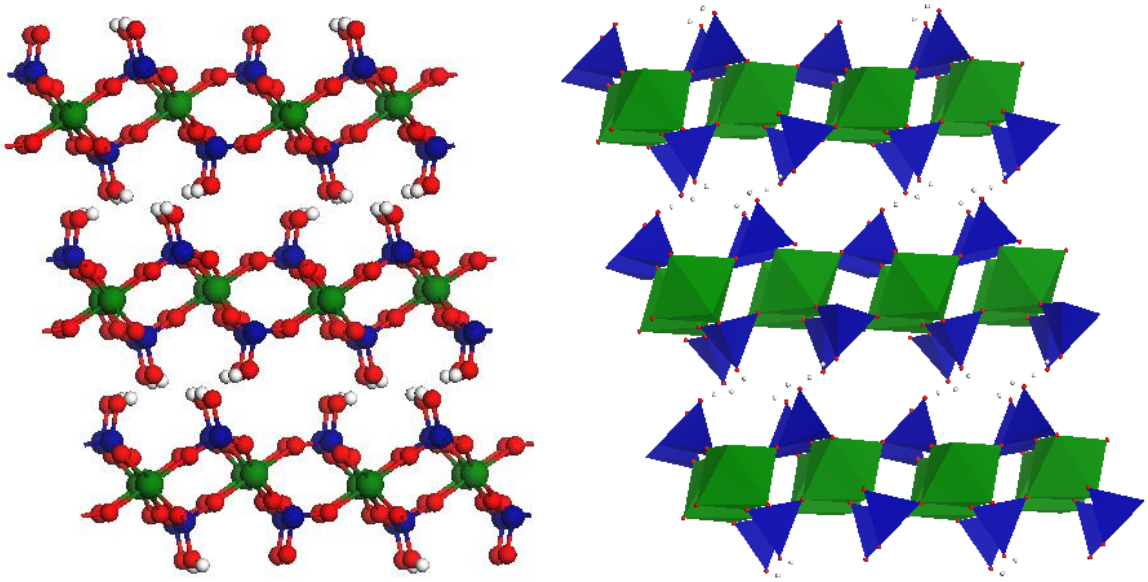

Figure 1-2. Models showing the structure and geometry of α-ZrP. Zirconium is green and has an octahedral geometry. Phosphorus is blue and has a tetrahedral geometry. Oxygen is red, and hydrogen is white. The interstitial water molecules are omitted for clarity. Input parameters from Troup and Clearfield.[39]

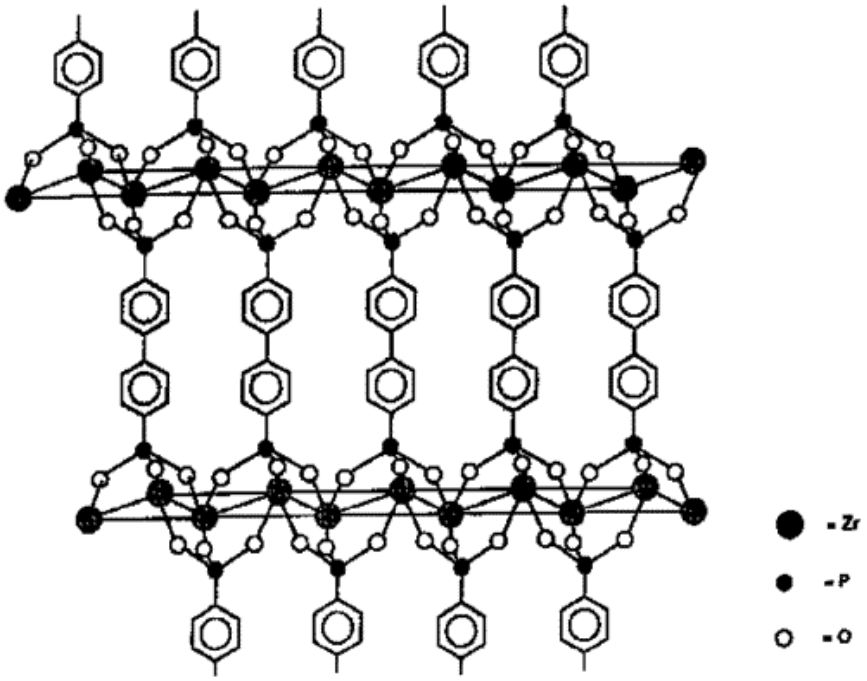

Figure 1-3. Schematic representation of idealized structure of the pillared material zirconium biphenylenebis(phosphonate), Zr(PO_3-Ph-Ph-PO_3). Reprinted with permission from Wang, Z.; Heising, J. M.; Clearfield, A. *J. Am. Chem. Soc.* **2003***, 125*, 10375-10383. Copyright 2003 American Chemical Society.

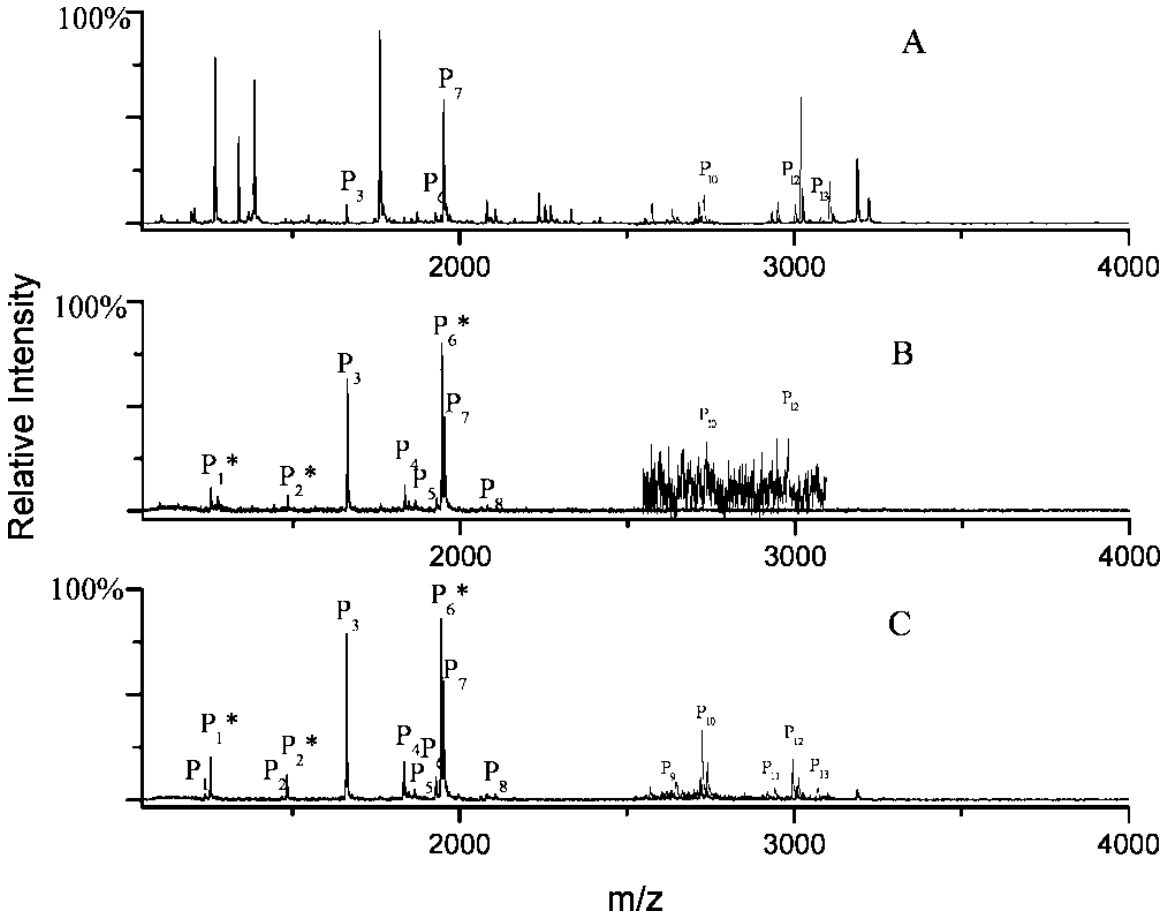

Figure 1-4. A tryptic digest of α-casein (400 fmol) analyzed by MALDI-TOF MS: A) direct analysis, B) neat α-ZrP, C) α-ZrP treated with excess $ZrOCl_2$ prior to use. $P_{\#}$ indicates a phosphopeptide; an asterisk marks a phosphopeptide with an oxidized M residue. Reprinted with permission from Xu, S.; Whitin, J. C.; Yu, T. T.; Zhou, H.; Sun, D.; Sue, H.; Zou, H.; Cohen, H. J.; Zare, R. N. *Anal. Chem.* **2008***, 80*, 5542-5549. Copyright 2008 American Chemical Society.

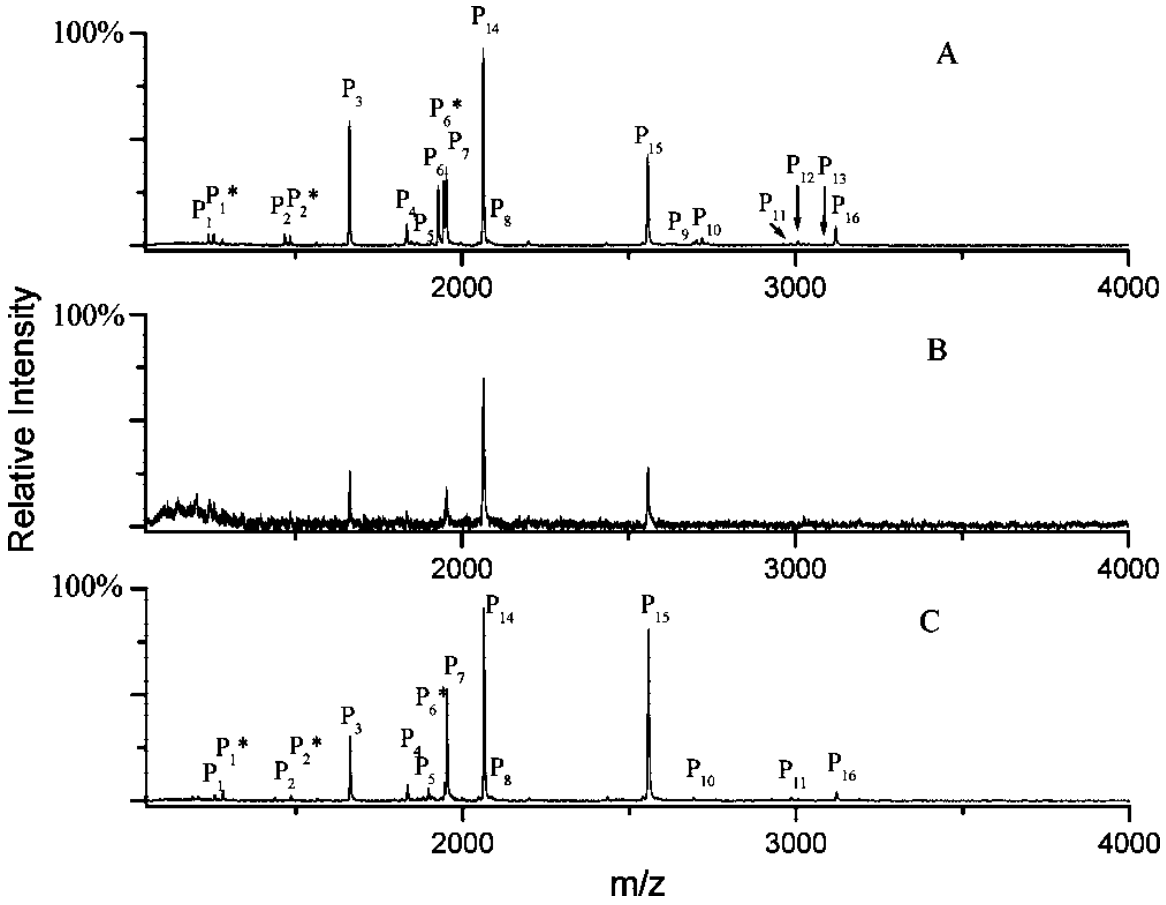

Figure 1-5. A tryptic digest of α-casein and β-casein analyzed by MALDI-TOF MS after using A) treated α-ZrP, B) treated α-ZrP and $ZrOCl_2$, C) treated α-ZrP and $FeCl_3$. $P_{\#}$ indicates a phosphopeptide; an asterisk marks a phosphopeptide with an oxidized M residue. Reprinted with permission from Xu, S.; Whitin, J. C.; Yu, T. T.; Zhou, H.; Sun, D.; Sue, H.; Zou, H.; Cohen, H. J.; Zare, R. N. *Anal. Chem.* **2008***, 80*, 5542-5549. Copyright 2008 American Chemical Society.

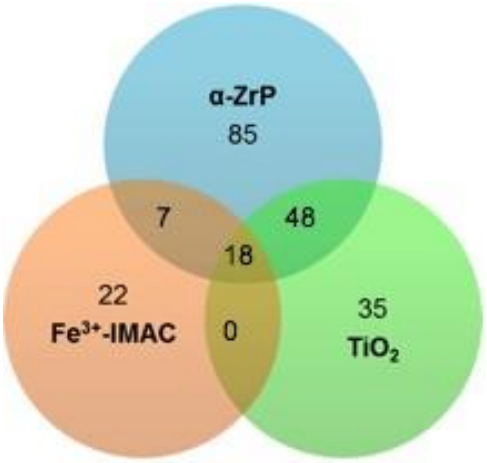

Figure 1-6. The overlap of the phosphopeptides observed in mouse liver lysate after enrichment with α-ZrP, TiO_2, and Fe^{3+}-IMAC. Adapted with permission from Xu, S.; Whitin, J. C.; Yu, T. T.; Zhou, H.; Sun, D.; Sue, H.; Zou, H.; Cohen, H. J.; Zare, R. N. *Anal. Chem.* **2008***, 80*, 5542-5549. Copyright 2008 American Chemical Society.

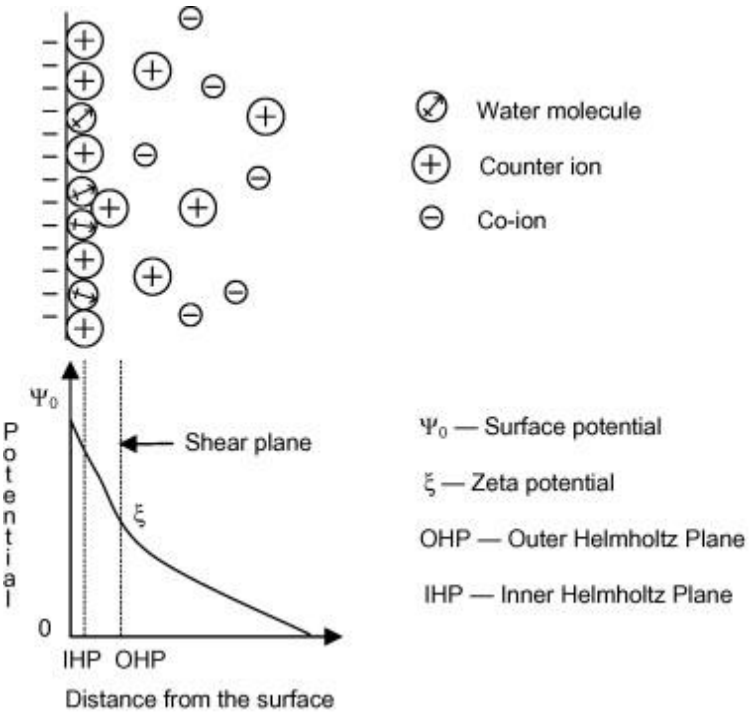

Figure 1-7. A schematic showing the composition of the electrical double layer and the position of the ζ relative to the surface potential. Reprinted from Minerals Engineering, 23, Alvarez-Silva, M.; Uribe-Salas, A.; Mirnezami, M.; Finch, J. A., The point of zero charge of phyllosilicate minerals using the Mular–Roberts titration technique, 383-389.[26] Copyright 2010, with permission from Elsevier.

CHAPTER 2
ISOELECRIC POINTS OF ENRICHMENT MATERIALS

Isoelectric Points

Metal oxide affinity chromatography (MOAC) has become one of the most common techniques for phosphopeptide enrichment. Yet, the mechanism by which this enrichment occurs is largely unknown. One possibility is that an electrostatic attraction exists between a positively charged metal oxide surface and a negatively charged phosphate.[40] Researchers have observed that lower pH, where TiO_2 is positively charged and competing carboxylates are neutralized, improves the results.[1] Another possibility is that a coordinate covalent bond is formed between the metal center and the phosphate; other researchers have observed a bidentate binding mode of phosphates to metal oxides.[41] Additionally, some reports have shown preferential differences in phosphopeptide enrichment using ZrO_2 compared to TiO_2 without an explanation of why this might be[42]

New enrichment materials such as α-ZrP have shown promise, however a discussion of enrichment mechanism with this material is lacking.[16] Clearly, the mechanism of these enrichments needs to be studied further especially for new enrichment materials such as zirconium phosphate and zirconium phosphonate. We have probed the electrokinetic potential of phosphopeptide enrichment materials by measuring the zeta potential (ζ) as a function of pH. The ζ is a reflection of the surface charge of a material, and the pH where the ζ is zero is the isoelectric point (IEP) of the material. Knowing the IEP of phosphopeptide enrichment materials will give us insight into enrichment mechanisms.

Kosmulski has published a series of reviews outlining the IEP of metal oxides,[24, 43-46] and in another review Kosmulski specifically discusses the published distributions of the IEP for TiO_2 and other common metal oxides.[47] In this work, he finds the universal IEP of TiO_2 to be about 5.8. A universal IEP, as described by Kosmulski, is independent of specific material specimen, detailed solution composition, and specific experimental conditions such as specific instrument or sample pretreatment. For ZrO_2, another common MOAC material, no universal IEP is found; rather the published results span a range of 4-8.[47] Additionally, only one entry is found for the IEP of α-ZrP.[48] Beyond our aim of understanding the IEP within the frame of phosphopeptide enrichment, it is important to determine the IEP of materials as a contribution to colloid science where this information relates to the stability of the suspension[49] and the effect of pH changes on the uptake of ions.[50]

The IEP of a colloid can be determined using any of several techniques. Two techniques of note are electrokinetic and potentiometric titrations. Between these techniques, there are differences in the way the IEP is determined and in what the value represents. The IEP is the pH at which no net charge exists at the slipping plane around the particle. Potentiometric techniques more accurately find the point of zero charge (PZC) instead of the IEP. The PZC is the pH at which the surface charge of the material is zero. Potentiometric techniques usually compare the behavior of a dispersion with the repeated additions of strong acid or base to a blank handled in the same way. The difference between the dispersion and the blank reveal the surface charge density of the dispersion as a function of pH and thus allows researchers to determine the PZC.[51] Electrokinetic titrations measure the change in ζ as a function of

pH using electroosmosis, electrophoresis, or electroacoustics. All electrokinetic measurements involve detecting the motion of either the solvent in the presence of a surface of interest (electroosmosis) or the particle of interest in suspension (electrophoresis and electroacoustics). The motion of the entity is then related to the ζ, the potential at the slipping plane of the electrical double layer above a charged surface using well established models. In most cases, the IEP and the PZC of materials are approximately the same. However, this might not the case with anisotropic materials such as talc, chlorite, and serpentine[26, 52] or for α-ZrP. Electrokinetic measurements consider the potential at the slipping plane, and therefore the technique reports an average of the potential contributing moieties on the surface. When a material is anisotropic, the contributions from one surface type can be very different from the other, and a shift in the ratio of the different surface moieties could have a large effect on the IEP. In this work, the IEP of phosphopeptide enrichment materials are determined by plotting the ζ, measured using electrophoretic techniques, as a function of pH. By determining the IEP of phosphopeptide enrichment materials in this work, we will be able to make inferences about the mechanism of phosphopeptide enrichment in future work. Similar strategies of using IEPs to make mechanistic inferences have been reported previously.[53-56]

Experimental Section

Titanium(IV) oxide nanopowder (TiO_2), zirconium(IV) oxide nanopowder (ZrO_2), and 1,8-octanediphosphonic acid (OBP) where purchased from Aldrich. Zirconyl chloride octahydrate was purchased from Acros Organics. Potassium chloride, potassium hydroxide, hydrochloric acid and *o*-phosphoric acid 85% were purchased

from Fisher. All materials were used as received. Water was purified to a resistivity of 17.2 MΩ·cm or greater using a Barnstead E-pure filtration system.

Synthesis of Materials

α-Zirconium phosphate ($Zr(HPO_4)_2 \cdot H_2O$, α-ZrP) was prepared similarly to the reflux method previously described by Clearfield and Stynes.[10] Zirconyl chloride octahydrate (3 mmol) was dissolved in 2.5 mL of water, and 7.5 mL of 4 M phosphoric acid was heated to 97 °C. The zirconyl chloride solution was quickly added to the heated phosphoric acid solution (1:10 Zr:P reaction ratio), and the resulting precipitant was allowed to reflux at 97 °C for one day. The particles were recovered by centrifugation for 10 min at 11,300 x g, and the supernatant was discarded. The particles were washed with 90 mL of water three times. The washed particles were dried overnight at 65 °C, and the dried particles were ground into a fine white powder with mortar and pestle forming neat α-ZrP. Neat α-ZrP was post-synthetically treated with excess zirconium ions by suspending particles 1 mg/mL in a solution of 20 mM zirconyl chloride octahydrate overnight with vigorous mixing. The treated particles were recovered by centrifugation, washed with 300 mL water twice, dried overnight at 65 °C, and ground into a fine white powder with mortar and pestle forming treated α-ZrP.

Neat $Zr(O_3P\text{-}(CH_2)_8\text{-}PO_3)$, hereafter known as Zr-OBP, has been prepared previously by Hong *et al*. where they formed a microcrystalline solid using fluorine complexation to aide in microcrystal development.[23] In this work, treated Zr-OBP was prepared similarly to α-ZrP. Zirconyl chloride octahydrate (0.37 mmol) was dissolved in 96 mL water, and 64 mL containing 0.73 mmol OBP was heated to 97 °C. The zirconyl chloride solution was quickly added to the heated phosphonic acid solution (1:3.9 Zr:P reaction ratio), and the resulting precipitant was allowed to reflux at 97 °C for one day.

The particles were recovered by centrifugation for 10 min at 11,300 x g, and the supernatant was discarded. The particles were washed with 180 mL of water three times. The washed particles were dried overnight at 65 °C, and the dried particles were ground into a fine white powder with mortar and pestle. The neat material was post-synthetically treated with excess zirconium ions by suspending particles 1 mg/mL in a solution of 20 mM zirconyl chloride octahydrate overnight with vigorous mixing. The treated particles were recovered by centrifugation, washed with 300 mL water twice, dried overnight at 65 °C, and ground into a fine white powder with mortar and pestle.

Characterization of Materials

The Fourier transfer infrared (FTIR) spectra of the synthesized particles was collected using a Nicolet 6700 Thermo Scientific spectrophotometer from 4000-500 cm^{-1} at a resolution of 1 cm^{-1} as the average of 16 scans. The particles were mounted in a pressed KBr pellet, and the background absorbance of KBr was subtracted. Scanning electron microscopy (SEM) micrographs of the samples were obtained using a Hitachi S-4000 FE-SEM located at the Major Analytical Instrument Center (MAIC) at the University of Florida. SEM samples were mounted on silica slides and coated with carbon prior to imaging. For neat and treated α-ZrP and neat Zr-OBP, powder X-ray diffraction (XRD) was collected on a PANalytical X'PERT Powder diffractometer located at MAIC with CuKα radiation by mounting of the powdered materials to a glass substrate with double-sided adhesive. The 2θ angle was scanned from 5-50° at a step size of 0.008° and a scan rate of 10.2 sec per step. For treated Zr-OBP, powder XRD was collected on a Bruker DUO diffractometer with CuKa radiation (λ = 1.54178 Å) from an ImS power source, multi-layered mirror optics, and an APEXII CCD area detector (1024x1024 detection format) positioned 150 mm from the sample. Powder samples

were packed into 0.3 mm diameter boron-rich thin walled capillary tubes purchased from the Charles Supper Company. Diffraction patterns were collected between 5 and 50 degrees with a 600 sec/image collection time. The Ma group of University of South Florida kindly completed gas sorption measurements on a Micromeritics ASAP 2020 surface area analyzer using nitrogen at 77 K. Complete Analysis Laboratory, Inc. in Parsippany, NJ conducted elemental analysis.

Zeta Potential Titrations

Titration experiments were carried out on a Malvern Zetasizer Nano-ZS equipped with an MPT-2 autotitrator and an auto-degas unit using a Malvern folded capillary cell. The pH probe was calibrated prior to each session. Samples were suspended in 10 mL of 1 mM KCl and sonicated for 20 min prior to titration. Titrations were carried out at room temperature (23.0-23.5 °C). The materials were titrated by the addition of acid or base across the IEP of the material using a program specific to each material. TiO_2 was suspended approximately 1 mg/mL and was titrated from pH 3.5 to 8.0 with 0.5 step size and ±0.1 target pH threshold using 0.25 M HCl, 0.025 M KOH, and 0.25 M KOH. ZrO_2 was suspended approximately 1 mg/mL and was titrated from pH 8.5 to 5.0 with 0.5 step size and ±0.1 target pH threshold using 0.25 M HCl, 0.025 M HCl, and 0.25 M KOH. Neat α-ZrP was suspended approximately 1 mg/mL and was titrated from resting pH to pH 1.0 with 0.5 step size and ±0.1 target pH threshold using 1.0 M HCl. Treated α-ZrP was suspended approximately 1 mg/mL and was titrated from resting pH to pH 1.5 with 0.5 step size and ±0.1 target pH threshold using 1.0 M HCl. Neat Zr-OBP was suspended approximately 0.2 mg/mL and was titrated from pH 3.5 to 1.0 with 0.5 step size and ±0.1 target pH threshold using 1 M HCl. Treated Zr-OBP was suspended

approximately 0.2 mg/mL and was titrated from pH 5.0 to 2.0 with 0.5 step size and ±0.2 target pH threshold using 1 M HCl, 0.25 M HCl, and 0.25 M KOH.

Results and Discussion

Characterization of Materials

We have synthesized two materials for this work: α-ZrP and Zr-OBP, and we have characterized both materials with FTIR, powder XRD, SEM, nitrogen sorption, and elemental analysis. The FTIR spectra recorded for α-ZrP and Zr-OBP (Figure 2-1) are consistent with the published spectra. For neat and treated α-ZrP, the peaks in the region 1330-900 cm^{-1} represent the stretching modes of phosphate. The broad absorbance from 3600-2900 cm^{-1}, the two sharp peaks at ~3598 and ~3511 cm^{-1}, and the feature observed at ~3155 cm^{-1} are attributed to vibrations of water held in α-ZrP in different configurations (zeolitic or H-bonded water).[57] For neat and treated Zr-OBP, the phosphonate stretches are observed as an unresolved single peak centered at ~1040 cm^{-1}. Asymmetric and symmetric stretches of $-CH_2-$ are observed near ~2931 and ~2857 cm^{-1}, respectively. Symmetric bending of $-CH_2-$ is observed near ~1467 cm^{-1}, and $-CH_2-$ scissoring is observed near ~1409 cm^{-1}.[23] For both materials, we do not observe significant differences related to the treatment of the particles.

Powder XRD for the synthesized samples are shown in Figure 2-2. Some peaks are observed for α-ZrP, and their positions are consistent with literature reports for the material. The poor signal to noise ratio and larger peak breadth can be attributed to small particles, limited amount of sample, or more amorphous material. For Zr-OBP, we observe a large interlayer distance indicated by the peaks at 6 and 12 °2θ. This can be attributed to pillaring of the phosphonic acid. We do not observe peaks at higher

angles, which would indicate organized structure of a shorter inter-atomic distance; only the broad peak attributed to the mounting glass is observed above 15 °2θ.

SEM micrographs of α-ZrP (Figure 2-3A-C and E-F) are consistent with aggregated platelets of approximately 100 nm in length, as reported previously.[58] SEM micrographs of Zr-OBP (Figure 2-3D and G-H) show that the particles are similar to α-ZrP in size and shape. Comparatively, TiO_2 nanopowder particles are less than 25 nm in diameter. Surface area analysis by nitrogen sorption shows BET surface areas of 86.3 m^2/g for treated α-ZrP and 182.3 m^2/g for treated Zr-OBP. Comparatively, TiO_2 has a surface area by BET of 45-55 m^2/g, according to the manufacturer.

Elemental analysis of Zr-OBP_N is consistent with the theoretical weight percentages for the molecular formula; the theoretical percentages for Zr, P, O, C, and H are 25.24, 17.14, 26.56, 26.59, and 4.46 respectively, and the experimental values are 25.19, 17.01, 26.86, 26.48, and 4.54 respectively. The error is approximately ±0.4%. Experimental oxygen percentages are determined by mass balance from the observed values of the other four elements. The slight increase of mass percentages of oxygen and hydrogen, and the corresponding slight decrease in C, P, and Zr, between theoretical to experimental values are most likely due to the incorporation of water in the lattice. This is confirmed by the modest absorbance near 3400 cm^{-1} in the FTIR spectra (Figure 2-1).

Isoelectric Point Determination

The ζ as a function of pH for each material is shown in Figure 2-4. Raw data was binned into x-axis categories, and the data points plotted here represent the mean x and y position of raw data. The lines between the points represent point a to point b straight-line connections. The x error bar represents the standard deviation of pH values

within the bin. The y error bar represents the standard deviation of the ζ within the x-axis bin. The IEP of each material can be visualized as the point at which the titration curve crosses ζ = 0 mV. We calculated the IEP for each material by a graphical method visualized in Figure 2-5. The black data points represent the mean value for repeated titrations of the material on the Zetasizer as described in Figure 2-4. The x-axis and y-axis error bars (black) represent the standard deviation (σ) of the mean. For the purpose of determining the IEP, the x-axis error is ignored because it is sufficiently small. Points were defined at (pH, ζ) and (pH, ζ ± σ). Lines (red) were drawn through all pairs of points and the x-axis; the x-axis intercept represents a possible IEP. The material IEP reported recorded below and presented here (Figure 2-5, blue points) represents the mean plus or minus the standard deviation (blue error bars) of the possible IEPs for the given pair of data points.

Using the method described above, we calculated the IEPs of phosphopeptide enrichment materials (Table 2-1). The IEP we found for TiO_2 is within the range of the universal IEP, and the IEP we found for ZrO_2 falls within the broad range of IEPs reported previously.[47] The IEP we found for neat α-ZrP is in agreement with the value published by Mercado *et al.*[48] After treating α-ZrP with zirconium ions, we observe a dramatic shift in the IEP from ca. pH 1 to ca. pH 3. Interestingly, the IEP found for treated α-ZrP is similar to that reported for zirconium pyrophosphate.[48] However the FTIR (Figure 2-1) and XRD (Figure 2-2) of the treated material are consistent with α-ZrP and not zirconium pyrophosphate.[57, 59] This indicates our treatment with excess zirconium ions has reduced the number of acidic sites on the surface of the material without disrupting the overall structure. We observe similar behavior for neat and

treated Zr-OBP. This is a reflection of the similar surface chemistries of the zirconium phosphate and the zirconium phosphonate.

In spite of the large IEP shifts we observe upon treatment, we do not observe an increase in mass percentage of zirconium (see above). For α-ZrP, roughly 3% of the zirconium present in a particle is positioned on the surface, and in post-synthetic treatment we are only adding zirconium to phosphoric acid not already fully coordinated to three zirconium atoms. Thus, it is not surprising that we cannot detect a change by elemental analysis. We propose that the dramatic shift observed in the IEP upon treatment is rooted in the anisotropic nature of the particle surface. When we synthesize α-ZrP and Zr-OBP, the phosphate/phosphonate are in excess and the reaction is carried out in an acidic aqueous environment, therefore on the edge of these particles and any defects in the faces, zirconium is likely coordinated to water or phosphate/phosphonate that is not fully coordinated to three zirconium atoms. In the treatment step, we can add zirconium into these spaces.

The dramatic IEP shifts we observe from our neat materials to our treated materials suggest we have changed the ratio of the two surface moieties by increasing the Zr and decreasing the P. We have also observed incomplete treatment by a smaller shift in the IEP (data not shown). If the IEP of the “treated” material is not above approximately 2.6, the treatment has failed, and the material must be treated again with excess zirconium ions. The treatment failure is related to poor mixing conditions, and after treating a second time with better mixing conditions, the IEP approaches 3. This observation further supports the proposed theory of shifting the ratio of surface sites with an increase in Zr and a decrease in P.

Summary

We have synthesized α-ZrP and Zr-OBP in neat and treated forms. The characterizations of our neat materials match what has been published previously with the exception of the XRD of our Zr-OBP. We attribute this to having, by design, a more amorphous material than Hong *et al*.[23] The FTIR, SEM, and XRD do not change appreciably between the neat and treated forms of the materials; this demonstrates that the treatment has not affected the bulk structure of the particles. The IEP of neat α-ZrP, TiO_2 and ZrO_2 are in agreement with published values. The IEP of neat Zr-OBP is similar to neat α-ZrP, as one would expect. The dramatic shift we observe in the IEP from neat to treated materials is attributed to a shift in the ratio of Zr to P sites on the surface of these anisotropic materials. We observe IEPs in three clusters: neat zirconium phosphate/phosphonate around pH 1, treated zirconium phosphate/phosphonate around pH 3, and TiO_2 and ZrO_2 between pH 6 and 7. In subsequent work, we will use the knowledge of the IEP for each material to make inferences about the mechanism of phosphopeptide enrichment.

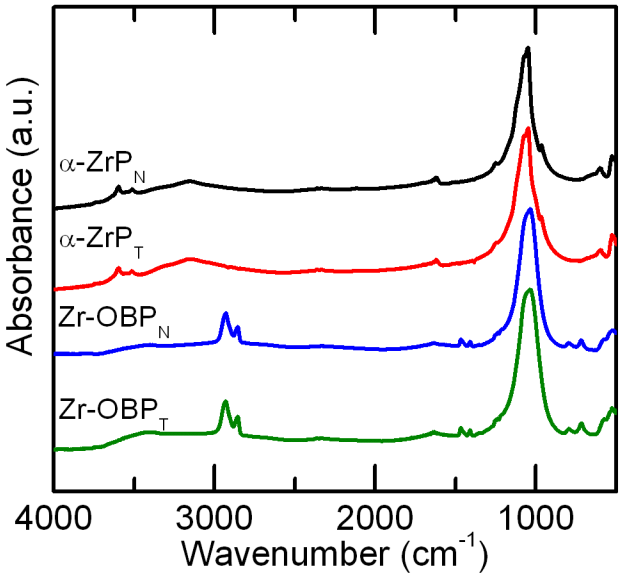

Figure 2-1. FTIR spectra of neat and treated α-ZrP and Zr-OBP. Absorbance signal was normalized to one. The peaks centered around 1000 cm^{-1} are attributed to phosphate/phosphonate stretching. CH stretching is observed in Zr-OBP just under 3000 cm^{-1}. Broad water stretching is observed 3500-3000 cm^{-1}. Additional interstitial water stretching is observed above 3500 cm^{-1} in α-ZrP.

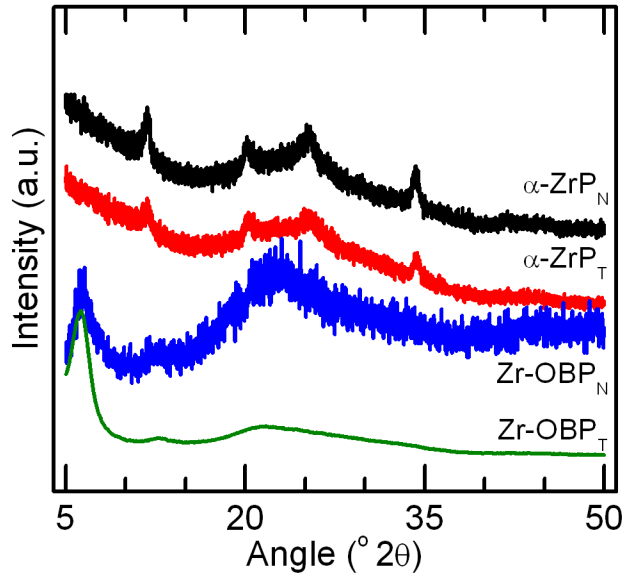

Figure 2-2. Powder XRD of neat and treated α-ZrP and Zr-OBP. We observe peaks in our α-ZrP diffraction that are consistent with published work. The diffraction for Zr-OBP shows only an ordered interlayer spacing al low angles indicating a large *d* spacing.

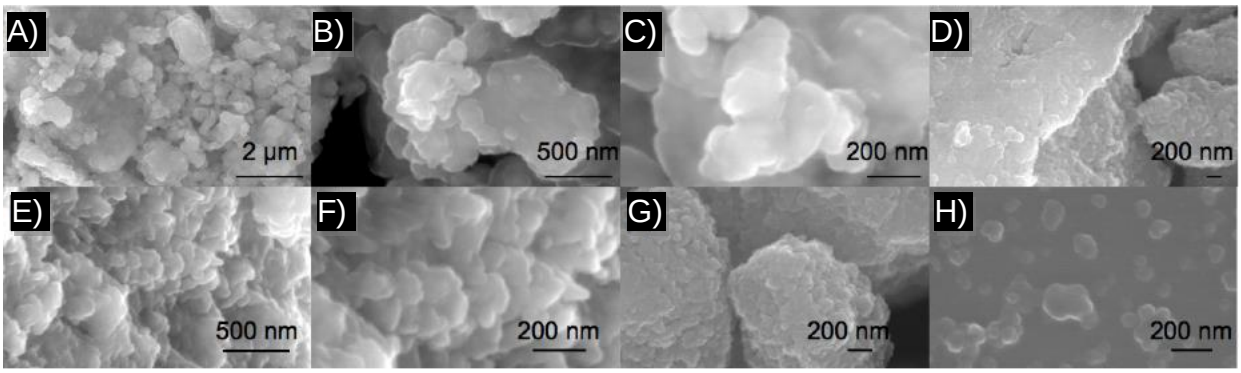

Figure 2-3. SEM of materials: A-C) treated α-ZrP, D) treated Zr-OBP, E-F) neat α-ZrP, and G-H) neat Zr-OBP.

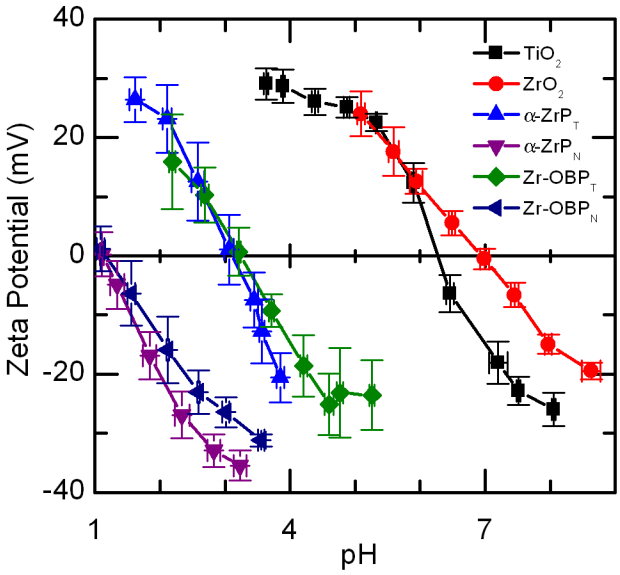

Figure 2-4. The ζ of the materials with respect to pH.

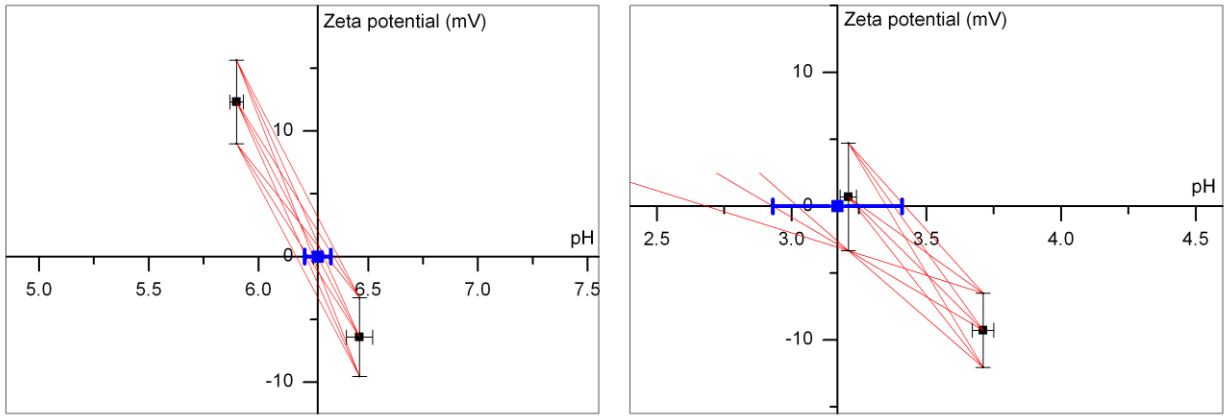

Figure 2-5. Our method for determining the IEP is illustrated. TiO_2 (left) and Zr-OBP_T (right) are shown as representative examples. Using the nearest data points with error on either side of 0 mV we draw nine lines between the points and the points ± the standard deviation. We calculate the average pH value of the nine points where these lines cross 0 mV. This mean ± the standard deviation is reported.

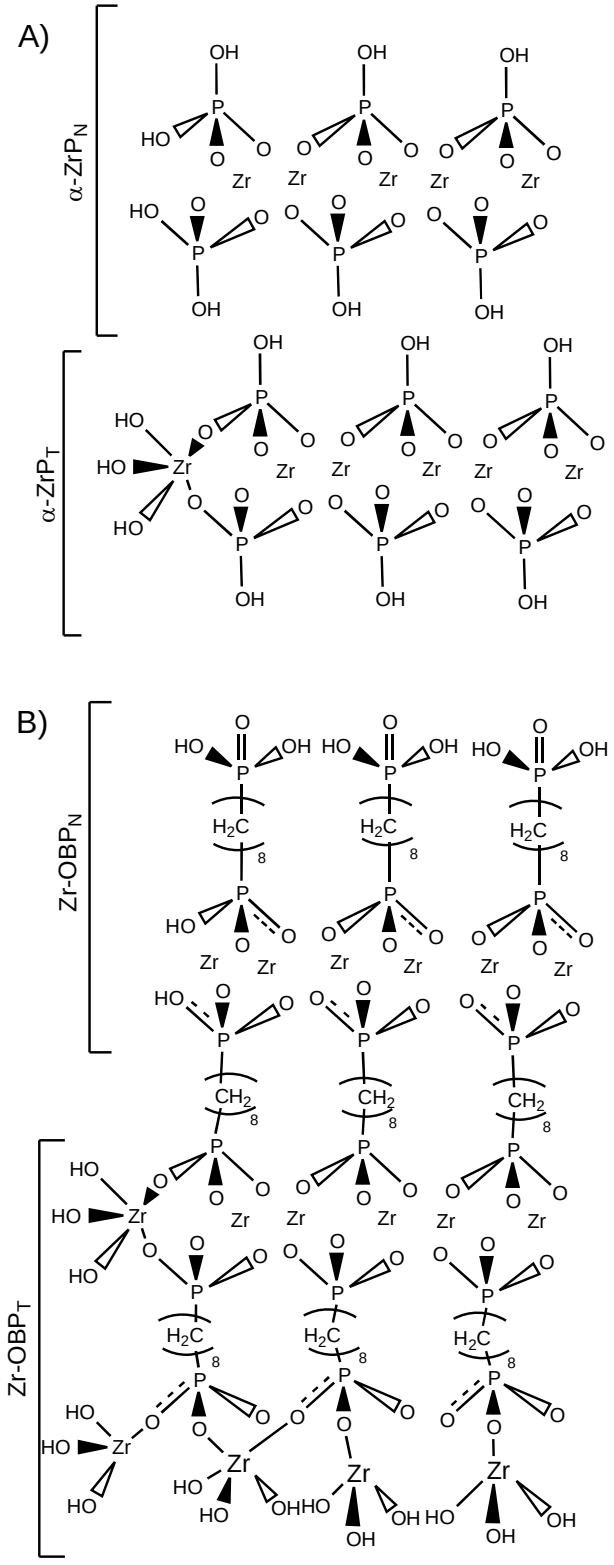

Figure 2-6. Schematic showing the hexagonal surface (top and bottom) and edge surface (left) for A) α-ZrP and B) Zr-OBP before and after treatment with excess Zr ions.

Table 2-1. The isoelectric point ± the standard deviation for phosphopeptide enrichment materials.

TiO_2	ZrO_2	α-ZrP_T	α-ZrP_N	Zr-OBP_T	Zr-OBP_N
6.3 ± 0.1	7.0 ± 0.1	3.1 ± 0.4	1.1 ± 0.3	3.2 ± 0.2	1.2 ± 0.3

CHAPTER 3
ADSORPTION STUDIES

Separation and Adsorption

Liquid chromatography is a long-standing technique invoked for the separation of components in solution. The essence of the technique is separating components of a mixture in space.[60, 61] A liquid chromatography separation can be divided into four processes: adsorption, washing, desorption, and regeneration.[27] Adsorption is the process of mixture components interacting with the separation medium. Washing is the process of removing unwanted components that have also bound to the material. Elution is the process of recovering the component of interest, and regeneration is the process of restoring the stationary phase to its original form for subsequent use.

In this work we have focused on developing two stationary phases, α-ZrP and Zr-OBP (described in Chapter 2), and we now present a study of the adsorption step of phosphopeptides and non-phosphopeptides onto these materials in comparison to a common phosphopeptide enrichment material TiO_2. Specifically, we will compare the binding capacity and binding efficiency for the adsorption of model peptides onto enrichment materials, and we will determine each material's selectivity of the phosphopeptide over the non-phosphopeptide. To this end, we have prepared adsorption isotherms for a variety of materials, peptides, and conditions. These factors of interest can be quantified by the parameters of fitting model equations to experimental data and subsequently comparing fitting parameters quantitatively. One of the most common models for adsorption is the Langmuir adsorption isotherm. The Langmuir model assumes monolayer coverage onto a homogeneous surface and provides parameters for binding efficiency and binding capacity.[62] Selectivity can be

defined in several ways. One option is the ratio of the initial slopes of the adsorption isotherm.[63, 64] Another option is a ratio of the distribution coefficients.[65] By calculating the selectivity quotient, we will have a semi-quantitative method to compare the abilities of these materials to preferentially bind phosphopeptides over non-phosphopeptides. This chapter will focus on the adsorption of two model peptides, one phosphopeptide and one non-phosphopeptide, onto three enrichment materials at different pH values in a buffered solution. By fitting the adsorption data with isotherm models, we will be able to compare properties that help to define the adsorption step in an enrichment system.

Using this data, we will consider the binding mechanisms that drive the adsorption of peptides onto each of the adsorbents. The binding mechanism that controls MOAC enrichment is debated. One possibility is that an electrostatic attraction exists between a positively charged metal oxide surface and a negatively charged phosphate.[40] Researchers have observed that lower pH, where TiO_2 is positively charged and competing carboxylates are neutralized, improves the results.[1] Another possibility is that a coordinate covalent bond is formed between the metal center and the phosphate; other researchers have observed a bidentate binding mode of phosphates to metal oxides.[41] We present MOAC enrichment with an electrostatic binding mechanism. Conversely, the binding mechanism that controls adsorption onto zirconium phosphate and zirconium phosphonate is unexplored. We present a coordinate covalent binding mechanism for the adsorption of phosphopeptide onto zirconium phosphate and zirconium phosphonate. The phosphate group of a phosphopeptide is capable of displacing weaker ligands around zirconium to coordinate with the metal center. The carboxylate group on competing acidic non-

phosphopeptides is unable to coordinate under the same conditions. This could lead to preferential binding of phosphopeptides over non-phosphopeptides in competitive binding situations such as those encountered in phosphopeptide enrichment experiments.

Experimental Section

Materials

α-ZrP and Zr-OBP were as described in Chapter 2; all work detailed in this chapter was done with the treated form of the adsorbents. TiO_2 was purchased from Aldrich. All other chemicals were purchased from Sigma or Fisher and used as received unless described otherwise. Water was purified to a resistivity of 17.2 MΩ·cm or greater using a Barnstead E-pure filtration system. A buffer capable of buffering the pH range 2.2-10.6 was prepared at 200 mM strength using a 200 mM concentration of each of the five following components: 2-(N-morpholino)ethanesulfonic acid sodium salt (MES), 2-amino-2-(hydroxymethyl)-1,3-propanediol (Tris base), glycine, acetic acid, and KCl. The buffer was adjusted to the desired pH using concentrated HCl or 10 M KOH.

Peptide Preparation

Phosphorylated delta sleep inducing peptide (pDSIP, sequence WAGGDA(pS)GE) and delta sleep inducing peptide (DSIP, sequence WAGGDASGE) were purchased from Mimotopes (Clayton, Victoria, Australia). Upon receipt of the lyophilized material, it was dissolved in 0.1% aqueous acetic acid and distributed into aliquots. Each aliquot contained 264 nmol of peptide in 11.2 µL of solution. The aliquots were frozen at -20 °C until use. Upon use, the aliquot was thawed and brought up to volume with the desired buffer. There was no detectable pH change from the original buffer solution to the buffer-peptide solution.

Peptide Adsorption

Adsorption onto TiO_2

The interaction of pDSIP with TiO_2 at pH 3.0 and at pH 4.5 was carried out in buffer using 1 mg of particles (Cahn C-33 microbalance) and an amount of peptide ranging from 4.6-77.4 nmol; a blank with an equivalent amount of particles and 0 nmol peptide and a five-point standard curve of peptide were run in parallel. Particles were suspended in 100 µL of buffer. A volume of peptide solution in buffer with the appropriate amount of peptide was added to the particle suspension. The total volume of the interaction was brought up to 200 µL using additional buffer as necessary. The interaction was mixed overnight at room temperature.

For the interaction of pDSIP with TiO_2 at pH 7.4, 5 mg of TiO_2 was used; for the interaction of DSIP with TiO_2 at pH 3.0, 1 mg of particles and an amount of peptide ranging from 9.3-77.4 nmol were used. All other conditions remained the same.

Adsorption onto α-ZrP

The interactions with α-ZrP were carried out in the same manner as described above for TiO_2 with the following differences: for pDSIP at pH 7.4, 10 mg of α-ZrP was used; for DSIP at pH 3.0, 10 mg of α-ZrP and a peptide range of 13.7 to 114.3 nmol was used. All other interaction conditions remained the same.

Adsorption onto Zr-OBP

The interaction of Zr-OBP with pDSIP consisted of 0.4 mg adsorbent and a peptide range of 6.8-114.3 nmol in pH 3.0 buffer. The interaction with DSIP consisted of 1.0 mg of particles and a peptide range of 9.3 to 77.4 nmol. All other conditions remained the same as those described above.

Peptide mass balance by UV absorbance spectroscopy

The interaction suspensions were centrifuged 5 min at 12k RPM on a Hermle microcentrifuge Z230MR equipped with a Hermle 220.59 VO4 rotor. One hundred microliters of the supernatant was transferred to a Corning UV-transparent 96-well microplate purchased from Fisher. The absorbance of the supernatant was measured over the range 200-500 nm using a Tecan Safire microplate spectrophotometer. The well volume of 100 µL equates to a path length of 2.8 mm. The absorbance value at 278 nm was attributed to peptide, and the absorbance at 500 nm was considered the background and was used for correcting baseline shifts. The amount of material in solution (C_e) was determined using a standard curve prepared separately for each experiment. The amount of material bound per mass of particles (q_e) was determined by mass balance (Equation 3-1) where C_i is the amount of peptide added in nmol and m is the mass of particles in mg.

$$q_e = \frac{C_i - C_e}{m} \tag{3-1}$$

Data was plotted as q_e with respect to C_e and was fit with the Langmuir adsorption isotherm (Equation 3-2) using Origin 8.5; q_e is the amount of peptide bound per mass of particles, C_e is proportional to the concentration in solution, Q_{max} is proportional to the adsorption capacity under the conditions, and K_L is the relative Langmuir equilibrium constant and represents binding efficiency.

$$q_e = \frac{Q_{\max} K_L C_e}{1 + K_L C_e} \tag{3-2}$$

Results

We studied the interaction of two model peptides pDSIP and DSIP with three adsorbents TiO_2, α-ZrP, and Zr-OBP. The data was fit with the Langmuir adsorption isotherm. Using the parameters of the Langmuir adsorption isotherm, we compare differences in adsorption as a result of peptide phosphorylation, adsorbent, and pH. We also attempted to fit the data with Freundlich adsorption isotherms; these fits were poorer than the Langmuir adsorption isotherm fits in all cases. Details on the Freundlich adsorption isotherm and the fitted data are available in Appendix B.

Adsorption onto TiO_2

TiO_2 is one of the most commonly used phosphopeptide enrichment materials. We have studied adsorption onto TiO_2 as a basis for comparison to alternative enrichment materials. Figure 3-1 shows mean data points fit with Langmuir adsorption isotherms for the interaction of pDSIP with TiO_2 from sets of data at pH values 3.0, 4.5, and 7.4. The isotherm at pH 3.0 shows a steep initial slope and approaches an asymptote near 40 nmol/mg. The parameters of the fit are shown in Table 3-1. The parameter K_L quantifies the steepness of the initial slope and relates to the binding efficiency the adsorbent has for the adsorbate. The Q_{max} value corresponds well to the asymptote we observe in the data plot. As we move to higher pH, we observe a decrease in the slope (Figure 3-1) and the corresponding K_L (Table 3-1). The results show that the binding of pDSIP onto TiO_2 is most favorable at pH 3.0.

We studied the binding of DSIP onto TiO_2 at pH 3.0 for comparison. Figure 3-2 shows the mean data points fit with the Langmuir adsorption isotherm. We observe a gradual slope, but we do not observe an asymptote. The parameters (Table 3-2) give a very small K_L value and a Q_{max} value with a large error. The size of the error is directly

related to the data not extending far enough to observe an asymptote. The results indicate the binding efficiency of DSIP onto TiO_2 at pH 3.0 is quite low and an adsorption maximum has not been satisfactorily defined.

We compare the binding onto TiO_2 at pH 3.0 of pDSIP versus DSIP. The binding efficiency parameter K_L is an order of magnitude larger for pDSIP than for DSIP indicating the binding of the phosphopeptide is significantly better, an important characteristic for a phosphopeptide enrichment material.

Adsorption onto α-ZrP

α-ZrP was recently reported as a phosphopeptide enrichment material.[16] We present a study focused on the adsorption step onto α-ZrP. Figure 3-3 shows mean data points fit with the Langmuir adsorption isotherm for the interaction of pDSIP with α-ZrP from sets of data at pH values 3.0, 4.5, and 7.4. We observe a moderate initial slope at pH 3.0 and an adsorption maximum above 30 nmol/mg. The initial slope and adsorption maximum decrease as the pH increases. The parameters (Table 3-1) quantify the same observations with the best binding efficiency and capacity values at pH 3.0 for the interaction of pDSIP with α-ZrP.

Figure 3-4 shows mean data points for the interaction of DSIP with α-ZrP at pH 3.0. We do not observe appreciable adsorption below 60 nmol, and the data cannot be fit with the Langmuir adsorption isotherm. The results indicate that the binding efficiency is very poor, and we cannot define and adsorption maximum. The non-phosphopeptide does not bind efficiently to α-ZrP at pH 3.0.

We also considered the binding of pDSIP and DSIP to α-ZrP at pH 2.0. Figure 3-5 shows this interaction. Compared to the results at pH 3.0, we observe an increase in the binding efficiency and capacity for pDSIP onto α-ZrP. The data for DSIP at pH 2.0

demonstrate minimal binding out to 80 nmol of peptide. The appreciable adsorption of pDSIP onto α-ZrP in combination with minimal adsorption of DSIP under the same conditions at both pH 3.0 and pH 2.0 have some interesting implications as we consider this adsorbent as a phosphopeptide enrichment material; these will be discussed in the discussion section below.

Adsorption onto Zr-OBP

We explored peptide adsorption onto the zirconium phosphonate Zr-OBP, a material with attributes similar to α-ZrP. Figure 3-6 shows the mean data points fit with the Langmuir adsorption isotherm for the interaction of pDSIP and DSIP with Zr-OBP at pH 3.0. For the interaction with pDSIP, we observe a steep initial slope corresponding to good binding efficiency and a high asymptote corresponding to a high binding capacity (Table 3-1). For the interaction with DSIP, we observe a more gradual initial slope and an asymptote indicating a binding capacity at about a third of the binding capacity of pDSIP onto the same material (Table 3-2). Collectively, the superior binding of pDSIP onto Zr-OBP compared to the binding of DSIP onto Zr-OBP indicate the material could serve as a phosphopeptide enrichment material; we will discuss this further below.

Discussion

We have prepared Langmuir adsorption isotherms when possible for the interaction of adsorbents TiO_2, α-ZrP, and Zr-OBP with the adsorbates pDSIP and DSIP, two model peptides. In order to compare and contrast these materials with one another we will use the parameters of the Langmuir adsorption isotherm of binding capacity (Q_{max}) and binding efficiency (K_L). We also define selectivity – the ability of an

adsorbent to bind the phosphopeptide over the non-phosphopeptide – as a means to compare the phosphopeptide enrichment capability of the adsorbents.

Binding Capacity

The binding capacity is a measure of how much adsorbate can bind to the adsorbent under the experimental conditions. It can be thought of as the number of binding sites for the adsorbate on the adsorbent, which is dependent on the environment. The binding constant is quantified by the parameter Q_{max} in the Langmuir adsorption isotherm. The parameters from the Langmuir adsorption isotherms for the adsorption of pDSIP are tabulated in Table 3-1. In all these cases, the highest binding capacity is observed at pH 3.0. We can compare the capacity graphically in Figure 3-7, which shows the fits for the data at pH 3.0 on a common scale. We observe the highest capacity with Zr-OBP; TiO_2 and α-ZrP have the same capacity within error. Interestingly, when we tested the adsorption of pDSIP onto α-ZrP at pH 2.0, the capacity increased (Figure 3-5).

We attribute the superior binding capacity of Zr-OBP to the surface chemistry of the material (Figure 2-6B). Theoretically, the surface of Zr-OBP consists completely of available Zr metal centers. Conversely, only a fraction of the surface of α-ZrP has Zr available and the remainder of the surface is comprised of the hydroxyl groups of phosphoric acid (Figure 2-6A). Additionally, the binding capacity is measured in nanomoles of peptide per milligram of adsorbent. We have the surface area of the particles (Chapter 2), and so we have estimated the binding capacity as nanomoles of peptide per square meter of adsorbent (Table 3-3). When we compare the binding capacity using the alternative units, Zr-OBP has approximately the same capacity as TiO_2. This suggests that the surface of both of these materials is fully available to bind

phosphopeptide where as only a fraction of the surface of α-ZrP is available. Thus, the apparent superiority for the binding capacity of Zr-OBP over TiO_2 is diminished when we consider the surface area of the materials. Additionally, our calculation suggests that the full surface area of α-ZrP is not accessible for binding phosphopeptide.

Binding Efficiency

The binding efficiency is a measure of how well the adsorbate binds to the adsorbent under the experimental conditions. It is quantified by the parameter K_L in the Langmuir adsorption isotherm. The parameters from the Langmuir adsorption isotherm for the adsorption of pDSIP are tabulated in Table 3-1. In all these cases, the most efficient binding is observed at pH 3.0. We can compare the efficiency graphically in Figure 3-7, which shows the fits for the data at pH 3.0 on a common scale. We observe the most efficient binding with Zr-OBP followed by TiO_2 and then α-ZrP. We attribute the superior efficiency of Zr-OBP to the availability of Zr metal centers over the entire surface of the material (Figure 2-6B). Conversely, TiO_2 does not offer free metal centers or Zr to bind phosphopeptides, and although α-ZrP has Zr metal centers available on the surface of the treated material, only a fraction of the surface has Zr available and the remainder of the surface is comprised of the hydroxyl groups of phosphoric acid (Figure 2-6A). A proposed binding mechanism and the related importance of Zr metal centers will be discussed below.

Interestingly, the efficiency for the binding of pDSIP onto α-ZrP at pH 2.0 increases above the efficiency of Zr-OBP at pH 3.0 (Figure 3-5). However, this data represents a single replicate, and we do not have comparable data for Zr-OBP at pH 2.0. Additional experiments for both zirconium-based materials should be done at or even below pH 2. Unfortunately, the buffering capacity of our buffer does not extend

below pH 2.2, and an alternative experimental system should be developed to explore these conditions further.

We also compare the binding efficiencies for the adsorbate DSIP; these Langmuir adsorption isotherm parameters are available in Table 3-2. We observe the same trend as with pDSIP – the highest efficiency for binding DSIP is seen with Zr-OBP followed by TiO_2 and then α-ZrP. Since we are considering these adsorbents as phosphopeptide enrichment materials and DSIP is a non-phosphopeptide, it would be ideal for the adsorbents to have a low efficiency for binding DSIP. In this respect, α-ZrP demonstrates the preferred binding efficiency toward DSIP.

Selectivity

An important characteristic of phosphopeptide enrichment materials is the ability to separate phosphopeptides from non-phosphopeptides. This can occur during the adsorption step if the adsorbent preferentially binds the phosphopeptide over the non-phosphopeptide; this is called selectivity. Selectivity can be defined in several ways.[63-65] Like Banerjee *et al.* and Liebl *et al.*, we use the initial slope of the adsorption isotherm, which is also the binding efficiency parameter K_L. We calculate the selectivity of a given adsorbent as the quotient the K_L for binding pDSIP over the K_L for binding DSIP. It is a ratio of the binding efficiencies for the phosphopeptide over the non-phosphopeptide.

We calculate the selectivity quotient for TiO_2 at 35 and for Zr-OBP at 6. The selectivity is ca. fivefold better for TiO_2 compared to Zr-OBP. This can be attributed to the more favorable binding of DSIP to Zr-OBP versus DSIP to TiO_2. Since we cannot use the Langmuir adsorption isotherm to fit the adsorption of DSIP onto α-ZrP, we cannot mathematically determine the selectivity for α-ZrP using K_L; this indicates the

selectivity is very good on this adsorbent, perhaps three or more orders of magnitude better than either TiO_2 or Zr-OBP. We attribute the exceptional selectivity of α-ZrP to the surface chemistry of the material. Although the surface chemistry of Zr-OBP is similar to α-ZrP, the selectivity is not comparable. This is likely related to significantly more surface area available for binding on Zr-OBP that led to more binding of DSIP. In this sense, perhaps binding capacity and selectivity are opposing characteristics. In order to better understand our selectivity observations and to increase the relevancy for phosphopeptide enrichment materials, it would be necessary to attempt competitive enrichment experiments where both phosphopeptides and non-phosphopeptides are exposed to the material simultaneously. However, based on our observations in this work, α-ZrP has the best selectivity; this could be an indication that it would outperform TiO_2 and Zr-OBP in phosphopeptide enrichment.

Binding Mechanisms

To explore potential binding mechanisms with the experimental methods and data we have presented here, we approach the discussion from a standpoint of considering the feasibility of an electrostatic adsorption mechanism. To begin, we must first establish an estimate of the peptide charge across a range of pH. We already have an estimate of the particle charge across a broad pH range (chapter2). The IEP of a peptide (pI) and charge state of a peptide across a range of pH can be estimated with readily available online calculators. However, these calculators do not account for the acidic nature of phosphate groups. Gauci *et al.* developed a java script that calculates the pI of modified peptides,[66] but this provides only a pI and no graphical representation of the charge across a pH range. Therefore, a simple Matlab script was kindly developed by Zheng, Z. to display the predicted charge of phosphopeptide across a

range of pH.[67] All peptide charge calculators are limited by the accuracy of the pK_a values input and in the assumption that the pK_a for any group is independent of the surrounding environment. Therefore, these calculators are especially weak for short sequences and outside the pH range of 4-8.[68] Nonetheless, the developed calculator provides an estimation of the peptide charge for DSIP and pDSIP, shown overlaid with the ζ titrations for the enrichment materials (Figure 3-8). The pI of DSIP is estimated to be 3.0; and the pI for pDSIP is estimated to be 2.1.

Given this information, we consider the adsorption isotherms and adsorption parameters as a function of pH in order to assess the possibility of an electrostatically driven binding mechanism. A summary of the peptide charges or adsorbent ζ at the pH conditions tested is available in Table 3-4. At pH 7.4 all peptides and particles are negatively charged. We do not observe any appreciable pDSIP adsorption under these conditions, and we can attribute this to electrostatic repulsion between peptide and particle surface or the unavailability of binding sites due to charge states. At pH 4.5, TiO_2 is positively charged, α-ZrP is negatively charged, and pDSIP is negatively charged. We see appreciable adsorption of pDSIP onto TiO_2 and onto α-ZrP. For TiO_2, this observation supports the theory of electrostatic attraction between peptide and surface, however for α-ZrP electrostatic attraction does not seem plausible given that both peptide and surface are likely to be negative. At pH 3.0 TiO_2 and α-ZrP are positively charged, pDSIP is negatively charged, and DSIP is at its estimated pI indicating charge balance rather than a lack of charge. With TiO_2 at pH 3.0, we observe increased binding efficiency, capacity, and favorability for the adsorption of pDSIP compared to pH 4.5. We observe less favorable adsorption of DSIP compared to

pDSIP under these conditions. This further supports the theory of electrostatic interaction. With α-ZrP at pH 3.0, we observe favorable binding of pDSIP and unfavorable binding of DSIP. If we consider only the pH 3.0 data with the modeled charges of the peptides and what we know about the surface of α-ZrP, the interaction at pH 3.0 could be electrostatic. However, it is unreasonable to suspect a different mechanism is in control based only on a shift in pH, and the data at pH 4.5 does not support an electrostatic mechanism. At pH 2.0 α-ZrP is positively charged, DSIP is positively charged, and pDSIP is near but below its pI and thus might also have a positive charge. We see improved adsorption parameters for pDSIP compared to pH 3.0 and worsened adsorption parameter for DSIP. Like the data at pH 4.5, the data at pH 2.0 for α-ZrP and pDSIP further refutes the idea of electrostatic interaction controlling the binding mechanism. The decrease in adsorption for DSIP could be attributed to electrostatic repulsion, which could further contribute to an underlying mechanism that prevents DSIP adsorption onto α-ZrP.

Our data supports the theory of an electrostatic binding mechanism onto TiO_2 as evident by binding between the positively charged surface and negatively charged peptides. Additional studies with TiO_2 at pH 2.5 where DSIP is positively charged and pDSIP is negatively charged and at pH 1.0 where pDSIP is also positively charged would provide more complete insight regarding the electrostatic binding mechanism. However, as mentioned previously, the limit of the buffering range for our buffer is pH 2.2, and an alternative system must be developed in order to run these experiments.

Unlike with TiO_2, our data does not support an electrostatic binding mechanism onto α-ZrP. At pH 4.5, both pDSIP and α-ZrP are negatively charged yet we observe

binding. Again at pH 2.0, both pDSIP and α-ZrP are positively charged, and we also observe binding. Again, future study of DSIP binding at pH 4.5 and pDSIP binding at pH 1.0 would be instructive in further supporting or refuting this theory.

As an alternative to electrostatic binding, we propose a coordinate covalent interaction is the primary binding mechanism whereby the phosphate groups of phosphopeptides are able to displace weaker ligands and coordinate to available Zr sites on the surface of α-ZrP (Figure 1-1F). Conversely, carboxylate groups of non-phosphopeptides are not strong enough to displace the ligands on Zr resulting in the unfavorable adsorption mechanism we observe. This mechanism explains the exceptional selectivity we observe with α-ZrP.

Based on the limited data we have for Zr-OBP, we cannot make an accurate assessment of the binding mechanism that controls peptide adsorption. Based on the similar surface chemistry for α-ZrP and Zr-OBP discussed in previous chapters, we would expect similar mechanisms for both of these materials. However we see a surprising amount of DSIP adsorption onto Zr-OBP, which could be related to the increased surface area on Zr-OBP. More experiments at different pH would help us understand the mechanism of adsorption onto Zr-OBP.

Summary

We have demonstrated a new potential phosphopeptide enrichment material in particulate Zr-OBP and compared it to α-ZrP and TiO_2. The Q_{max} (nmol/mg) for Zr-OBP far exceeds those for the other materials we tested, but when considered in the unit nmol/m^2, the adsorption capacity of Zr-OBP is comparable to that for TiO_2. The selectivity for Zr-OBP at pH 3 is close to that of TiO_2, but it could be improved by exploring conditions with lower pH.

Our findings support the theory of electrostatic interaction of peptides with the surface of TiO2, and they suggest an alternative mechanism is involved in the binding of peptides to α-ZrP. The unfavorable binding observed for the interaction of DSIP with α-ZrP results in excellent selectivity at pH 3.0 and pH 2.0. We attribute this to a coordinate covalent binding mechanism where only phosphate groups, and not carboxylate groups, are basic enough to displace the ligands around Zr. Additional adsorption isotherm work is required to strengthen this theory, and isothermal titration calorimetry would further support it. We expect the surface chemistry of Zr-OBP to mimic that of the Zr sites on α-ZrP, and with this relationship, we also expect a similar binding mechanism for phosphopeptides. With refinement of synthetic conditions and exploration of alternative phosphonic acids, we may be able to pair the full surface availability of Zr-OBP with the selectivity of α-ZrP.

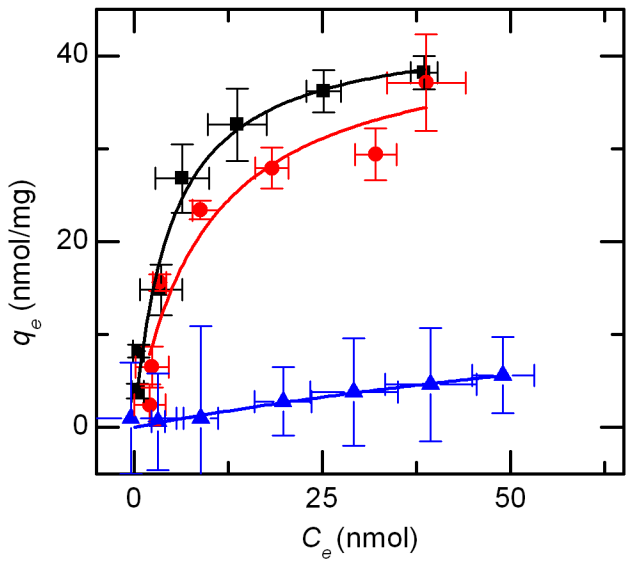

Figure 3-1. Langmuir adsorption isotherms for the interaction of pDSIP with TiO_2 at pH 3.0 (black), pH 4.5 (red), and pH 7.4 (blue). Error bars represent ± the standard deviation for n = 3 sets.

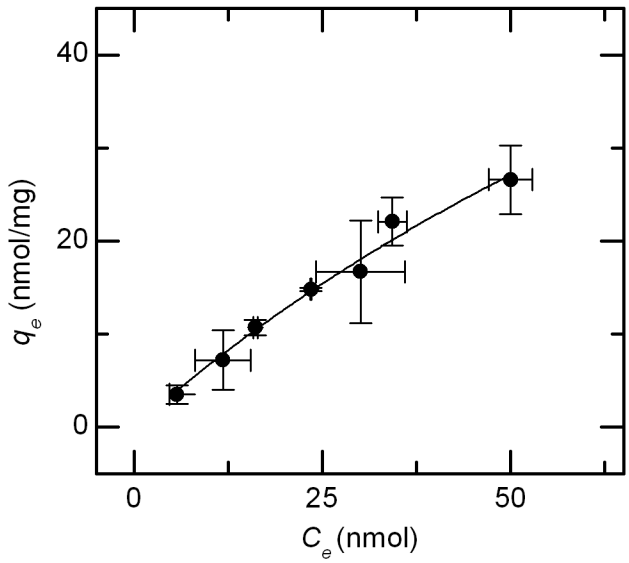

Figure 3-2. Langmuir adsorption isotherm for the interaction of DSIP with TiO_2 at pH 3.0. Error bars represent ± the standard deviation for n = 2 sets.

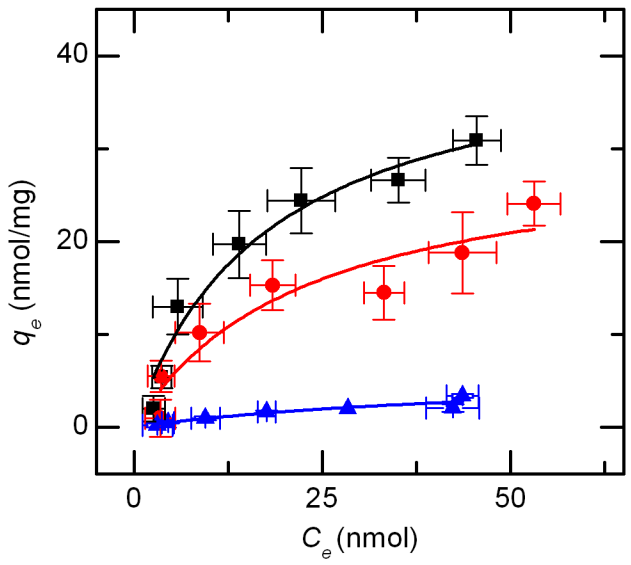

Figure 3-3. Langmuir adsorption isotherms for the interaction of pDSIP with α-ZrP at pH 3.0 (black), pH 4.5 (red), and pH 7.4 (blue). Error bars represent ± the standard deviation from n=2 to n=5 sets.

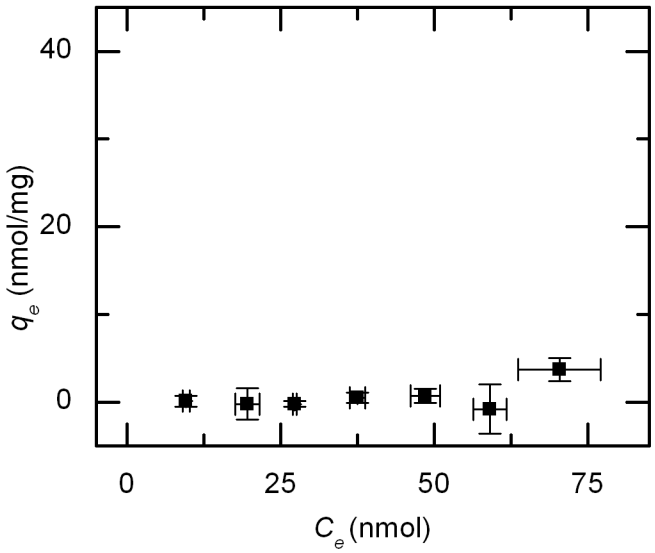

Figure 3-4. Adsorption isotherm for the interaction of DSIP with α-ZrP at pH 3.0. The data cannot be fit with the Langmuir isotherm. Error bars represent ± the standard deviation for n = 4 sets.

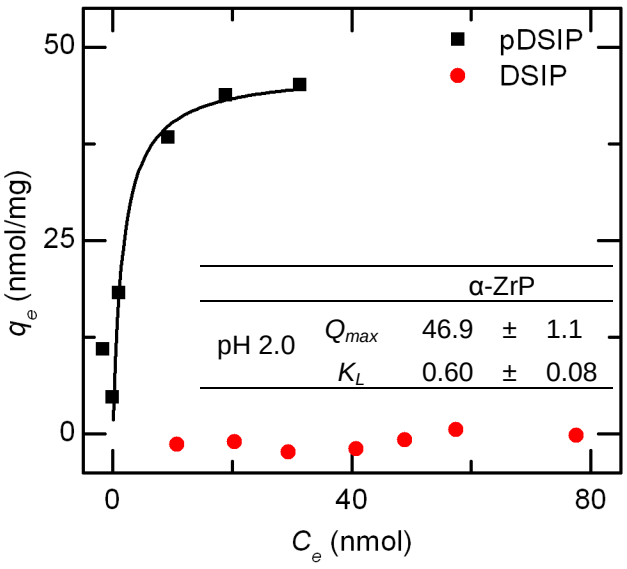

Figure 3-5. Adsorption isotherm for the interaction of pDSIP and DSIP with α-ZrP at pH 2.0 shown with overlaid Langmuir fitting curve for pDSIP. The inset shows the Langmuir equation parameters Q_{max} (nmol/mg) and K_L (nmol^{-1}).

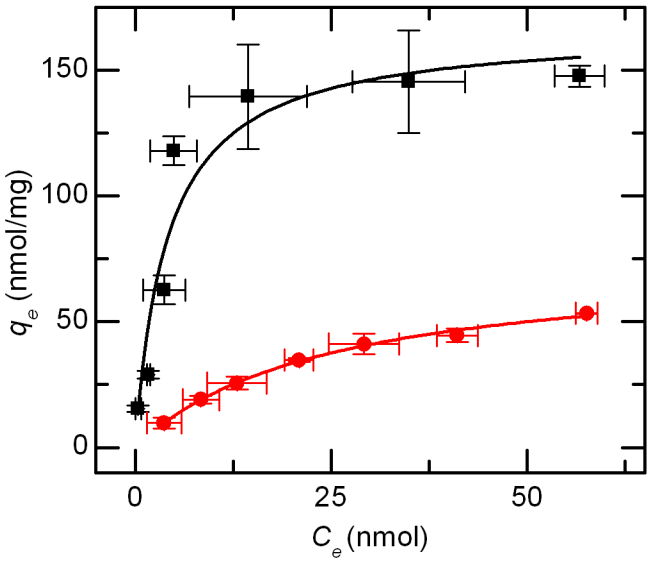

Figure 3-6. Langmuir adsorption isotherms for the interaction of pDSIP (black) and DSIP (red) with Zr-OBP at pH 3.0.

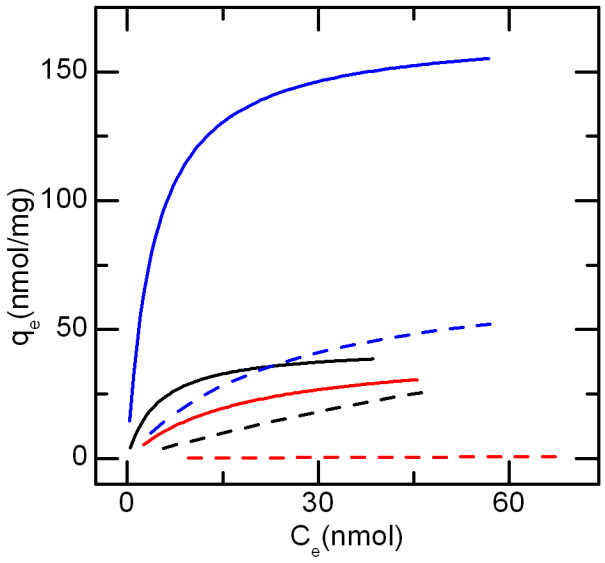

Figure 3-7. A comparison of the Langmuir adsorption isotherms for the adsorbents TiO_2 (black), α-ZrP (red), and Zr-OBP (blue) with the adsorbates pDSIP (solid) and DSIP (dashed) in pH 3.0 buffer. Note that for DSIP onto α-ZrP the fit shown is not a Langmuir adsorption isotherm but rather a linear fit through the origin and the data points.

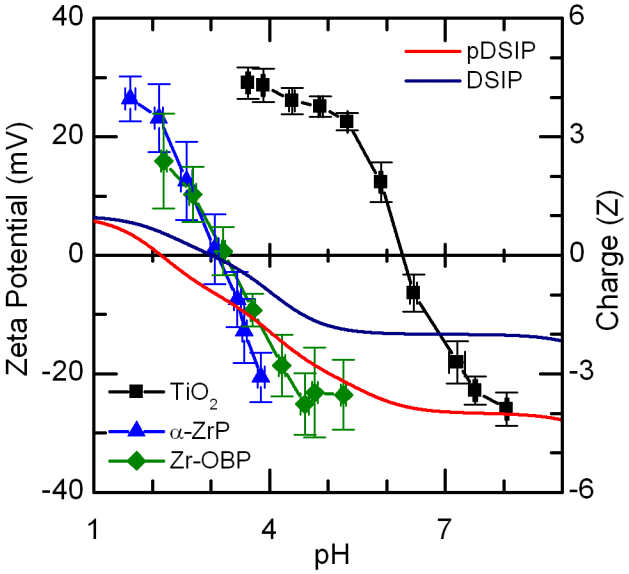

Figure 3-8. The modeled peptide charge as a function of pH (right axis) is shown overlaid with the ζ titrations of the adsorbents (left axis). The ζ data were described in Chapter 2.

.

Table 3-1. The Q_{max} (nmol/mg) and K_L ($nmol^{-1}$) values of the Langmuir fits ± the standard error for the interaction of pDSIP with TiO_2, α-ZrP, and Zr-OBP.

		TiO_2	α-ZrP	Zr-OBP
pH 3.0	Q_{max}	43 ± 3	42 ± 6	167 ± 16
	K_L	0.21 ± 0.05	0.06 ± 0.02	0.24 ± 0.08
pH 4.5	Q_{max}	43 ± 6	30 ± 7	not tested
	K_L	0.11 ± 0.04	0.04 ± 0.02	
pH 7.4	Q_{max}	22 ± 7	6 ± 3	
	K_L	7E-3 ± 3E-3	0.02 ± 0.02	

Table 3-2. The Q_{max} (nmol/mg) and K_L ($nmol^{-1}$) values of the Langmuir fits ± the standard error for the interaction of DSIP with TiO_2 and Zr-OBP. The interaction of DSIP with α-ZrP cannot be fit with the Langmuir adsorption isotherm.

		TiO_2	α-ZrP	Zr-OBP
pH 3.0	Q_{max}	113 ± 47	undefined	75 ± 3
	K_L	6E-3 ± 3E-3	undefined	4.1E-2 ± 4E-3

Table 3-3. Binding capacity considered by mass and by surface area for pDSIP at pH 3.0 onto the materials.

	Q_{max} (nmol/mg)	Surface area (m^2/g)	Q_{max} ($nmol/m^2$)
TiO_2	43	45-55	782-956
α-ZrP	42	86	490
Zr-OBP	167	182	918

Table 3-4. Estimations of the charge for peptides or the sign of ζ for particles at the pH values considered in the work.

	2.0	3.0	4.5	7.4
pDSIP	+	-	-	-
DSIP	+	0	-	-
TiO_2	+	+	+	-
α-ZrP	+	+	-	-
Zr-OBP	+	+	-	-

CHAPTER 4
EXPLORATORY WORK INTO DESORPTION AND ENRICHMENT

Overview

Two characteristics are essential to phosphopeptide enrichment: good separation of phosphopeptides from non-phosphopeptides and the ability to recover phosphopeptides for further analysis. Enrichment can be related to chromatography, which consists of four steps: adsorption, washing, desorption, and regeneration.[27] Adsorption was covered extensively in Chapter 3. Washing is the desorption process of non-specifically bound non-phosphopeptides. Desorption, in order to disambiguate, will be referred to hereafter as elution. Elution is the desorption process of specifically bound phosphopeptides. Regeneration is the process by which the adsorbent is returned to its original state so that it can be used again.

The work in the previous chapter demonstrated the adsorption step for phosphopeptides and non-phosphopeptides onto TiO_2, α-ZrP, and Zr-OBP, but adsorption alone does not equate to enrichment. In this chapter we will demonstrate mock enrichment as we show in sequence the adsorption and desorption of pure model peptides. We will also demonstrate a simple enrichment scenario using an enzymatically digested phosphoprotein β-casein.

Experimental Section

All materials and instruments are the same as mentioned previously. Additionally, Trizma buffer was purchased from Sigma-Aldrich while trifluoroacetic acid (TFA) and ammonium bicarbonate (ABC) were purchased from Fisher.

Mock Enrichment on α-ZrP

Determining the limit of mass dependence

Treated α-ZrP (α-ZrP_T) was prepared and characterized as described in Chapter 2. Amounts of α-ZrP_T ranging from 0.1-18 mg were mixed overnight at room temperature with 26.4 nmol of peptide in buffer at pH values 3.0, 4.5, and 7.4. The suspensions were centrifuged. The amount of peptide in solution was determined by UV absorbance spectroscopy in comparison to a standard control.

Testing enrichment independent of adsorbent mass

Peptide solutions were reconstituted from frozen aliquots containing 264 nmol of peptide to a final volume of 1000 µL using buffer at the desired pH. α-ZrP_T particles (2.0-2.2 mg) were suspended in 100 µL buffer. Interactions at pH 3.0, 4.5 and 7.4 were carried out in quadruplicate by adding 26.4 nmol of peptide in solution to the particle suspensions and mixing overnight at room temperature. The suspensions were centrifuged, and the supernatant was retained for analysis.

The particles were washed with 200 µL of 0.01% TFA for 4 h at room temperature with mixing. The suspensions were centrifuged, and the supernatant was retained for analysis. The particles were washed a second time with 200 µL of 1% TFA for 2 h at room temperature with mixing. The suspensions were centrifuged, and the supernatant was retained for analysis.

Peptide remaining on the particles was eluted with 200 µL of 300 mM ABC overnight at room temperature with mixing. The suspensions were centrifuged, and the supernatant was retained for analysis.

At pH 3.0 and 7.4, a similar experiment was carried out using 19.8-20.0 mg of α-ZrP_T. A second elution step was done with 200 µL of 300 mM ABC mixed overnight at room temperature. All other conditions remained the same.

Positive controls were prepared in duplicate with 26.4 nmol of peptide and 0 mg of α-ZrP_T. Negative controls were prepared in quadruplicate with 2.0-2.2 mg or 19.8-20.0 mg α-ZrP_T and 0 nmol peptide with 200 µL of buffer. Negative controls were handled identically to the experimental samples.

The amount of peptide in the supernatant of each fraction in comparison to the positive controls was determined by UV absorbance at 278 nm using 100 µL of sample, a Tecan Safire microplate spectrophotometer, and Corning UV-transparent 96-well microplates (Fisher).

Mock Enrichment on Titania

The limit of mass dependence with TiO_2 was carried out as reported above for α-ZrP_T. The enrichment independent of adsorbent mass with TiO_2 was carried out identically to α-ZrP_T except only pH 3.0 was considered.

Mass Spectrometry after Mock Enrichment

α-ZrP_T and Zr-OBP_T particles were suspended 5 mg/mL in aqueous solution of 0.1% formic acid and 0.01% TFA. From this suspension, 100 µL containing approximately 0.5 mg of particles was combined with 26.6 nmol peptide in 100 µL 10 mM Trizma buffer with 100 mM NaCl adjusted to pH 3.0. The remainder of the model enrichment remained the same as described above with the exception that only the first wash was performed.

MALDI-TOF mass spectra were obtained using an AB Sciex TOF/TOF 5800 (Framingham, MA) in reflection mode. Data were acquired from 600-1500 m/z. Spectra

of model peptides pDSIP (929.3 m/z) and DSIP (849.3 m/z) were sought by combining the supernatant of fractions with matrix α-cyano-4-hydroxycinnamic acid (Sigma-Aldrich) and spotting the mixture on a MALDI plate.

Enrichment and Mass Spectrometry of β-Casein Digest

The enzymatic digest of β-casein (Sigma-Aldrich) using trypsin (Sigma-Aldrich), the preparatory washing of α-ZrP_T, and the enrichment procedure followed published protocol.[16] MS analysis was competed as described above except that the data range was expanded to 600-4000 m/z.

Results and Discussion

The enrichment capability of α-ZrP_T and TiO_2 are explored beyond the adsorption step as we consider the desorption of non-phosphopeptides during the wash steps and the desorption of phosphopeptides during the elution step. First, we must ensure sample-to-sample variation in the mass of adsorbent does not affect the results.

Mass Independence

In Figure 4-1 we show the plot of peptide in solution as a function of the mass of α-ZrP_T in the sample. A value of 100% represents 26.4 nmol of peptide. When an increase in mass no longer results in a decrease of peptide in solution, mass independence has been achieved. Mass independence for the binding of pDSIP was found with approximately 2 mg of α-ZrP_T at pH 3.0 and 6 mg at pH 4.5. We estimate 20 mg would be necessary at pH 7.4 based on the data available at 18 mg. At pH 3.0, relatively little DSIP bound with mass independence occurring at or below the lowest mass tested, 0.5 mg. At pH 4.5 and pH 7.4, the data were more scattered, and we could not determine the point where mass independence is achieved. These results are summarized in Table 4-1. We chose to conserve adsorbent and proceed with additional

studies knowing that mass dependence could contribute to error in the data. For the same reason we chose to use 2 mg of adsorbent at both pH 3.0 and pH 4.5 in subsequent studies. Twenty milligrams of adsorbent was necessary at pH 7.4.

In Figure 4-2 we show the plot of peptide in solution as a function of the mass of TiO_2 in the sample. At pH 3.0 and pH 4.5, mass independence for the binding of pDSIP was achieved with as little as 1-2 mg of TiO_2; at pH 7.4, 4 mg or more was necessary. For DSIP, at pH 3.0 approximately 4 mg or more of TiO_2 was necessary to achieve mass independence; at pH 4.5, 10 mg is necessary. We observe only minimal DSIP binding at pH 7.4, but mass independence may be occurring with as little as 2 mg of TiO_2. These results are summarized in Table 4-1. Since the goal of subsequent work was to maximize pDSIP adsorption while minimizing DSIP adsorption 2 mg was chosen as the constant mass for further pH 3.0 and pH 4.5 studies, and 10 mg was chosen as the constant mass for further pH 7.4 studies. Unfortunately, further studies at pH 4.5 and pH 7.4 were never realized due to unmitigated problems with the pH 3.0 work (see below).

Mock Enrichment with UV Detection

α-ZrP_T as the adsorbent

Using the known points of mass independence, we conducted a focused study of the four-step mock enrichment on α-ZrP. Figure 4-3 shows the percentage of peptide in the supernatant of each fraction after the adsorption, wash, and desorption steps for the interaction of pDSIP with ca. 2 mg of α-ZrP_T. At pH 3.0 and pH 4.5 we observe near complete adsorption of the peptide. At pH 7.4, a large amount of peptide remains in the supernatant after the adsorption step. This can be attributed to insufficient mass of material (Figure 4-1). In the wash steps, minimal amount of pDSIP is removed from the

particles and present in the supernatant. In the elution step, more than 50% of the peptide adsorbed under pH 3.0 or pH 4.5 conditions is recovered from the particles. We do not observe pDSIP in the elution step of the pH 7.4 adsorption sequence because the majority of peptide did not bind initially. Furthermore, it appears that if pDSIP bound at pH 7.4 is removed in the first wash. The results indicate that under pH 3.0 and pH 4.5 adsorption conditions, pDSIP adsorbs onto α-ZrP_T, remains bound during the wash steps, and is recovered in the elution step.

Using the same mass of particles, we tested the adsorption/desorption of DSIP with α-ZrP_T under the same conditions. Figure 4-4 shows the percentage of peptide in supernatant of each fraction. At all adsorption pH conditions tested, DSIP remains in the supernatant after the adsorption step. If any, only a minimal amount of peptide is observed in the subsequent steps. The results indicate that DSIP does not adsorb onto α-ZrP_T.

Collectively, the results in Figures 4-3 and 4-4 suggest that α-ZrP_T could be a good phosphopeptide enrichment material. We note the recovery of phosphopeptide in the elution step as a demonstration of this critical aspect of an enrichment material. While these results do not demonstrate the separation of phosphopeptides from non-phosphopeptides under competitive binding conditions, we can infer from the results that α-ZrP_T would be able to selectively bind phosphopeptide over non-phosphopeptide under such conditions. Further work under competitive binding conditions should be done, but the results here indicate that α-ZrP_T will likely be able to separate phosphopeptides from non-phosphopeptides during the adsorption step and

phosphopeptides would be recovered during the elution step. This makes α-ZrP_T a good adsorbent option for phosphopeptide enrichment work.

Additional amount of α-ZrP_T as the adsorbent

The earlier mass independence results (Figure 4-1) indicate that more α-ZrP_T is required for complete adsorption of pDSIP under pH 7.4 conditions. We completed a four-step mock enrichment experiment similar to the one described above with 20 mg of α-ZrP_T under pH 3.0 and pH 7.4 adsorption conditions (Figure 4-5). We observe near complete adsorption of pDSIP at both pH 3.0 and pH 7.4. A negligible amount of pDSIP is observed in either wash step. The first elution does not result in the desorption of pDSIP, however we observe ca. 50% of the pDSIP in the second elution of the pH 3.0 adsorption sequence and ca. 75% of the pDSIP in the second elution of the pH 7.4 adsorption sequence.

We were intrigued by the lack of peptide recovery after the first elution. When we tested the pH of the elution supernatant, the pH was neutral. We attribute this to residual 1% TFA after the second wash. The amount of residual solution was higher in this experiment than in previous experiments because the increased mass, and therefore volume, of particles trapped more residual solution than the lower mass experiment. Thus, we found it necessary to perform a second elution, and we chose 1 M KOH. After the second elution, the pH of the supernatant was at the expected pH 10, and we were able to recover an appreciable amount of pDSIP. The results indicate that with an increased mass of the adsorbent α-ZrP_T, phosphopeptide can be adsorbed at pH 7.4 and recovered during a subsequent elution step.

Using 20 mg of α-ZrP_T, we tested the adsorption/desorption of DSIP with the adsorbent under pH 3.0 and pH 7.4 conditions. Figure 4-6 shows the percentage of

peptide in the supernatant of each fraction. We observe ca. 60% of the DSIP in the pH 3.0 adsorption supernatant and ca. 80% of the DSIP in the pH 7.4 supernatant after adsorption. A negligible amount of peptide is observed in either wash step, and within the projected error of the results (± 20%), no peptide signal is observed in the elution steps.

The results indicate that an increase in mass of adsorbent results in an increase in the binding of the non-phosphopeptide. The binding of the non-phosphopeptide appears to be favored at the lower pH value. This indicates binding is more favorable at pH 3.0 than at pH 7.4. The relative lack of peptide signal in the subsequent steps could indicate that the DSIP that does bind to the adsorbent is not being removed. However, it seems more reasonable to conclude that the conditions of the wash and elution steps have not been optimized for the experimental setup. Additionally, the negative controls appear to be inappropriate for the system which is causing significant negative signal in the elution signals. We can conclude that DSIP will bind to α-ZrP_T under these conditions, but the wash and elution steps need to be further explored.

Combined, the results in Figures 4-5 and 4-6 show α-ZrP_T will readily bind pDSIP to a greater extent than it will bind DSIP. If competitive binding were attempted, the results suggest that α-ZrP_T will bind pDSIP preferentially over DSIP, a characteristic referred to as selectivity.

If we compare these results to those with one tenth of the adsorbent (Figures 4-3 and 4-4), we see complete adsorption of pDSIP at pH 3.0 with both masses of adsorbent. We observe complete adsorption of pDSIP at pH 7.4 only with 20 mg of adsorbent, which is consistent with the mass independence results (Figure 4-1). The

binding of DSIP increases with increased mass of adsorbent at both pH values tested. Collectively, the results suggest that increased mass could reduce the selectivity under competitive binding scenarios. This could be mitigated by carefully selecting the mass of adsorbent or by improving the desorption of non-phosphopeptide during the wash step prior to the desorption of phosphopeptide during the elution step. Overall, increased mass of α-ZrP_T led to complete adsorption of phosphopeptide at pH 7.4 while maintaining some selectivity for the phosphopeptide over the non-phosphopeptide.

TiO_2 as the adsorbent

We attempted similar four-step mock enrichment experiments on the well-documented MOAC enrichment material TiO_2 for use as a comparison to α-ZrP_T. Figure 4-7 shows the percentage of peptide in the supernatant of each fraction for the interaction of pDSIP with TiO_2 after adsorption in pH 3.0 buffer. We observe minimal peptide in the supernatant after the adsorption step and both wash steps. There is a large amount of error in the first wash step, which we attribute to the increased presence of particles in the microplate wells during the UV absorbance measurement. During the elution, ca. 25% of pDSIP is recovered. Between all four steps we observe only ca. 40% of the expected 100% of peptide signal. This indicates that either pDSIP remains on TiO_2 after all four steps or that the detection of the peptide during the steps shown by this UV absorbance method is inadequate. Overall, the relative amount of peptide signal in each step is in line with our expectations in that the only appreciable signal from pDSIP is in the elution step. The low percentage of peptide recovered in the elution step must me addressed further and will be discussed further below.

We also tested the adsorption/desorption of DSIP on TiO_2 at pH 3.0. Figure 4-8 shows the percentage of peptide in the supernatant of each fraction. We observe 25%

of the peptide in the supernatant after the adsorption step. In the following steps, we do not observe any appreciable amount of peptide in the supernatant. As we saw for the interaction of pDSIP with TiO_2 (Figure 4-7), the majority of the DSIP is not accounted for, which again suggests that either the DSIP remains on the TiO_2 after all four steps or the detection of the peptide during the steps by this UV absorbance method is inadequate. Since we are using a well-documented phosphopeptide enrichment material, it seems unlikely that both pDSIP and DSIP remain on the adsorbent after the wash and elution steps. We conclude that the detection method we have used is inadequate for studying the full interaction on TiO_2 even though the same method appears effective for the same study on α-ZrP_T. The results on TiO_2 (Figures 4-7 and 4-8) show the expected relative presence of peptide (DSIP in the unbound, pDSIP in the elution), but not at the expected percentages. For this reason, we did not pursue similar studies at pH 4.5 or pH 7.4. Instead, we shifted our focus to the adsorption step (Chapter 3).

Mock Enrichment with MS Detection

Mass spectrometry (MS) is a very common method of analysis for phosphopeptides after enrichment. As such, we wanted to demonstrate MS analysis of the model peptides after adsorption and elution in similar mock enrichment studies as those described above.

MALDI-TOF MS after mock enrichment on α-ZrP

Figure 4-9 shows the MALDI-TOF spectrum of the supernatant after the adsorption of pDSIP onto α-ZrPT. We observe $[M+H]^+$ and $[M+Na]^+$ peaks indicating pDSIP is still present in the supernatant after the adsorption step. Corresponding UV absorbance of the same supernatant indicates ca. 5% of the peptide remains in the

supernatant (data not shown). The interaction took place in 10 mM Trizma buffer with 100 mM NaCl and adjusted to pH 3 before use. It was later determined that the buffer was ineffective at this pH and that the α-ZrP_T pulled the pH of the solution down to ca. pH 2.7. The presence of pDSIP in the unbound fraction does not indicate that adsorption has not occurred but rather suggests that some peptide is still present in the supernatant after the adsorption step.

Figure 4-10 shows the MALDI-TOF spectrum after the elution of pDSIP from α-ZrP_T using 300 mM ABC following the adsorption described above. The dominant peaks in the spectrum are attributed to the molecular ion peak or the sodium or potassium adducts. The results indicate that we are able to elute pDSIP from α-ZrP_T after the binding and washing steps. Thus, the results suggest that α-ZrP_T could serve as a phosphopeptide enrichment material and confirm the signal observed in the elution by UV absorbance (Figure 4-3) is rightly attributed to pDSIP.

MALDI-TOF MS after mock enrichment on Zr-OBP

We completed a mock enrichment using the adsorbent Zr-OBP_T instead of α-ZrP_T; all other conditions remained the same. Figure 4-11 shows the MALDI-TOF spectrum of the supernatant after the adsorption step. The phosphopeptide pDSIP is not detected. This indicates good adsorption of pDSIP onto Zr-OBP_T. Figure 4-12 shows the subsequent spectrum after elution. The dominant peaks in the spectrum are attributed to the molecular ion peak or the sodium or potassium adducts. The results indicate that we are able to elute pDSIP from Zr-OBP_T and suggest Zr-OBP_T could serve as a phosphopeptide enrichment material.

Simple Enrichment with MS Detection

The preceding results do not demonstrate competitive binding since a purified peptide as adsorbed and later removed. We repeated the enrichment experiment demonstrated by Xu *et al.* with the enrichment of the phosphopeptides present in the tryptic digest of β-casein. The spectra show the β-casein digest (Figure 4-13) and the supernatants after adsorption (Figure 4-14), washing (Figure 4-15), and elution (Figure 4-16). The spectrum of the digest shows the presence of both expected phosphopeptides at low intensity. Neither phosphopeptide peak is observed in the spectra of the supernatant of the adsorption or wash steps. Both phosphopeptide peaks are observed in the elution spectrum. The results we observe are consistent with the previously published report by Xu *et al.*, and further indicate that α-ZrP_T can be used as a phosphopeptide enrichment material.

Summary

We have demonstrated mock enrichment of pDSIP on α-ZrP_T as detected by UV absorbance spectroscopy. The UV signal observed in the elution off of α-ZrP_T and Zr-OBP_T was confirmed to be pDSIP by MALDI-TOF MS. Furthermore, we placed the UV signal attributed to DSIP primarily in the supernatant after the adsorption step above α-ZrP_T suggesting that the adsorbent would serve well as a phosphopeptide enrichment material. Finally, we were able to repeat the enrichment experiment demonstrated by Xu *et al.* where the phosphopeptides of β-casein were enriched from the tryptic digest of the phosphoprotein. Overall, the results indicate that both α-ZrP_T and Zr-OBP_T could serve as phosphopeptide enrichment materials.

Further work needs to be done to refine the desorption steps: the wash step for non-phosphopeptides and the elution step for phosphopeptides. Particularly in the work

with TiO_2, new experimental methods must be developed to track the peptide throughout the process since we cannot account for 100% of the peptide introduced to the system. This might be corrected by using different wash and elution buffers, or an alternative detection approach might be required. This shortcoming not withstanding, the results are promising that all the materials tested in this chapter can serve as phosphopeptide enrichment materials, and their effectiveness could be improved or better understood by further exploration of the conditions and detection methods.

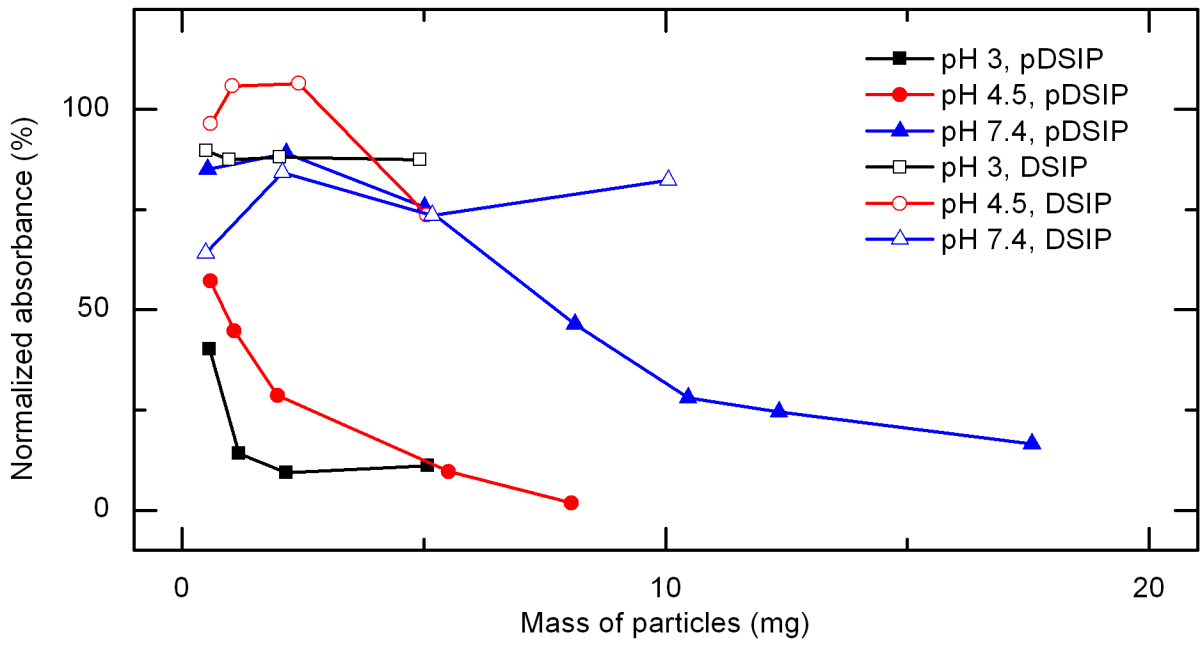

Figure 4-1. The mass dependent adsorption of pDSIP and DSIP onto α-ZrP_T. Approximately 3-5 mg of α-ZrP_T is necessary to completely bind pDSIP at pH 3.0 and 4.5; near 20 mg of α-ZrP_T is necessary at pH 7.4. The data for DSIP at this stage in inconclusive, but we can see that limited amounts of DSIP will bind under conditions favorable for the adsorption of pDSIP. We expect the error to be about 20%.

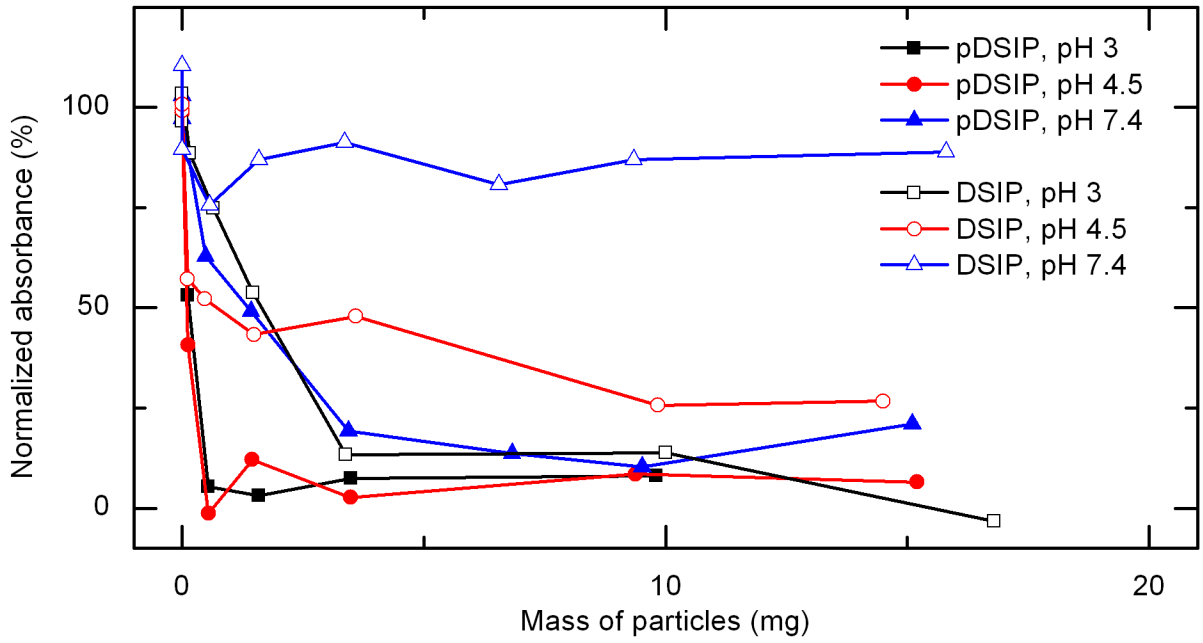

Figure 4-2. The mass dependent adsorption of pDSIP and DSIP onto TiO_2. The data shown reflect the amount of peptide in solution after an 18 h interaction. Only 1-2 mg of TiO_2 is necessary to completely adsorb all pDSIP at pH 3.0 and 4.5. Increasing to 5-10 mg of TiO_2 is necessary to completely adsorb all pDSIP at pH 7.4. The adsorption of DSIP requires more mass of particles than for pDSIP and has a more defined pH trend. We expect the error to be about 15%.

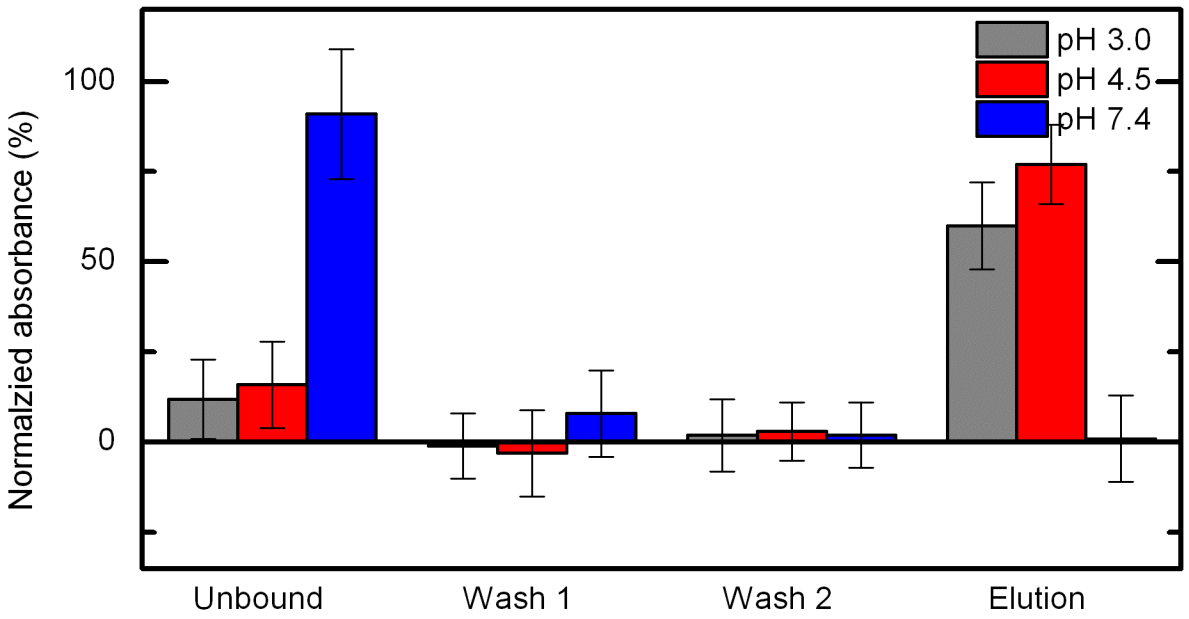

Figure 4-3. Full enrichment sequence study of pDSIP onto 2 mg of α-ZrP_T Near complete binding is observed at pH 3.0 and 4.5, and 50-75% recovery is observed in the elution step for the same setup. At pH 7.4, minimal binding is observed because there is not enough adsorbent available.

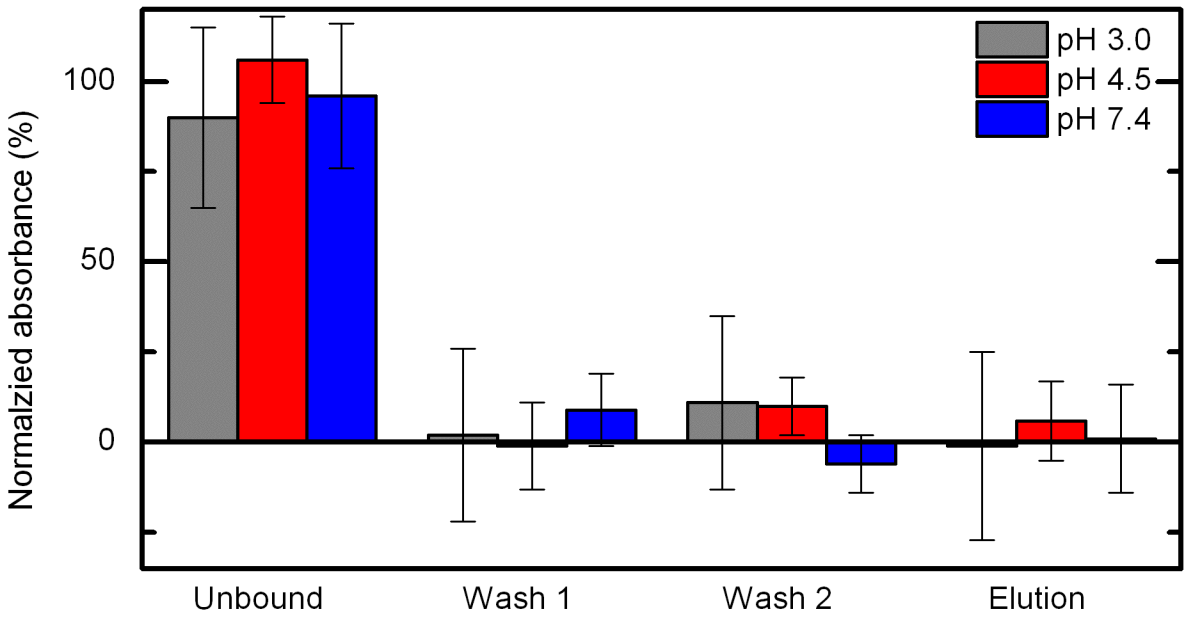

Figure 4-4. Full enrichment sequence study of DSIP onto 2 mg of α-ZrP_T. The majority of the peptide does not bind to the particles and is thus observed in the unbound fraction. Within error, almost no peptide is observed in the following steps. There is some indication that the first wash in 0.1% TFA removed DSIP bound at pH 7.4 and second wash in 1% TFA removed DSIP bound at pH 3.0 or 4.5.

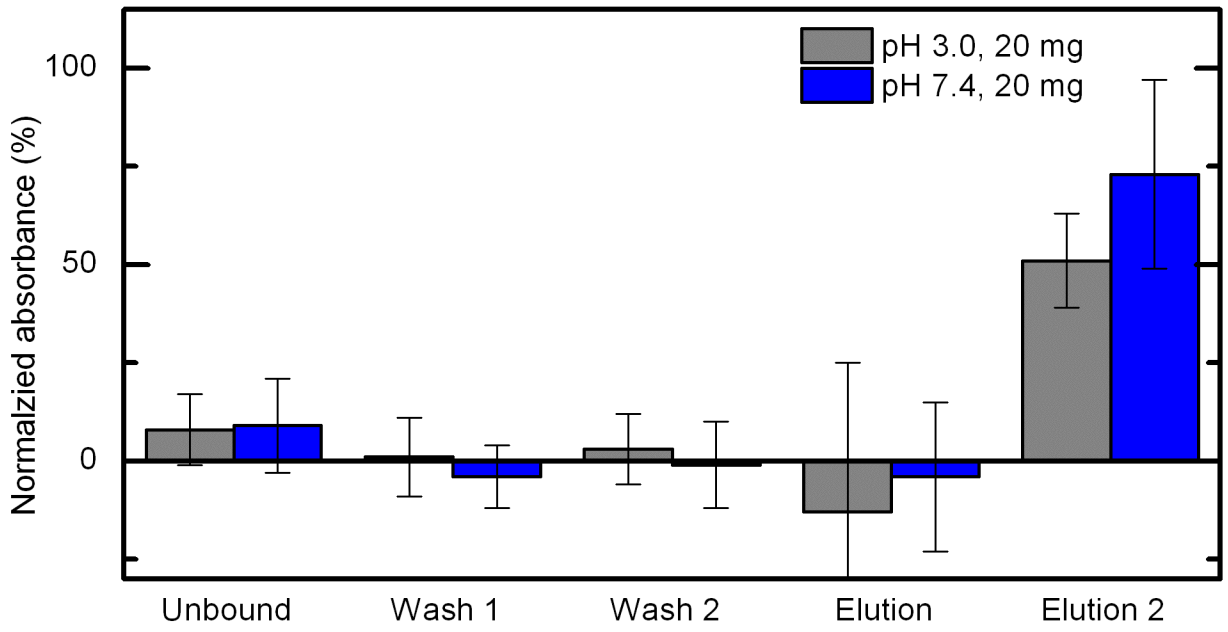

Figure 4-5. Full enrichment sequence study of pDSIP onto 20 mg of α-ZrP_T. With ten times more adsorbent, it is possible to almost completely adsorb pDSIP onto α-ZrP_T under pH 7.4 conditions. Following the adsorption at pH 7.4, approximately 75% of the peptide is recovered in the second elution step with 300 mM ABC.

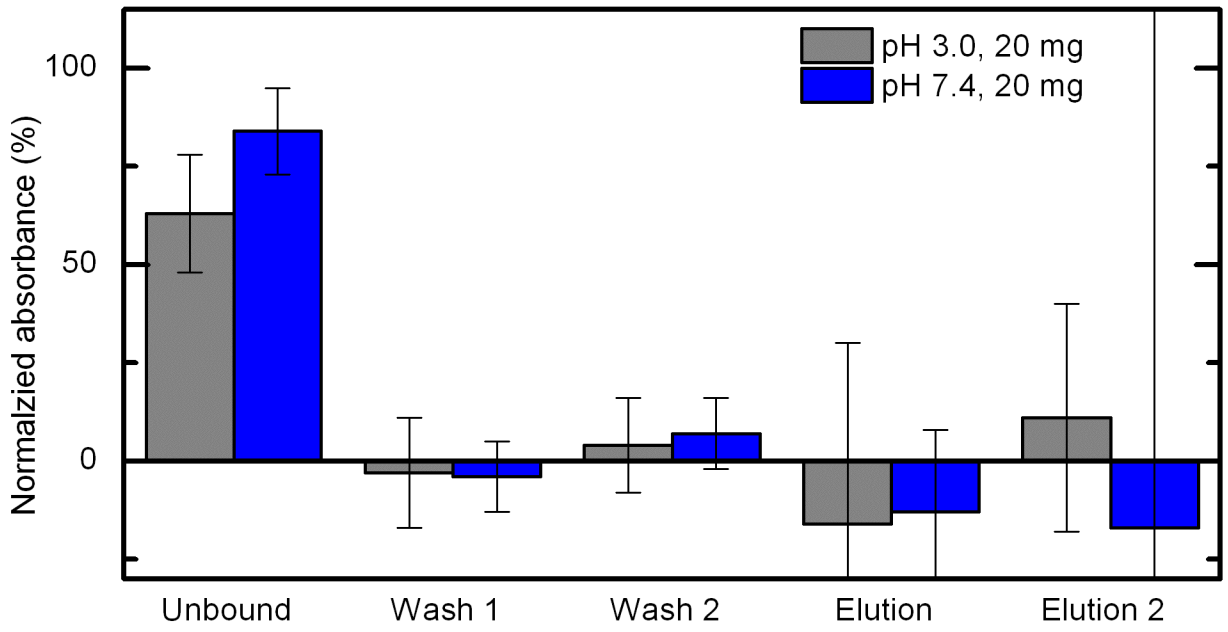

Figure 4-6. Full enrichment sequence study of DSIP onto 20 mg of α-ZrP_T. With more adsorbent available, we see an increase in the non-specific binding of DSIP onto α-ZrP_T. The results do not show sufficient recovery of the bound peptide in the following washing or elution steps. Exceptionally large error is present in the elution steps. The large error was caused by signal scattering problems in the negative controls.

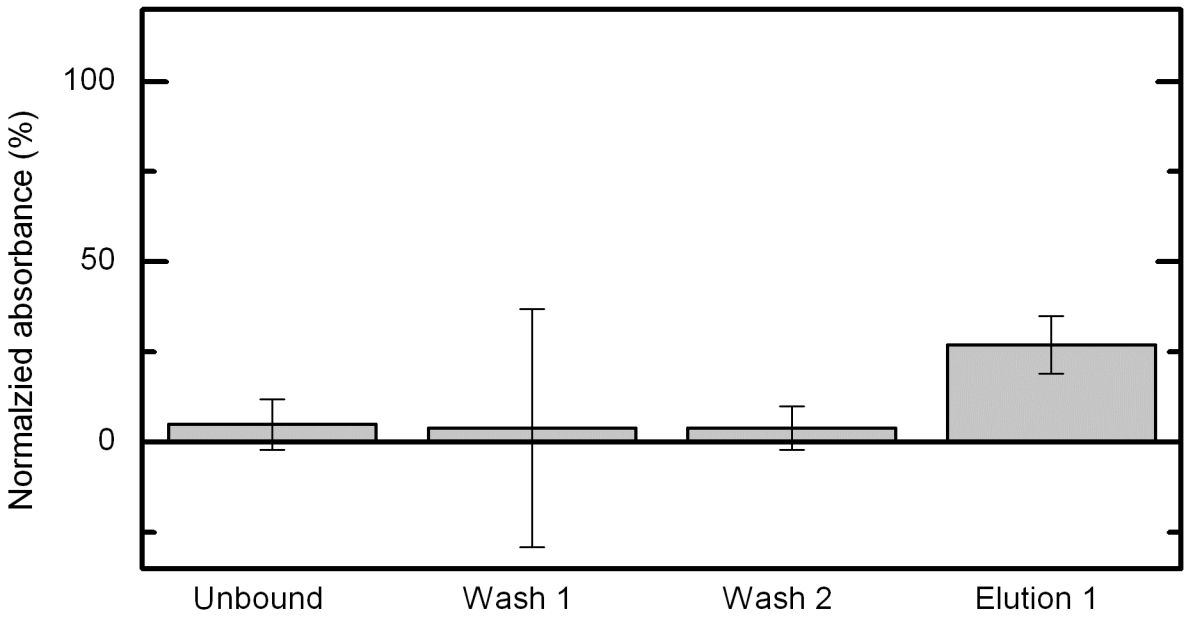

Figure 4-7. Full enrichment sequence study of pDSIP onto TiO_2. We could not achieve good mass balance due to error in the measurements. We diverted our attention to understanding the adsorption step more completely (Chapter 3).

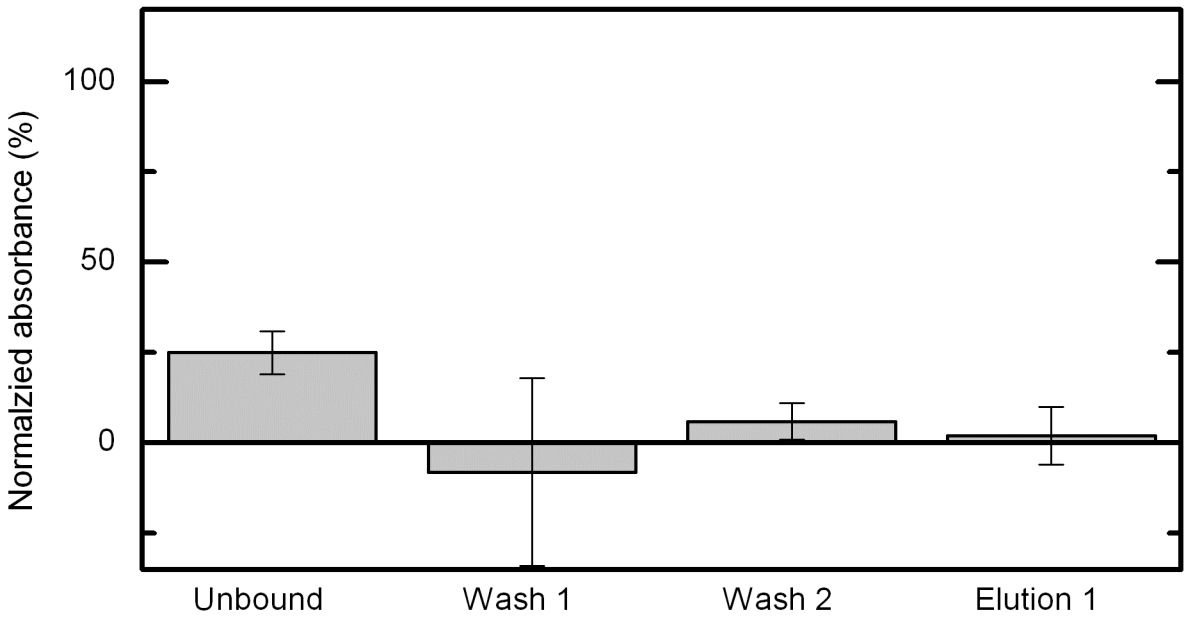

Figure 4-8. Full enrichment sequence study of DSIP onto TiO2. We could not achieve good mass balance. After several attempts including changing parameters, we diverted our attention to the adsorption isotherms (Chapter 3).

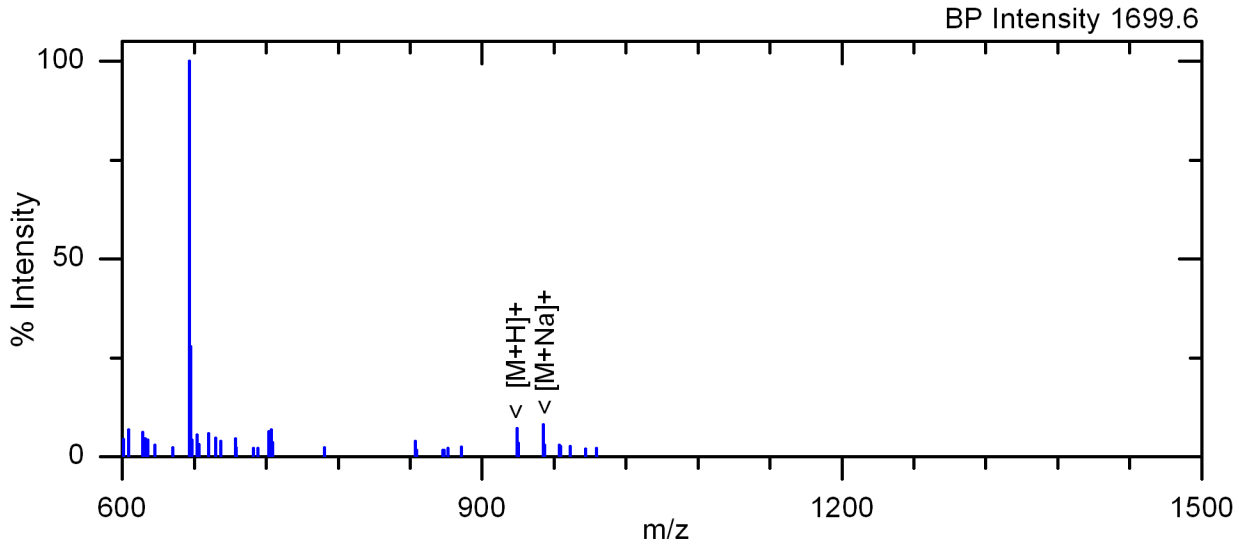

Figure 4-9. MALDI-TOF MS of the unbound fraction after the interaction of pDSIP with α-ZrP_T in pH 3.0 Trizma buffer. Two peaks indicating the presence of pDSIP can be observed.

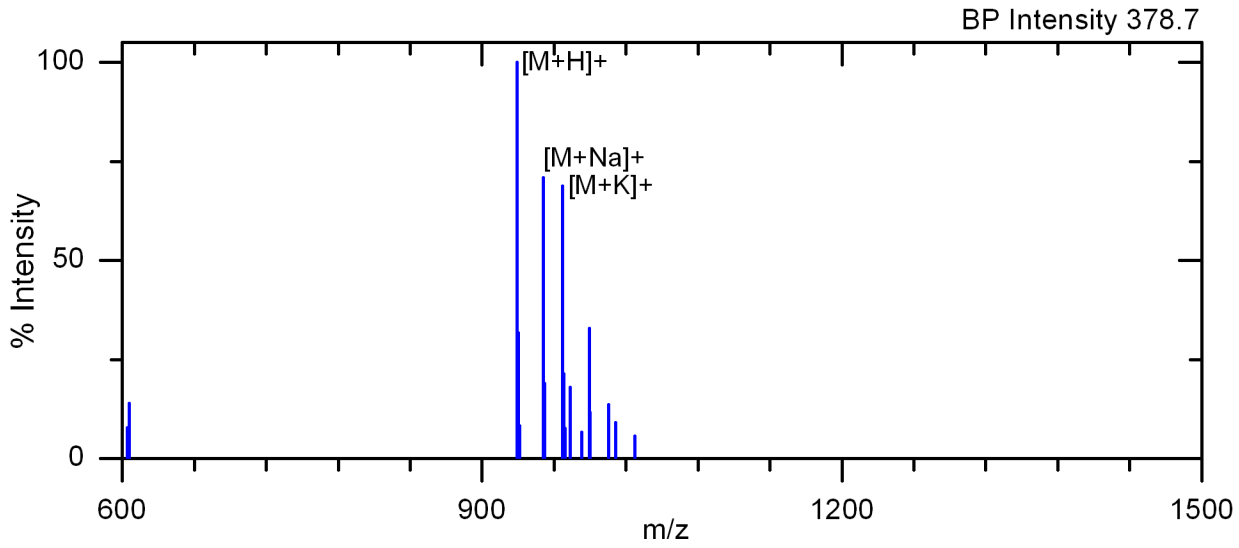

Figure 4-10. MALDI-TOF MS of the elution of pDSIP using 300 mM ABC after the interaction of pDSIP with α-ZrP_T. Multiple peaks indicating the presence of pDSIP are observed including the hydrogenated, sodiated, and potassiated molecular ion peaks.

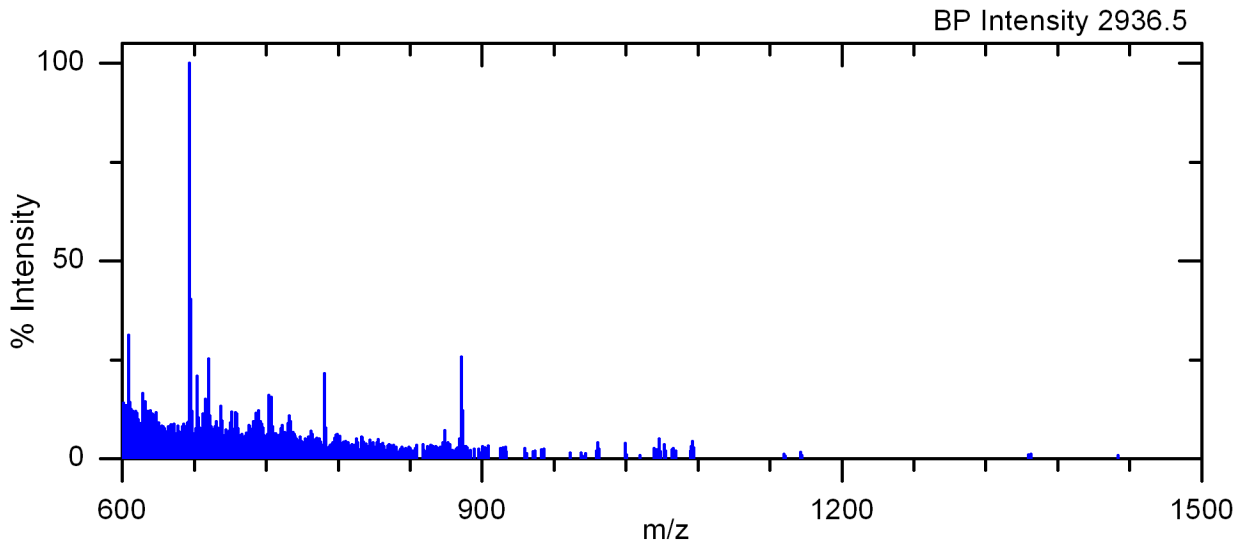

Figure 4-11. MALDI-TOF MS of the unbound fraction after the interaction of pDSIP with Zr-OBP.

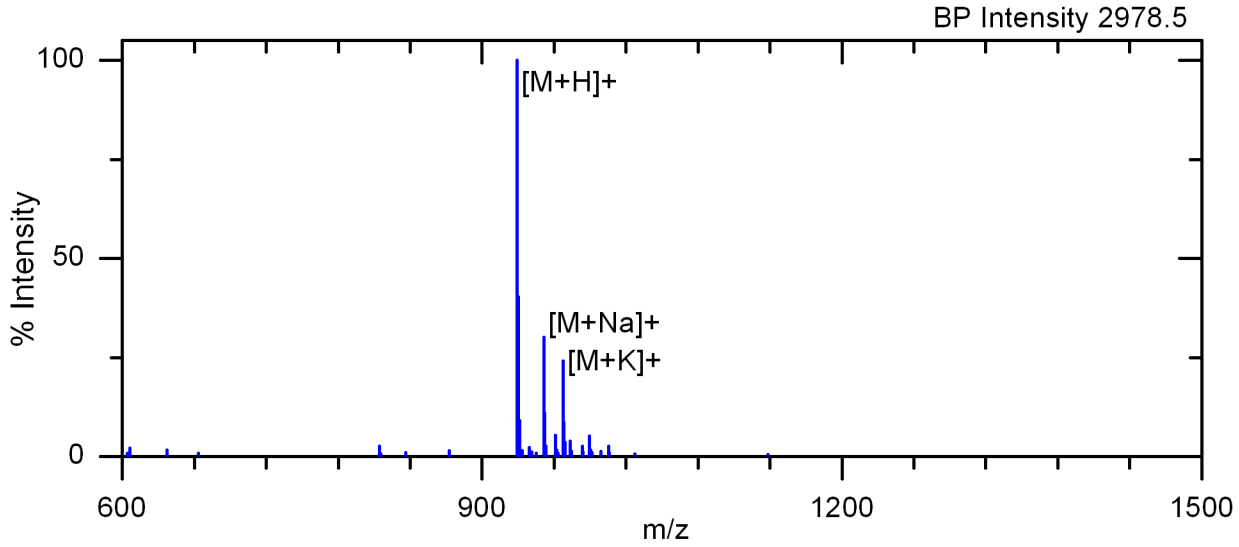

Figure 4-12. MALDI-TOF MS of the elution fraction after the interaction of pDSIP with Zr-OBP.

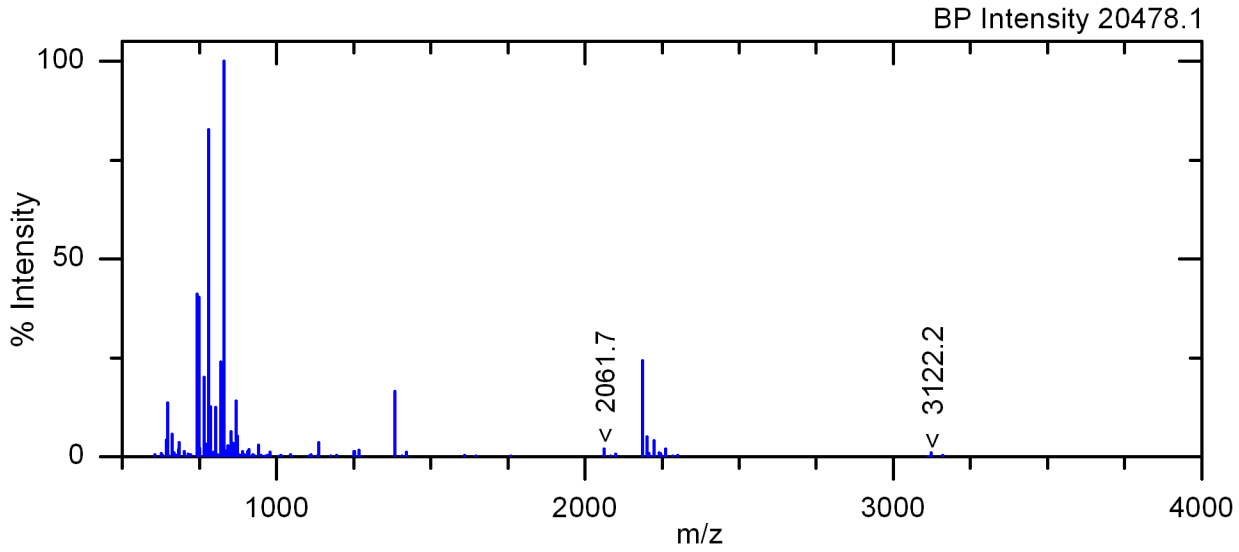

Figure 4-13. MALDI-TOF MS of the tryptic digest of β-casein. The phosphopeptides are labeled.

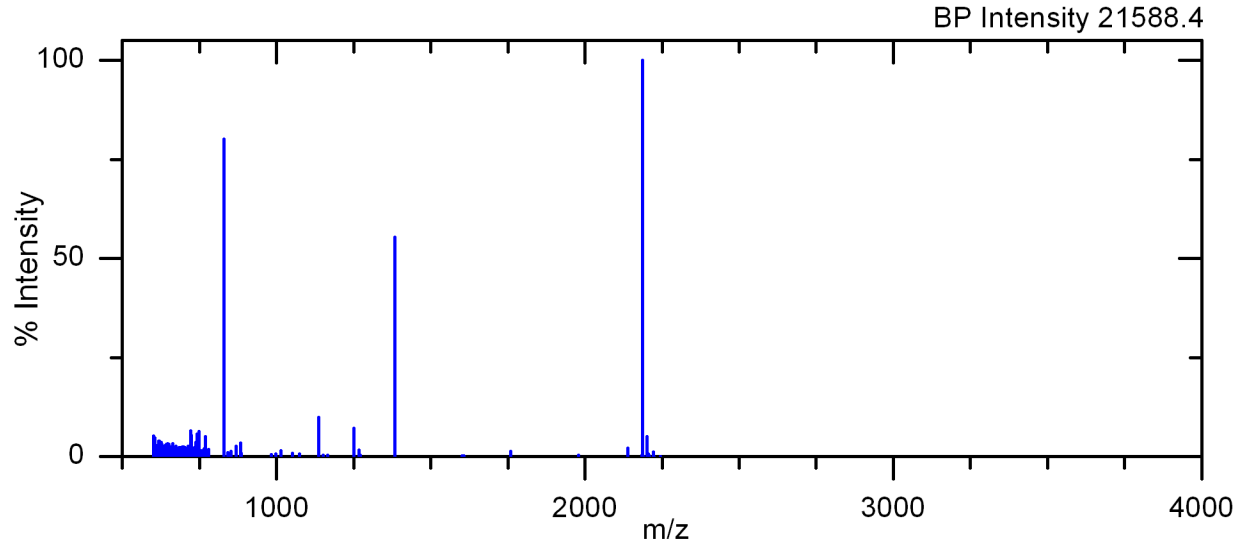

Figure 4-14. MALDI-TOF MS of the unbound fraction after the interaction of β-casein tryptic digest with α-ZrP. No phosphopeptides are observed.

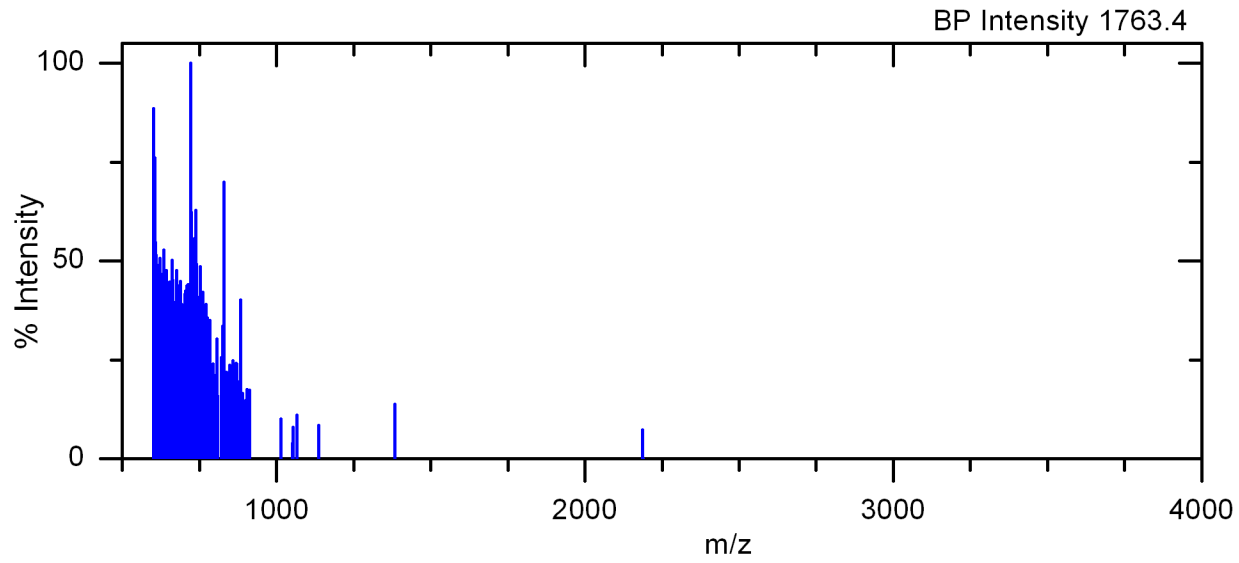

Figure 4-15. MALDI-TOF MS of the wash fraction after the interaction of β-casein tryptic digest with α-ZrP. No phosphopeptides are observed.

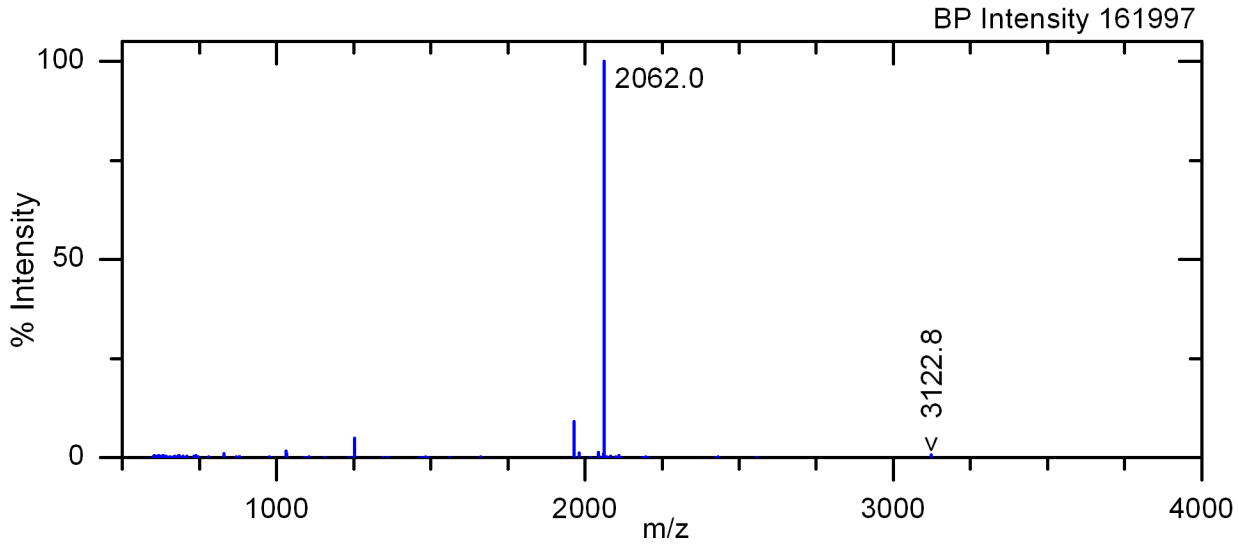

Figure 4-16. MALDI-TOF MS of the elution fraction after the interaction of β-casein tryptic digest with α-ZrP. The phosphopeptides are labeled.

Table 4-1. The approximate point of mass independence is tabulated when we can reasonably estimate it from the data in Figures 4-1 and 4-2. The point of mass independence is the point at which no additional peptide will bind even if more mass of adsorbent were available. The abbreviation unk is used for unknown when it seems unreasonable to assign an approximate value based on the data available.

	α-ZrP_T		TiO_2	
pH	pDSIP	DSIP	pDSIP	DSIP
3.0	2 mg	0.5 mg	0.5 mg	4 mg
4.5	6 mg	unk	0.5 mg	unk
7.4	20 mg	unk	4 mg	unk

CHAPTER 5
CONCLUSIONS

We have prepared two potential phosphopeptide enrichment materials α-ZrP and Zr-OBP and characterized them in comparison to published examples of these materials. As part of this characterization, we titrated the ζ as a function of pH and determined the IEP of the materials we prepared and commercial phosphopeptide enrichment materials. We found three clusters of IEPs: ca. pH 6.5 for metal oxides, ca. pH 1 for neat α-ZrP and neat Zr-OBP, and ca. pH 3 for treated α-ZrP and Zr-OBP. These clusters are a testament to different surface chemistries in the materials. We attribute the large shift in IEP from neat material to treated material to a shift in the ratio of Zr to P sites on the surface of the materials.

We conducted a study of the adsorption of a phosphopeptide and a non-phosphopeptide onto these materials with an understanding of the ζ as a function of pH for the materials and a prediction of charge as a function of pH for the pair of model peptides. We changed the pH of the interaction in an effort to elucidate any pH dependence in the results. We combined our understanding of the ζ and peptide charge as functions of pH with the pH dependence of the adsorption results. Our data supports the theory that TiO_2 has an electrostatic binding mechanism. In the same way, we found α-ZrP does not have an electrostatic binding mechanism. We propose coordinate covalent binding as an appropriate alternative mechanism on α-ZrP. We found α-ZrP has exceptional selectivity of the model phosphopeptide over the model non-phosphopeptide. This can also be attributed to a coordinate covalent binding mechanism where only the phosphate on a phosphopeptide is basic enough to displace the ligands around a Zr center. Conversely, a carboxylate is not basic enough, and thus

we do not observe any non-specific binding of non-phosphopeptide. We found Zr-OBP has the highest binding capacity of the materials tested. We attribute this to full surface availability, compared to α-ZrP, and a higher surface area compared to both α-ZrP and TiO_2. Ultimately through refinement of Zr-OBP synthesis or with an alternative zirconium phosphonate it may be possible to combine the exceptional selectivity we observe with α-ZrP and the increased amount of available surface area we observe with Zr-OBP.

We also demonstrated the ability to recover phosphopeptide during the elution step of mock enrichment and simple enrichment experiments. This provides assurance that the tested materials are suitable phosphopeptide enrichment materials because the desired adsorbate can be removed from the adsorbents for further analysis.

Several tiers of future work are conceivable hereafter. First, the exploration of a few more pH would further solidify our proposed binding mechanisms. In some cases, this will require either the use of a different buffer to control pH or external pH control. Second, additional zirconium phosphonates should be explored. Using different α,ω-bisphosphonic acids to prepare different solids could yield zirconium phosphonate particles with lower binding efficiency toward non-phosphopeptide thus improving the selectivity while maintaining the increased adsorption capacity. Third, the desorption step, which is essential to effective enrichment, should be explored further in order to improve the removal of non-phosphopeptides during the wash step and to improve the recovery of the phosphopeptide during the elution step. Fourth, the work should move forward toward competitive binding scenarios and realistic samples. This will require the development of an alternative analysis method.

APPENDIX A
RAW DATA

In this appendix we provide the raw data for the adsorption isotherm measurements. The category is consistent down each column and is thus labeled only in the first row.

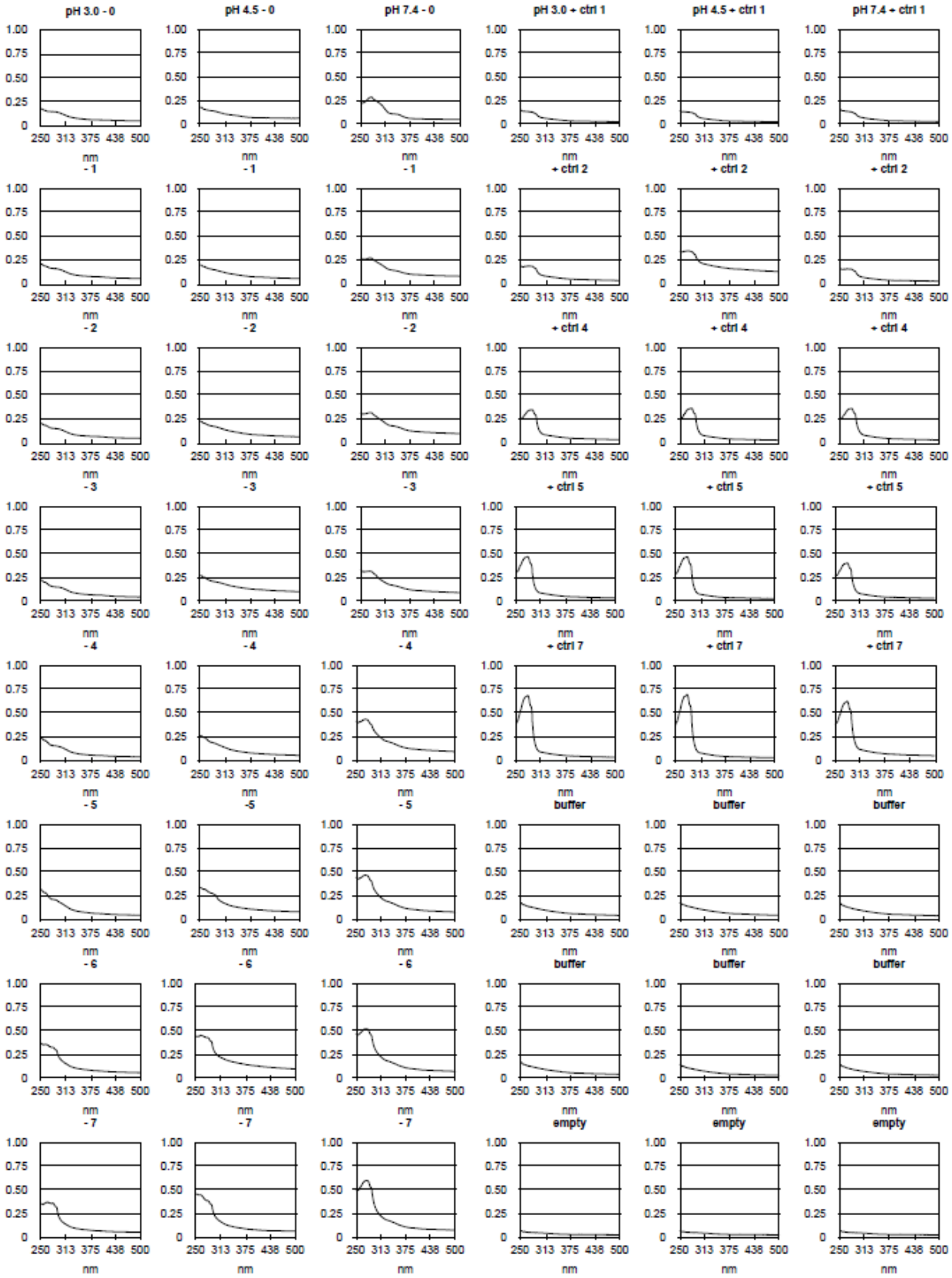

Figure A-1. TiO_2; pDSIP; pH 3.0, 4.5, 7.4; Set A; file 2013 03 14.

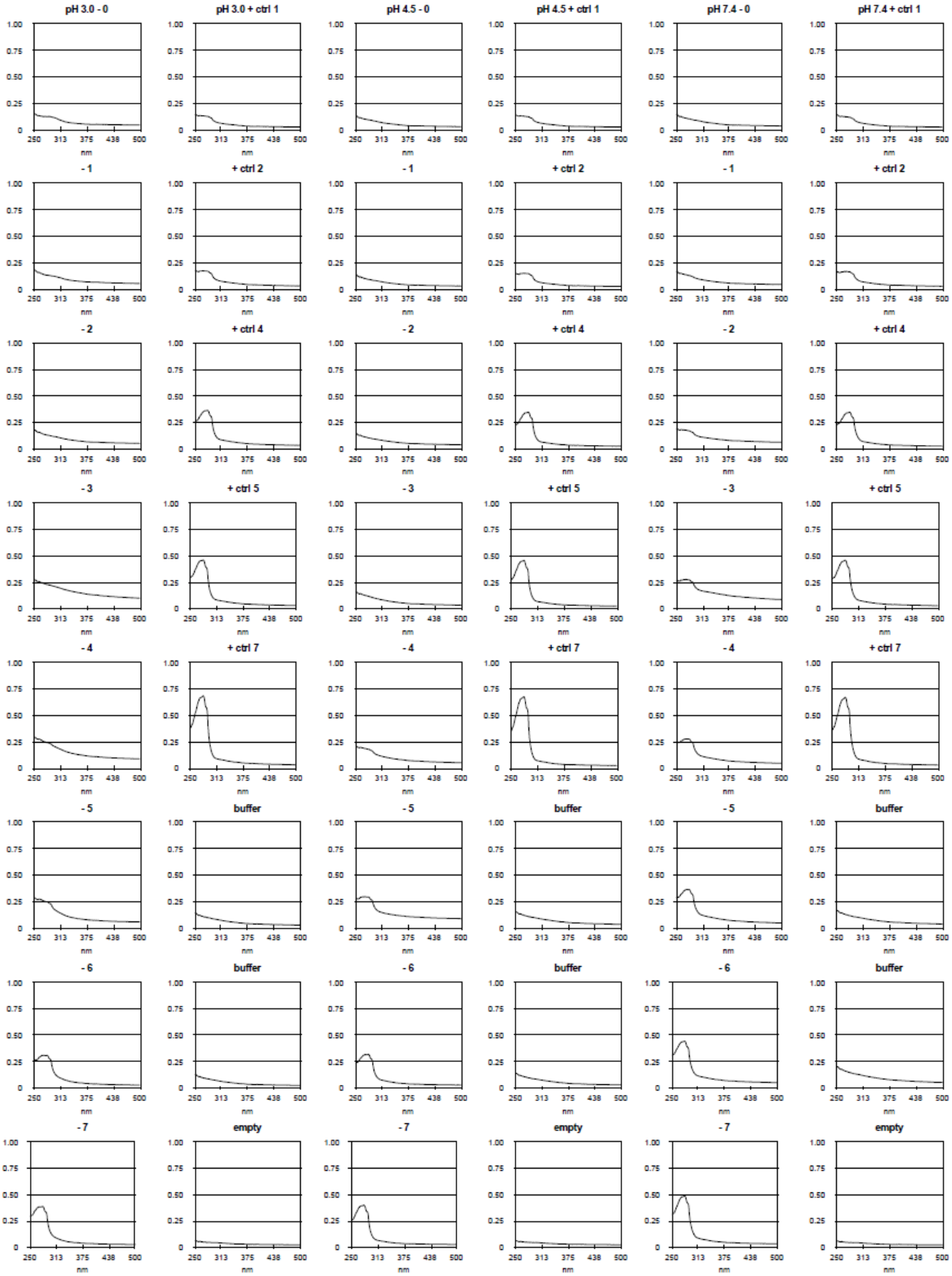

Figure A-2. TiO_2; pDSIP; pH 3.0, 4.5, 7.4; Set B; file 2013 03 15.

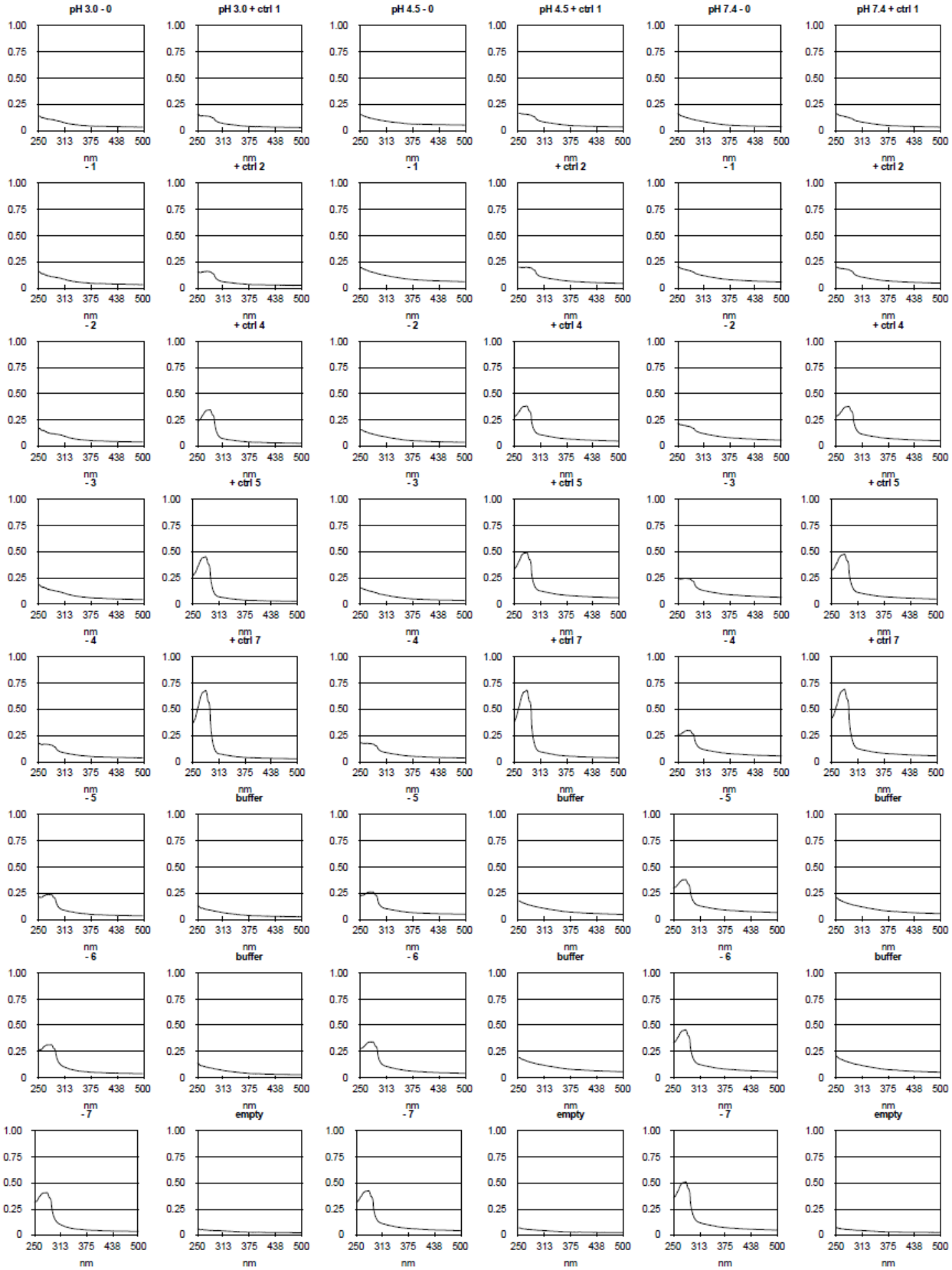

Figure A-3. TiO_2; pDSIP; pH 3.0, 4.5, 7.4; Set C; file 2013 03 15.

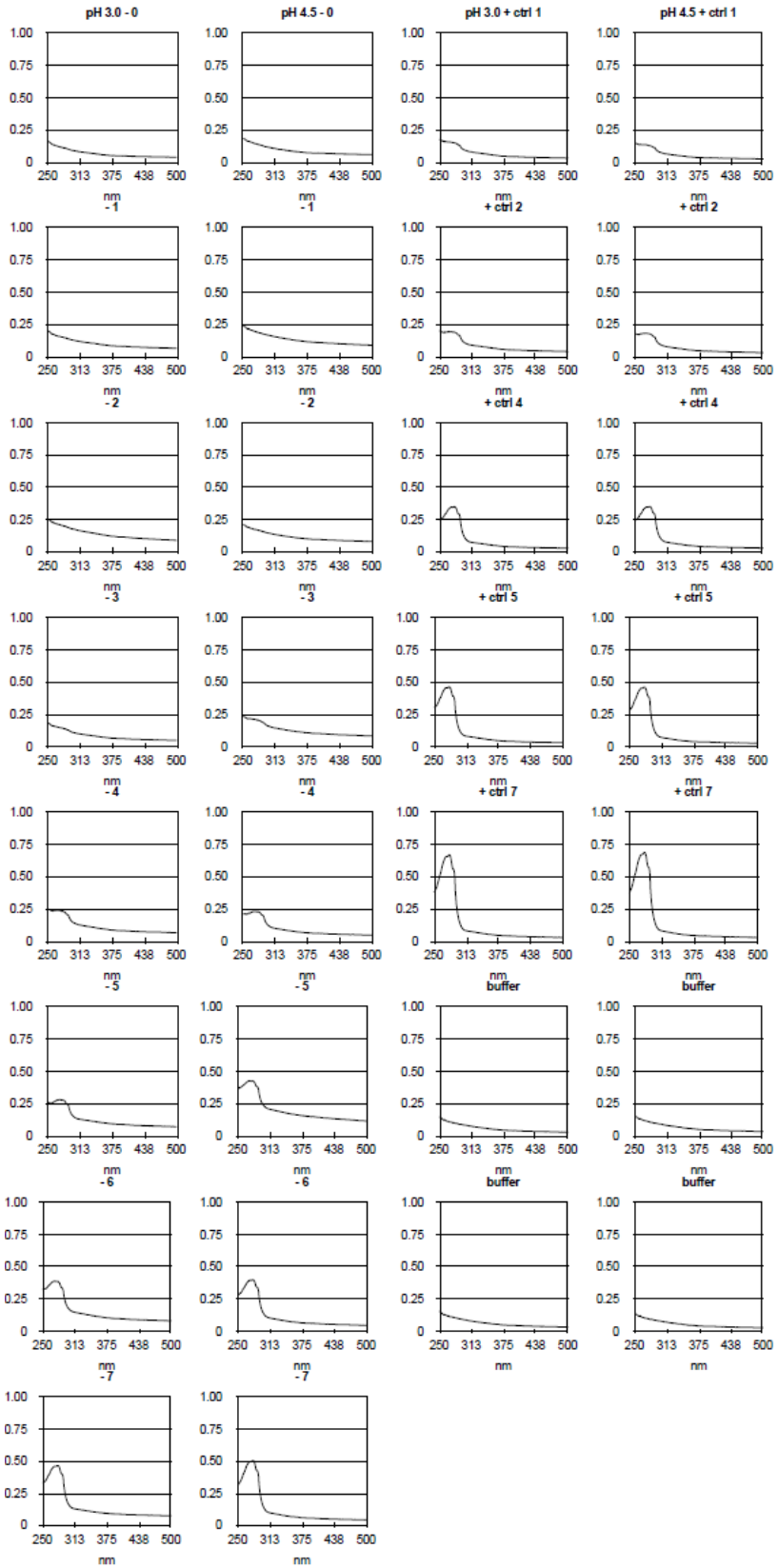

Figure A-4. α-ZrP; pDSIP; pH 3.0, 4.5; Set A; file 2013 03 06.

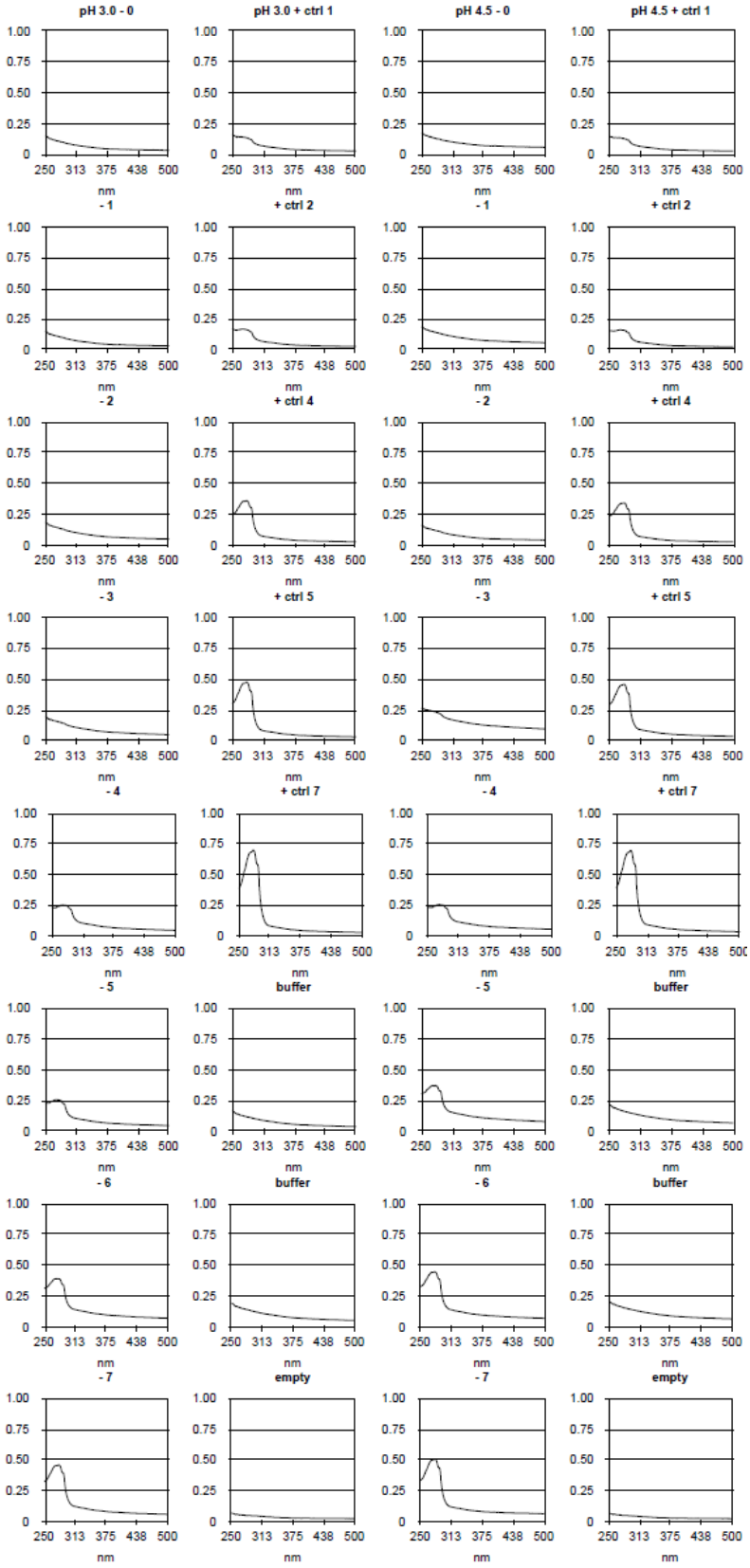

Figure A-5. α-ZrP; pDSIP; pH 3.0, 4.5; Set B; file 2013 03 07.

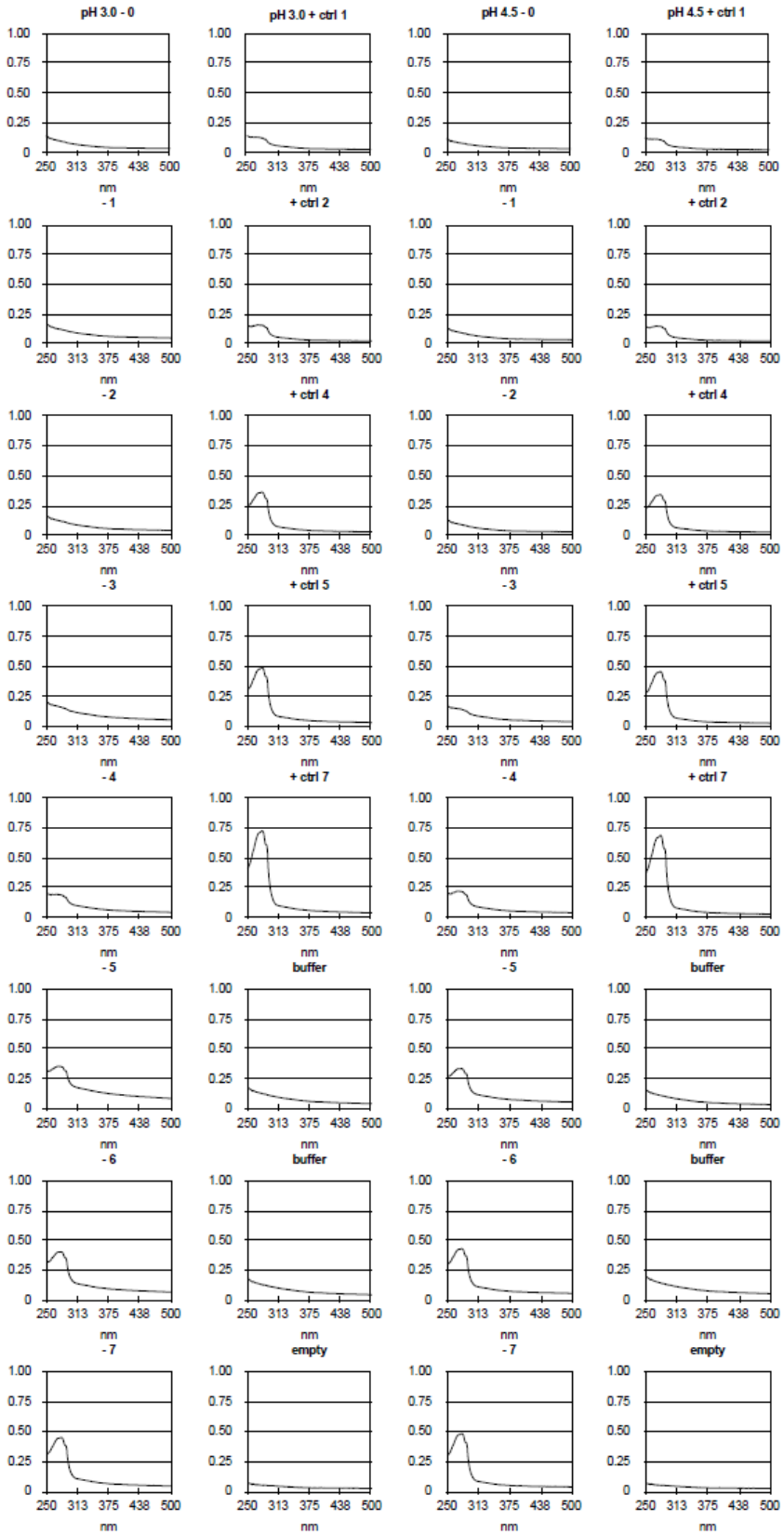

Figure A-6. α-ZrP; pDSIP; pH 3.0, 4.5; Set C; file 2013 03 07.

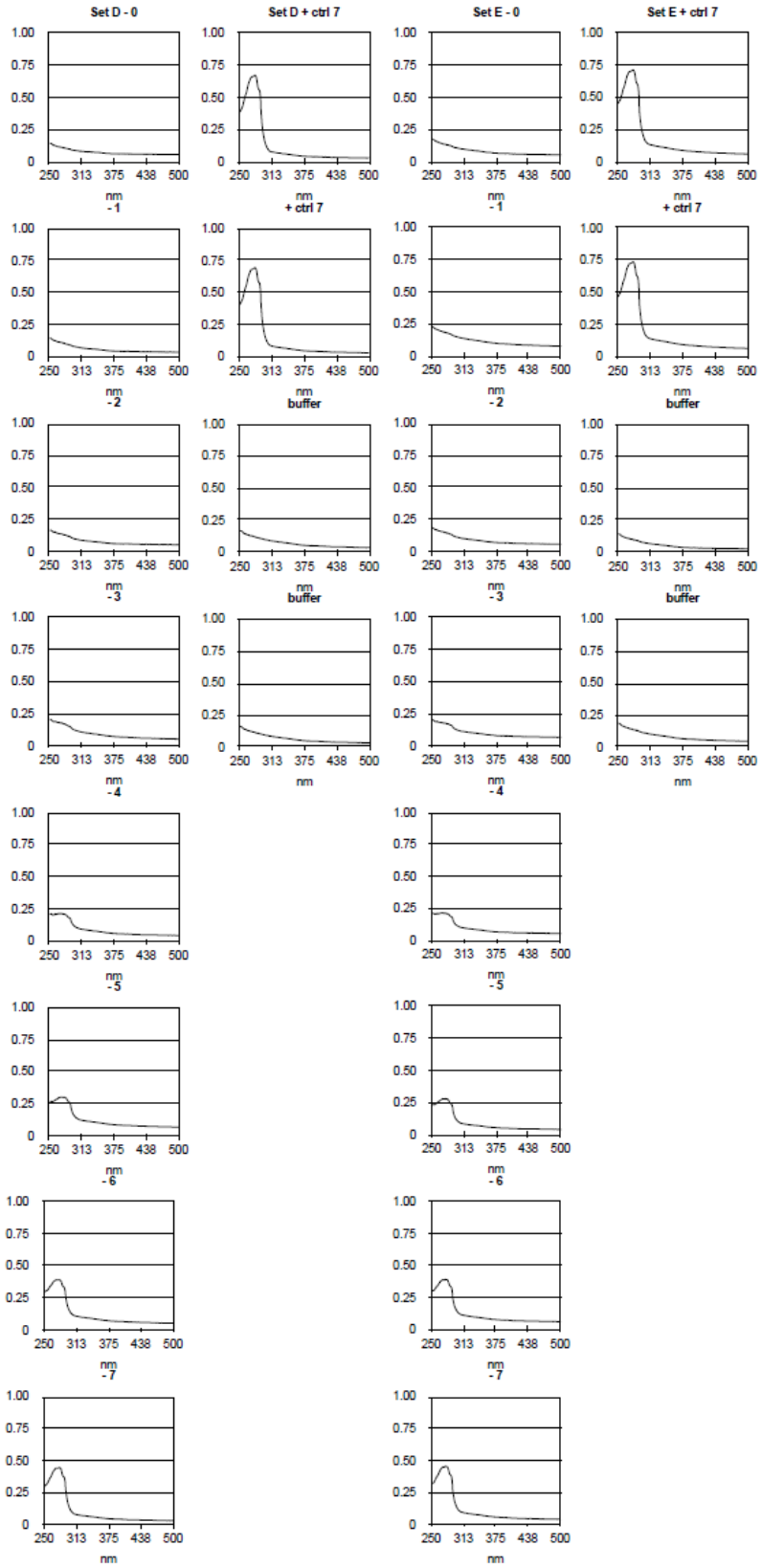

Figure A-7. α-ZrP; pDSIP; pH 3.0; Sets D,E; files 2013 02 05, 2013 02 07.

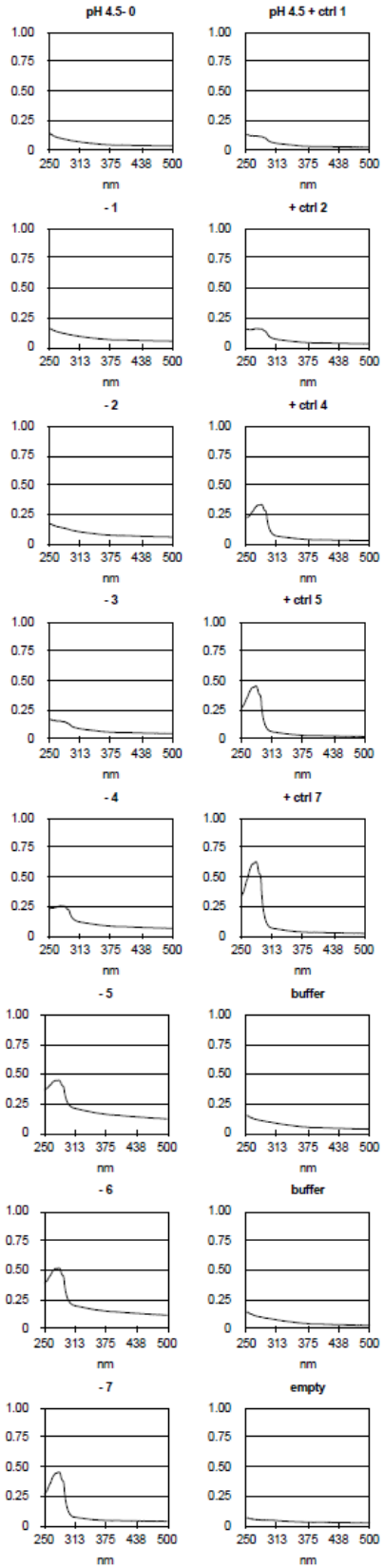

Figure A-8. α-ZrP; pDSIP; pH 4.5; Set D; file 2013 03 22.

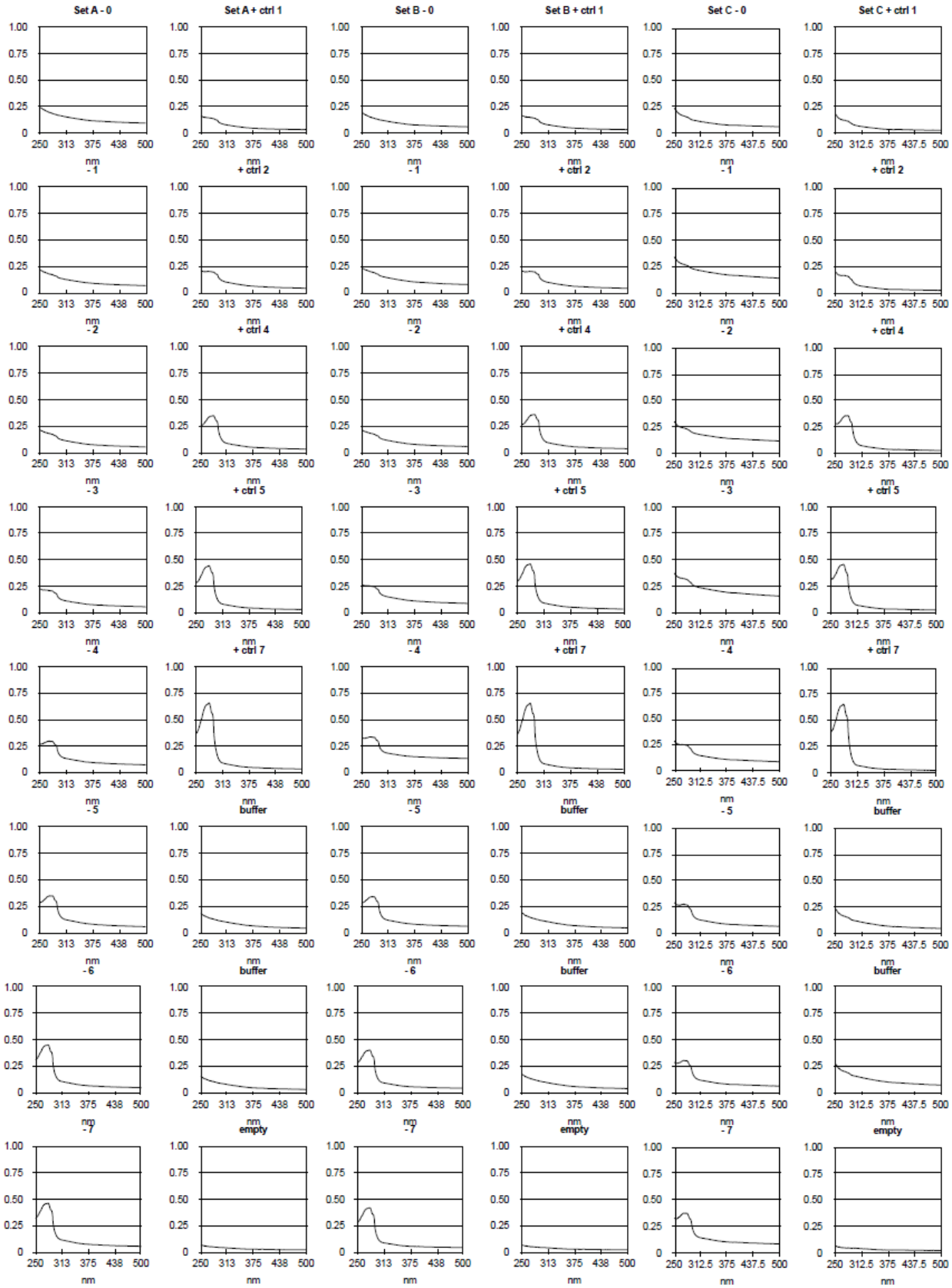

Figure A-9. α-ZrP; pDSIP; pH 7.4; Sets A-C; files 2013 03 15, 2013 03 22.

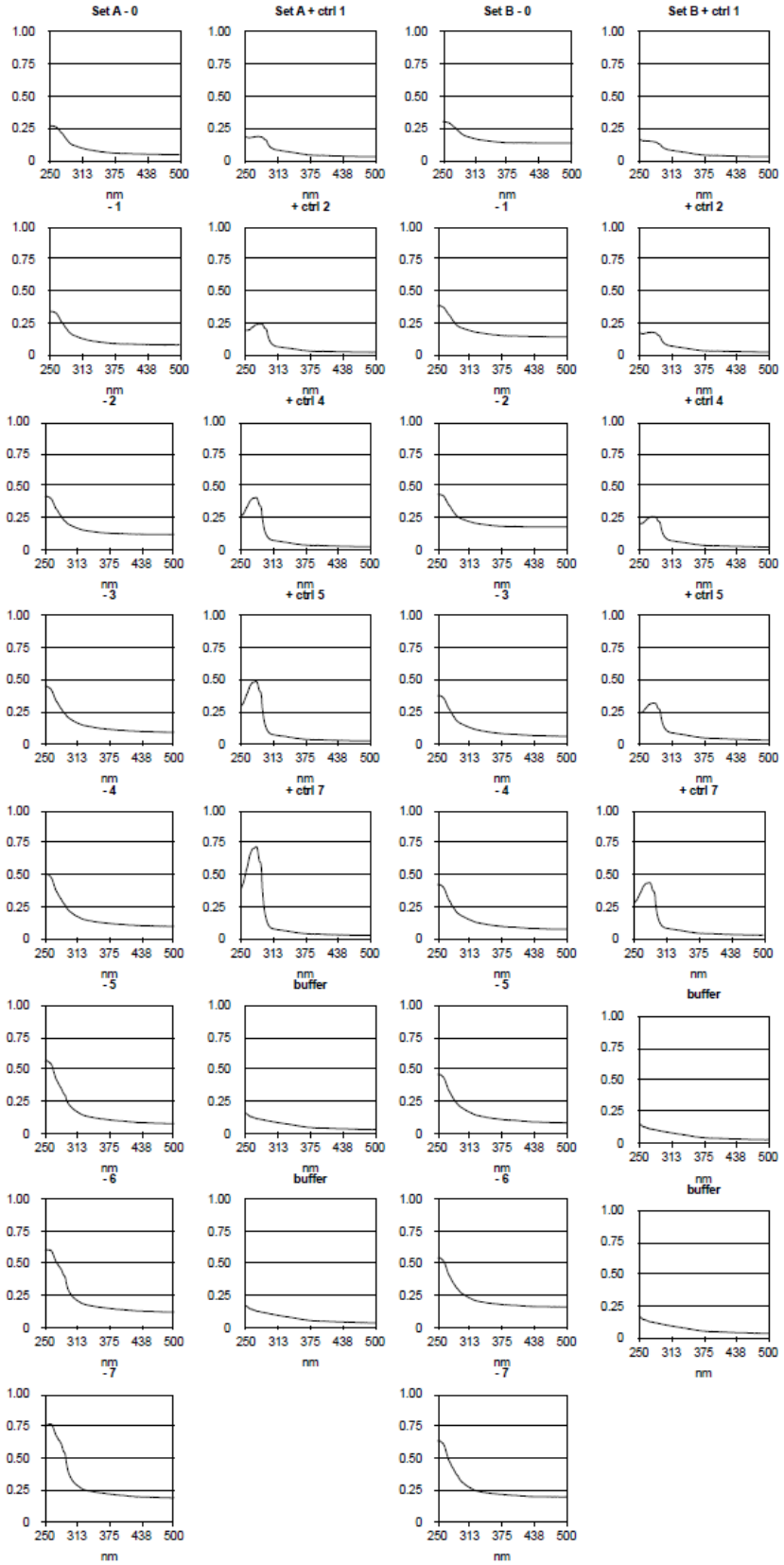

Figure A-10. TiO_2; DSIP; pH 3.0; Sets A-B; file 2013 05 23.

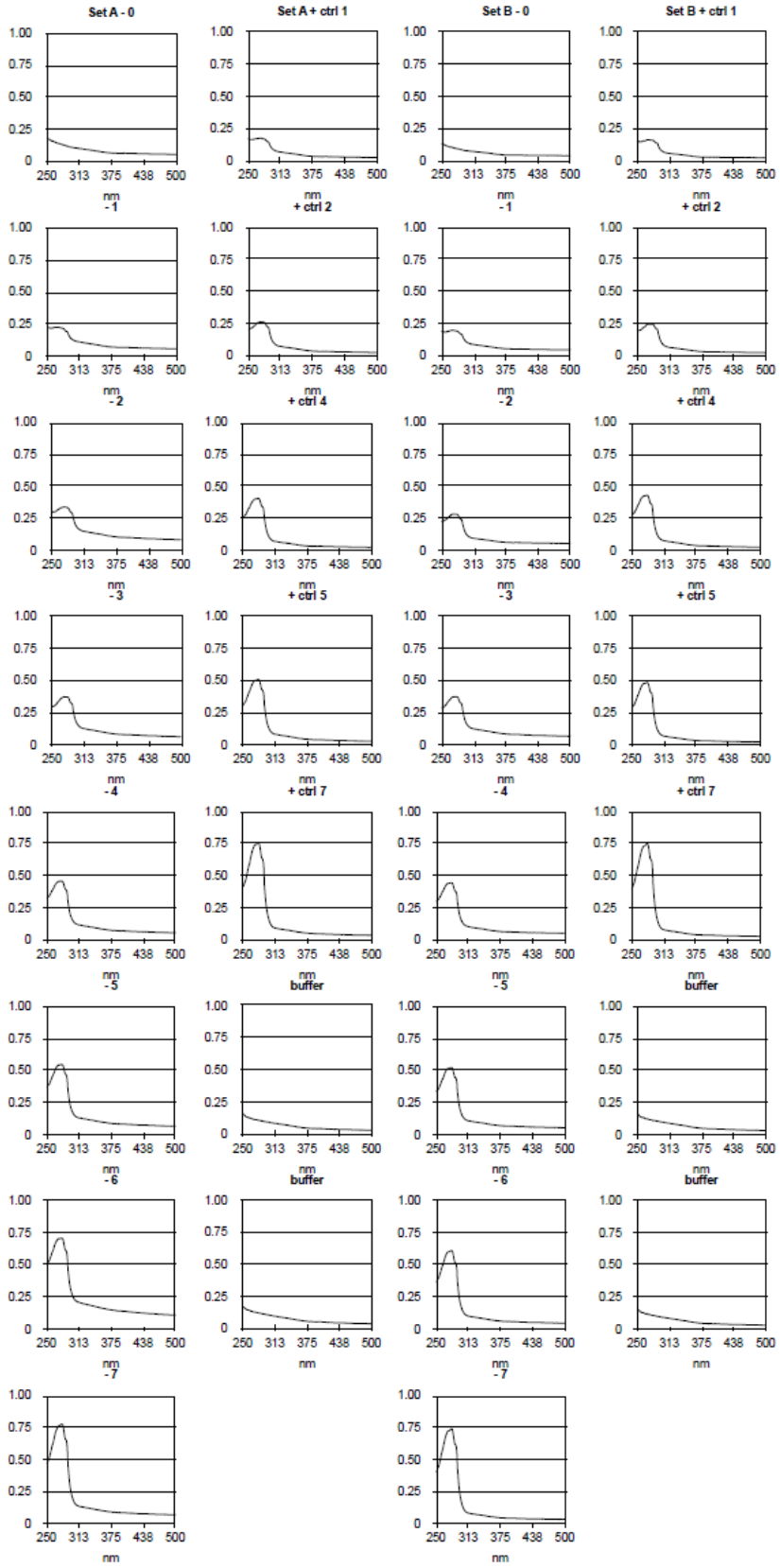

Figure A-11. α-ZrP; DSIP; pH 3.0; Sets A-B; files 2013 05 23, 2013 05 29.

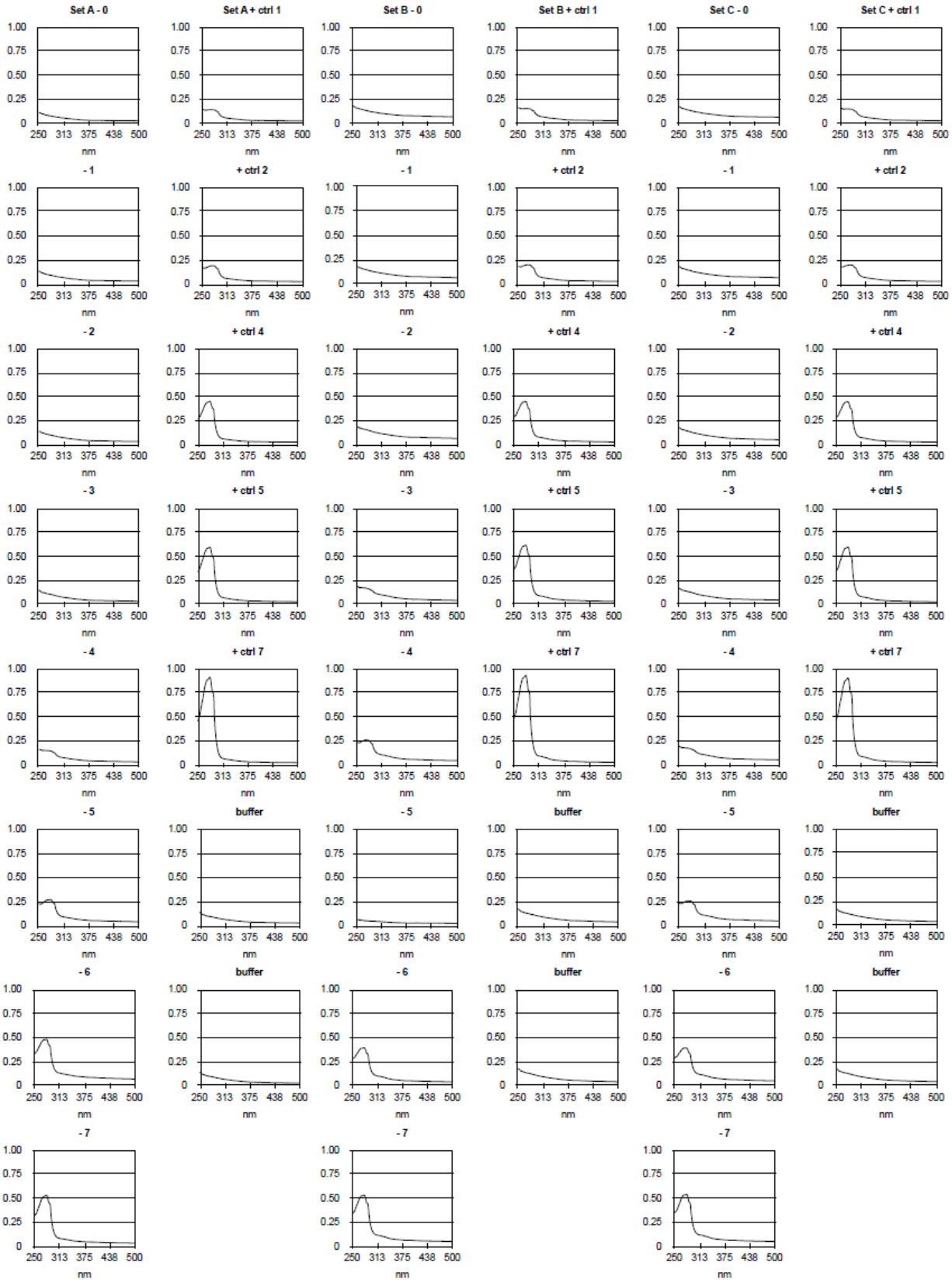

Figure A-12. Zr-OBP; pDSIP; pH 3.0; Sets A-C; files 2013 04 09, 2013 04 19. Samples B-4 and B-5 were removed due to a pipetteing error.

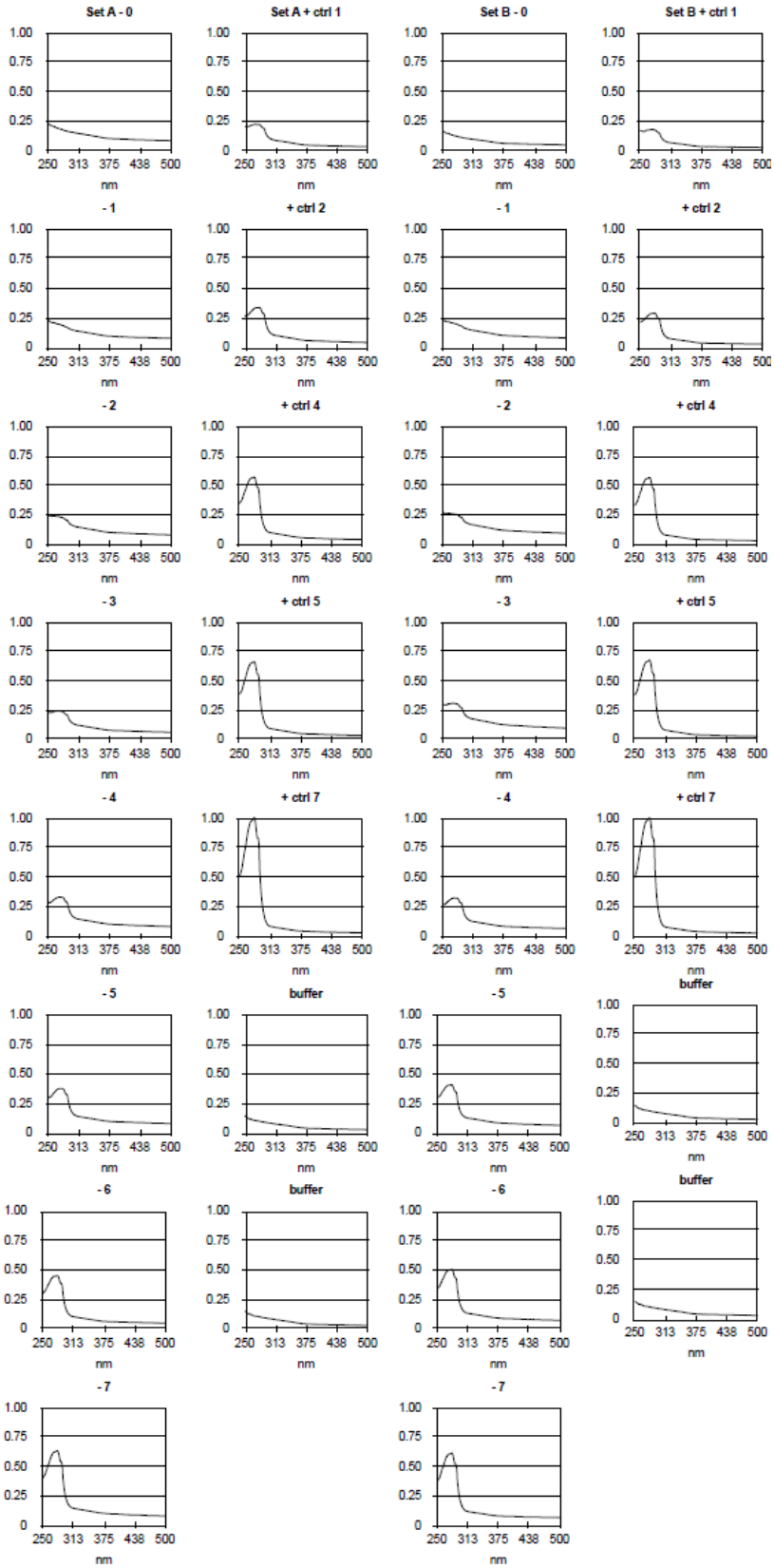

Figure A-13. Zr-OBP; DSIP; pH 3.0; Sets A-B; files 2013 05 31.

APPENDIX B
FREUNDLICH ADSORPTION ISOTHERMS

The data in Chapter 3 were also fit with the Freundlich adsorption isotherm. Equation B-1 is the Freundlich equation where the Freundlich constant K_F describes the adsorption capability (similar to capacity) and $1/n$ is a reflection of the adsorption intensity. When $1/n < 1$, binding is favorable. When $1/n = 1$, the plot is linear. When $1/n > 1$, binding is unfavorable.[62] Unlike the Langmuir model, the Freundlich model allows for multilayer adsorption onto a potentially heterogeneous surface. As such, there is no adsorption maximum by the Freundlich model.

$$q_e = K_F C_e^{1/n} \tag{B-1}$$

The figures in this appendix show the Freundlich adsorption isotherms for the data in Chapter 3. The tables in this appendix tabulate the parameters K_F and $1/n$ from the Freundlich adsorption isotherms. In most cases, the Langmuir adsorption isotherm was a better fit for the data. The only exception is the adsorption of DSIP onto α-ZrP; in this case, the Langmuir model could not fit the data. On the other hand, the Freundlich model could provide a fit for this data, but the fitting parameters have significant error associated with them.

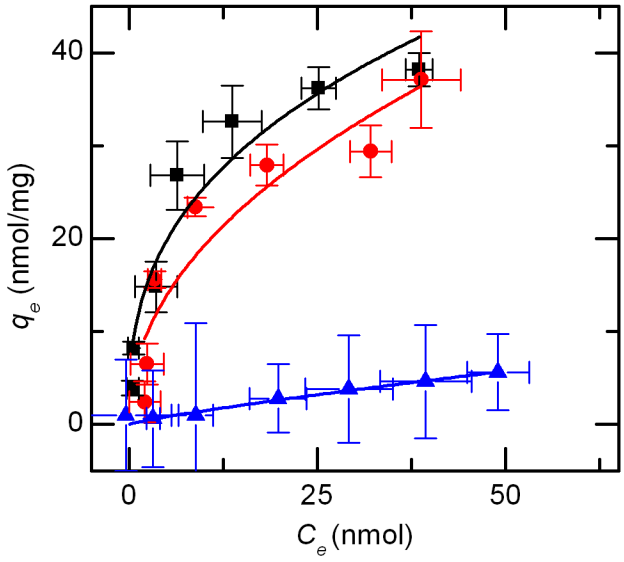

Figure B-1. Freundlich adsorption isotherms for the interaction of pDSIP with TiO_2 at pH 3.0 (black), pH 4.5 (red), and pH 7.4 (blue). Error bars represent ± the standard deviation for n = 3 sets.

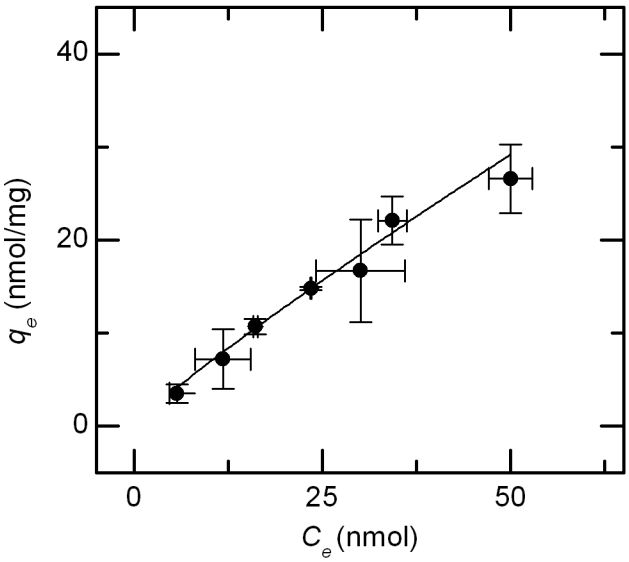

Figure B-2. Freundlich adsorption isotherm for the interaction of DSIP with TiO_2 at pH 3.0. Error bars represent ± the standard deviation for n = 2 sets.

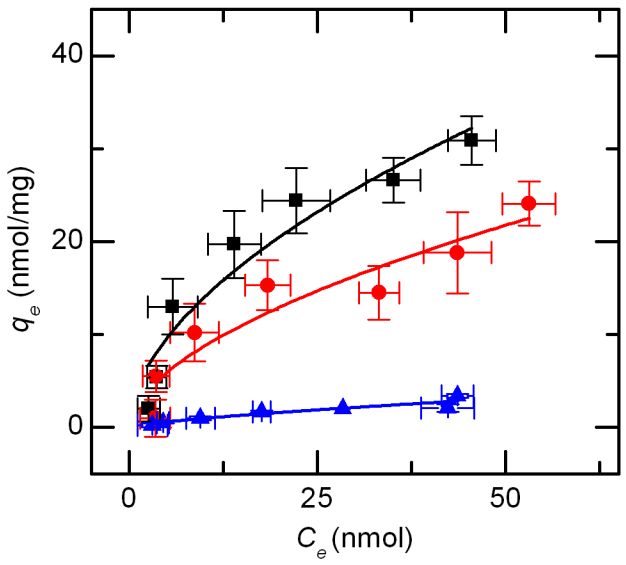

Figure B-3. Freundlich adsorption isotherms for the interaction of pDSIP with α-ZrP at pH 3.0 (black), pH 4.5 (red), and pH 7.4 (blue). Error bars represent ± the standard deviation from n=2 to n=5 sets.

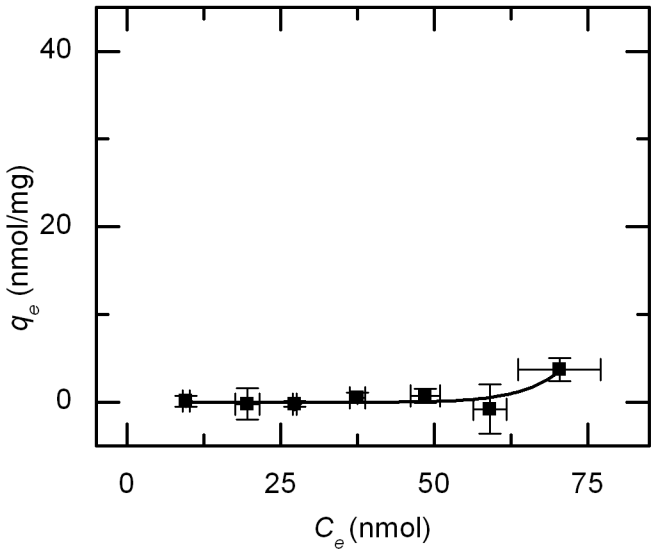

Figure B-4. Langmuir adsorption isotherm for the interaction of DSIP with α-ZrP at pH 3.0. Error bars represent ± the standard deviation for n = 4 sets.

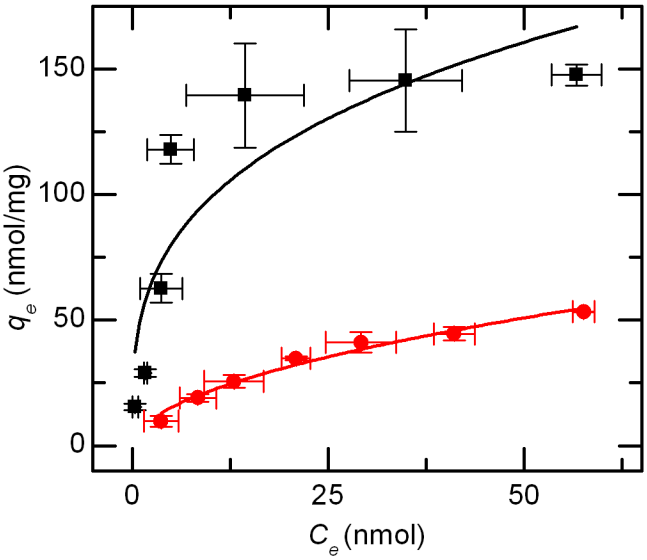

Figure B-5. Freundlich adsorption isotherms for the interaction of pDSIP (black) and DSIP (red) with Zr-OBP at pH 3.0.

Table B-1. The 1/*n* (unitless), and K_F (nmol/mg)(mg)$^{-n}$ values of the Freundlich fits ± the standard error for the interaction of pDSIP with TiO_2 and α-ZrP.

		TiO_2	α-ZrP
pH 3.0	1/*n*	0.36 ± 0.06	0.55 ± 0.09
	K_F	11.0 ± 2.1	4.0 ± 1.3
pH 4.5	1/*n*	0.47 ± 0.10	0.57 ± 0.12
	K_F	6.5 ± 2.2	2.4 ± 1.0
pH 7.4	1/*n*	0.85 ± 0.06	0.72 ± 0.18
	K_F	0.2 ± 0.1	0.2 ± 0.1

Table B-2. The 1/*n*, and K_F (nmol/mg)(mg)$^{-n}$ values of the Freundlich fits ± the standard error for the interaction of DSIP with TiO_2 and α-ZrP.

		TiO_2	α-ZrP
pH 3.0	1/*n*	0.90 ± 0.05	11 ± 8
	K_F	0.9 ± 0.1	4E-20 ± 1E-18

Table B-3. The 1/*n*, and K_F (nmol/mg)(mg)$^{-n}$ values of the Freundlich fits ± the standard error for the interaction of pDSIP and DSIP with Zr-OBP.

		pDSIP	DSIP
pH 3.0	1/*n*	0.30 ± 0.09	0.52 ± 0.04
	K_F	49.3 ± 14.2	6.6 ± 1.0

LIST OF REFERENCES

(1) Tichy, A.; Salovska, B.; Rehulka, P.; Klimentova, J.; Vavrova, J.; Stulik, J.; Hernychova, L. *J. Proteomics* **2011***, 74*, 2786-2797.

(2) Dunn, J. D.; Reid, G. E.; Bruening, M. L. *Mass Spectrom. Rev.* **2010***, 29*, 29-54.

(3) Han, G.; Ye, M.; Zou, H. *Analyst* **2008***, 133*, 1128-1138.

(4) Kan'shin, E. D.; Nifant'ev, I. E.; Pshezhetskii, A. V. *J. Anal. Chem.* **2010***, 65*, 1295-1310.

(5) Leitner, A.; Sturm, M.; Lindner, W. *Anal. Chim. Acta* **2011***, 703*, 19-30.

(6) Ficarro, S. B.; McCleland, M. L.; Stukenberg, P. T.; Burke, D. J.; Ross, M. M.; Shabanowitz, J.; Hunt, D. F.; White, F. M. *Nat Biotech* **2002***, 20*, 301-305.

(7) Wang, H.; Duan, J.; Xu, H.; Zhao, L.; Liang, Y.; Shan, Y.; Zhang, L.; Liang, Z.; Zhang, Y. *J. Sep. Sci.* **2011***, 34*, 2113-2121.

(8) Xue, Y.; Wei, J.; Han, H.; Zhao, L.; Cao, D.; Wang, J.; Yang, X.; Zhang, Y.; Qian, X. *J. Chromatogr. , B: Anal. Technol. Biomed. Life Sci.* **2009***, 877*, 757-764.

(9) Lu, J.; Li, Y.; Deng, C. *Nanoscale* **2011***, 3*, 1225-1233.

(10) Clearfield, A.; Stynes, J. A. *J. Inorg. Nucl. Chem.* **1964***, 26*, 117-129.

(11) Dines, M. B.; DiGiacomo, P. M. *Inorg. Chem.* **1981***, 20*, 92-97.

(12) Dines, M. B.; Digiacomo, P. M.; Callahan, K. P.; Griffith, P. C.; Lane, R. H.; Cooksey, R. E. In *Derivatized Layerd M(IV) Phosphonates;* Miller, J. S., Ed.; Chemically Modified Surfaces in Catalysis and Electrocatalysis; American Chemical Society: Washington, D.C., 1982; .

(13) Dines, M. B.; Cooksey, R. E.; Griffith, P. C.; Lane, R. H. *Inorg. Chem.* **1983***, 22*, 1003-1004.

(14) Wang, Z.; Heising, J. M.; Clearfield, A. *J. Am. Chem. Soc.* **2003***, 125*, 10375-10383.

(15) Clearfield, A. In *Metal Phosphonate Chemistry;* Karlin, K. D., Ed.; *Prog. Inorg. Chem.*; Wiley: New York, 1998.

(16) Xu, S.; Whitin, J. C.; Yu, T. T.; Zhou, H.; Sun, D.; Sue, H.; Zou, H.; Cohen, H. J.; Zare, R. N. *Anal. Chem.* **2008***, 80*, 5542-5549.

(17) Jin, W.; Dai, J.; Zhou, H.; Xia, Q.; Zou, H.; Zeng, R. *Rapid Commun. Mass Spectrom.* **2004***, 18*, 2169-2176.

(18) Dong, J.; Zhou, H.; Wu, R.; Ye, M.; Zou, H. *J. Sep. Sci.* **2007***, 30*, 2917-2923.

(19) Wang, P.; Zhao, L.; Wu, R.; Zhong, H.; Zou, H.; Yang, J.; Yang, Q. *J. Phys. Chem. C* **2009***, 113*, 1359-1366.

(20) Zhao, L.; Wu, R.; Han, G.; Zhou, H.; Ren, L.; Tian, R.; Zou, H. *J. Am. Soc. Mass Spectrom.* **2008***, 19*, 1176-1186.

(21) Zhou, H. J.; Xu, S. Y.; Ye, M. L.; Feng, S.; Pan, C. S.; Jiang, X. G.; Li, X.; Han, G. H.; Fu, Y.; Zou, H. F. *J. Proteome Res.* **2006***, 5*, 2431-2437.

(22) Feng, S.; Ye, M.; Zhou, H.; Jiang, X.; Jiang, X.; Zou, H.; Gong, B. *Mol. Cell. Proteomics* **2007***, 6*, 1656-1665.

(23) Hong, H. G.; Sackett, D. D.; Mallouk, T. E. *Chem. Mater.* **1991***, 3*, 521-527.

(24) Kosmulski, M. *J. Colloid Interface Sci.* **2002***, 253*, 77-87.

(25) Hunter, R. J. In *Zeta Potential in Colloid Science: Principles and Applications;* Academic Press: 1981.

(26) Alvarez-Silva, M.; Uribe-Salas, A.; Mirnezami, M.; Finch, J. A. *Minerals Eng* **2010***, 23*, 383-389.

(27) Mao, Q. M.; Hearn, M. T. W. *Biotechnol. Bioeng.* **1996***, 52*, 204-222.

(28) Stone, M. C.; Tao, Y.; Carta, G. *J. Chromatogr., A* **2009***, 1216*, 4465-4474.

(29) Watkins, R.; Weiss, D.; Dubbin, W.; Peel, K.; Coles, B.; Arnold, T. *J. Colloid Interface Sci.* **2006***, 303*, 639-646.

(30) Lin, F.; Chen, C.; Chen, W.; Yamamoto, S. *J. Chromatogr., A* **2001***, 912*, 281-289.

(31) Goobes, R.; Goobes, G.; Campbell, C. T.; Stayton, P. S. *Biochemistry (N. Y.)* **2006***, 45*, 5576-5586.

(32) Maharjan, P.; Hearn, M. T. W.; Jackson, W. R.; De Silva, K.; Woonton, B. W. *J. Chromatogr., A* **2009***, 1216*, 8722-8729.

(33) Perez-Almodovar, E. X.; Carta, G. *J. Chromatogr., A* **2009***, 1216*, 8339-8347.

(34) Zhou, X.; Li, W.; Shi, Q.; Sun, Y. *J. Chromatogr., A* **2006***, 1103*, 110-117.

(35) Lin, X.; Wu, J.; Fan, J.; Qian, W.; Zhou, X.; Qian, C.; Jin, X.; Wang, L.; Bai, J.; Ying, H. *J. Chem. Technol. Biotechnol.* **2012***, 87*, 924-931.

(36) Baker, H. M.; Massadeh, A. M.; Younes, H. A. *Environ. Monit. Assess.* **2008; 2009***, 157*, 319-330.

(37) Valero-Navarro, Á.; Gómez-Romero, M.; Fernández-Sánchez, J. F.; Cormack, P. A. G.; Segura-Carretero, A.; Fernández-Gutiérrez, A. *J. Chromatogr., A* **2011***, 1218*, 7289-7296.

(38) Bak, H.; Thomas, O. R. T.; Abildskov, J. *J. Chromatogr., B* **2007***, 848*, 131-141.

(39) Troup, J. M.; Clearfield, A. *Inorg. Chem.* **1977***, 16*, 3311-3314.

(40) Leitner, A. *TrAC, Trends Anal. Chem.* **2010***, 29*, 177-185.

(41) Connor, P. A.; McQuillan, A. J. *Langmuir* **1999***, 15*, 2916-2921.

(42) Kweon, H. K.; Hakansson, K. *Anal. Chem.* **2006***, 78*, 1743-1749.

(43) Kosmulski, M. *J. Colloid Interface Sci.* **2004***, 275*, 214-224.

(44) Kosmulski, M. *J. Colloid Interface Sci.* **2006***, 298*, 730-741.

(45) Kosmulski, M. *J. Colloid Interface Sci.* **2009***, 337*, 439-448.

(46) Kosmulski, M. *J. Colloid Interface Sci.* **2011***, 353*, 1-15.

(47) Kosmulski, M. *Colloids Surf. Physicochem. Eng. Aspects* **2003***, 222*, 113-118.

(48) Mercado, A.; Farfán-Torres, E. M.; Regazzoni, A. E.; Blesa, M. A. *Colloids Surf. Physicochem. Eng. Aspects* **2003***, 218*, 277-284.

(49) Hubbard, A. T. In *Encyclopedia of surface and colloid science, v3;* Marcel Dekker: New York, 2002.

(50) Kosmulski, M.; Maczka, E.; Jartych, E.; Rosenholm, J. B. *Adv. Colloid Interface Sci.* **2003***, 103*, 57-76.

(51) Lützenkirchen, J.; Preocanin, T.; Kovacevic, D.; Tomiscic, V.; Lovgren, L.; Kallay, N. *Croat. Chem. Acta* **2012***, 85*, 391-417.

(52) Fuerstenau, D. W.; Pradip *Adv. Colloid Interface Sci.* **2005***, 114–115*, 9-26.

(53) Wang, H.; Niu, C. H.; Yang, Q.; Badea, I. *Nanotechnology* **2011***, 22*, 145703.

(54) Adamczyk, Z.; Bratek-Skicki, A.; Dabrowska, P.; Nattich-Rak, M. *Langmuir* **2011***, 28*, 474-485.

(55) Nunes, A. P. L.; Peres, A. E. C.; de Araujo, A. C.; Valadão, G. E. S. *J. Colloid Interface Sci.* **2011***, 361*, 632-638.

(56) Lǔ, J.; Liu, H.; Liu, R.; Zhao, X.; Sun, L.; Qu, J. *Powder Technol.* **2013***, 233*, 146-154.

(57) Ali, A.; hanna, A.; Gad, A. *Phosphorus Research Bulletin* **2008***, 22*, 32-40.

(58) Sun, L.; Boo, W. J.; Sue, H.; Clearfield, A. *New J. Chem.* **2007***, 31*, 39-43.

(59) Ch. Srilakshmi; Ramesh, K.; Nagaraju, P.; Lingaiah, N.; Sai Prasad, P. S. *Catalysis Letters* **2005***, 106*, 115-122.

(60) Giddings, J. C. In *Unified separation science;* Wiley: 1991.

(61) Poole, C. F. In *The Essence of Chromatography;* London: 2003.

(62) El-Khaiary, M. I. *J. Hazard. Mater.* **2008***, 158*, 73-87.

(63) Banerjee, R.; Furukawa, H.; Britt, D.; Knobler, C.; O'Keeffe, M.; Yaghi, O. M. *J. Am. Chem. Soc.* **2009***, 131*, 3875-3877.

(64) Liebl, M. R.; Senker, J. *Chem. Mater.* **2013***, 25*, 970-980.

(65) Li, H.; Li, G.; Li, Z.; Lu, C.; Li, Y.; Tan, X. *Appl. Surf. Sci.* **2013***, 264*, 644-652.

(66) Gauci, S.; van Breukelen, B.; Lemeer, S. M.; Krijgsveld, J.; Heck, A. J. R. *Proteomics* **2008***, 8*, 4898-4906.

(67) Zheng, Z. *Unpublished work* **2011**.

(68) Wilkins, M.; Gasteiger, E.; Bairoch, A.; Sanchez, J.; Williams, K.; Appel, R.; Hochstrasser, D. *Methods Mol. Biol.* **1999***, 112*, 531-552.

BIOGRAPHICAL SKETCH

Emily graduated from Colorado State University with her Bachelor of Science degree in chemistry in May of 2007. At that time she commissioned into the United States Air Force and took her first assignment at Tyndall AFB, Florida. During this assignment, she completed a Professional Science master's degree in materials and chemical synthesis from Illinois Institute of Technology in December of 2009. In the fall of 2010, she began her research at the University of Florida, Department of Chemistry under the direction of Dr. Dan Talham. She completed her work toward her Doctor of Philosophy degree in analytical chemistry in August and graduated in December of 2013. Upon completion of her PhD, Emily returned to regular active duty service in the Air Force.